1973

Numerical simulation of heat, mass, and momentum transfer in an atmospheric boundary layer

Darrell W. Pepper

Department: Mechanical and Aerospace Engineering

NUMERICAL SIMULATION OF HEAT, MASS, AND MOMENTUM TRANSFER IN AN ATMOSPHERIC BOUNDARY LAYER

by

Darrell W. Pepper, 1946 -

A DISSERTATION

Presented to the faculty of the Graduate School of the

UNIVERSITY OF MISSOURI - ROLLA

In Partial Fulfillment of the Requirements for the Degree

DOCTOR OF PHILOSOPHY

in

MECHANICAL ENGINEERING

1973

Shen C. Lee
Advisor

H. F. Nelson

J. C. Carstens

R. B. Oetting

C. Y. Ho

ABSTRACT

Considerable interest has developed in recent years to understand transport phenomena in thermally stratified boundary layers. More complete knowledge in this field is needed to improve the prediction of the diffusion of air pollutants in the lower atmosphere as well as in forecasting air-water circulation for weather conditions.

The atmospheric boundary layer is modeled using the equations of continuity, momentum, energy, and concentration. Closure of this set of partial differential equations is hindered by the turbulence terms. Using turbulence kinetic energy, the system of equations is closed by internally determining the exchange coefficients of heat, mass, and momentum along with other atmospheric parameters. This approach makes it possible for the history of turbulent motion to be taken into account. Verification of this model is made by systematically comparing the numerical results with available wind tunnel data for neutral, stable, and unstable conditions. Application of the model is made to study the formation of advection fogs occurring over cold sea surfaces. However, the predicted results of liquid water and water vapor contents have yet to be verified with actual data obtained from field measurements.

ACKNOWLEDGMENTS

I personally wish to thank Dr. Shen C. Lee for his assistance and foresight during the period of research represented by this thesis. His enthusiasm and confidence gave me sufficient incentive to overcome numerous obstacles throughout this investigation. I should also like to thank Dr. John Carstens for his suggestions in the course of this research.

This project was supported by a research fellowship under THEMIS Contract N00014-68-A-0497 and ONR Contract N00014-69-A-0141-0006. I would like to extend my appreciation to Dr. J. L. Kassner, Director of the Cloud Physics Research Center, for making this fellowship possible and to Dr. J. Podzimek for his timely comments and guidance during the course of study. I am also thankful to Mrs. Janet Thompson for her assistance in the typing of this paper.

I would like to express my deep appreciation to my father, who, during his lifetime, gave me all of his encouragement and confidence. I would additionally like to thank Dr. H. P. Limbacher for instilling in me his desire for excellence of work and pursuit of education.

Finally, I wish to thank my wife for helping me prepare this thesis. I am deeply indebted to her for allowing me to pursue this research while doing without all but the barest necessities.

TABLE OF CONTENTS

LIST OF ILLUSTRATIONS

LIST OF TABLES

NOMENCLATURE

a	coefficient of the general parabolic equation
a_1	constant used to relate turbulent shear stress to turbulence kinetic energy
a_2	constant appearing in the dissipation term for turbulence kinetic energy
A_+	empirical constant in van Driest model for exchange coefficient of momentum
b	coefficient of the general parabolic equation
c	coefficient of the general parabolic equation
C_{max}	maximum concentration, mg/cc
C_{w_o}	wall concentration at initial x location, mg/cc
C^n	concentration of species
c'	fluctuation of concentration
C_s	source term for condensation or evaporation
C_p	specific heat of air at constant pressure
C_μ	empirical constant based upon Kolmogorov model for turbulence kinetic energy
d	coefficient of the general parabolic equation
D_c	molecular diffusion coefficient
D_Q	turbulence kinetic energy dissipation, newt/m^2-se
F	dissipation variable for turbulence kinetic energy in terms of frequency squared
F_i	tensor for body forces appearing in the Navier Stokes equation
G	constant strength of line source, mg/cm-sec
g	acceleration due to gravity, m/sec^2

H	total, or stagnation, enthalpy, m^2/sec^2
h	static enthalpy, m^2/sec^2
h'	enthalpy fluctuation
h^n	enthalpy generation of species n
J_H	diffusional flux for total enthalpy
J_C	diffusional flux for species, or concentration
k	von Karman constant, .41
K	Kelvin scale
K_m	exchange coefficient of momentum, newt-sec/m^2
K_m^*	K_m/density, m^2/sec
K_h	exchange coefficient of heat, newt-sec/m^2
K_Q	exchange coefficient of turbulence kinetic energy, newt-sec/m^2
K_c	exchange coefficient of species, newt-sec/m^2
K_w	mean mass absorption coefficient for fog
K_p	pressure gradient coefficient
L	Monin-Obukhov stability length scale, m
L_h	latent heat of condensation
ℓ	Prandtl mixing length, m
ℓ_μ, ℓ_k	empirical mixing lengths based upon Kolmogorov model, m
ℓ_D	mixing length for the dissipation of turbulence kinetic energy, m
$\dot{m}_w$	mass flux at a surface
$\dot{m}_I$	wall boundary entrainment rate
$\dot{m}_E$	free boundary entrainment rate

m_v	mass of water vapor
m_a	mass of dry air
N	number of droplets per unit volume
P	static pressure, newt/m^2
p'	fluctuating pressure
p_v	partial pressure of water vapor
p_a	partial pressure of dry air
Q	turbulence kinetic energy, m^2/sec^2
q	heat flux
q_s	scalar velocity in second order closure method
R	radiative flux divergence
R_v	universal gas constant for water vapor
R_a	universal gas constant for dry air
R_t	Reynolds number of turbulence
R_i	gradient Richardson number
R_f	flux Richardson number
S^n	production of species concentration due to chemical reaction
T	temperature, ^oK
T_w	surface temperature, ^oK
T_∞	free stream temperature, ^oK
T_m	average absolute temperature of the boundary layer
t*	friction temperature
t	time, sec

t'	fluctuating temperature
U	mean velocity in the x-direction, m/sec
u'	fluctuating velocity in the x-direction
U_∞	free stream velocity, m/sec
U_j	mean velocity in the j direction, m/sec
u'_j	fluctuating velocity in the j direction
u_i	Eulerian velocity
u^*	friction velocity
u^+	dimensionless velocity in the x-direction
v	specific volume
W	mean velocity in the z-direction, m/sec
W_L	liquid water content
W_t	terminal velocity of fog droplets
W_v	water vapor mixing ratio
X_1, X	coordinate in the main flow direction, m
X_2, Y	coordinate lateral to main flow direction, m
X_3, Z	coordinate normal to main flow direction, m
X_s	distance from source of concentration in the main flow direction, m
α	thermal conductivity
β	power law exponent for velocity profile in Couette flow region
β'	fraction of radiation emitted from earth's surface (long wave radiation)
β_1	local pressure gradient parameter
β_2	blowing fraction

β_3, β^*	empirical constants to account for thermal stratification
Γ	adiabatic lapse rate, g/C_p
γ	power law exponent for dependent variables in the Couette flow region
Δ	dimensionless grid interval
δ	boundary layer thickness, m
δ_o	boundary layer thickness at initial x location, m
δ_t	thermal boundary layer thickness, m
ε	ratio of R_a/R_v
ε_m	eddy coefficient of momentum, newt-sec/m^2
ε_h	eddy coefficient of heat
ε_c	eddy coefficient of concentration
ζ	empirical constant used in subgrid scale method
η	constant associated with the van Driest mixing length model
θ	potential temperature, ^oK
Λ_α	scalar length
λ	characteristic height where $C = \frac{1}{2}C_{max}$, m
λ^*	characteristic height where $T = \frac{1}{2}T_w$, m
μ	dynamic viscosity, newt-sec/m^2
ν	kinematic viscosity, m^2/sec
ξ	non-dimensional height, Z/L
ρ	density, newt-sec^2/m^4
Σ	energy dissipation parameter, m^2/sec^3

σ	Stefan Boltzmann constant
σ_{h_l}	laminar Prandtl number
σ_{h_t}	turbulent Prandtl number
σ_{c_l}	laminar Schmidt number
σ_{c_t}	turbulent Schmidt number
σ_h	mixed Prandtl number
σ_c	mixed Schmidt number
σ_k	equivalent mixed Prandtl number for turbulence kinetic energy
τ	local shear stress, newt/m^2
Φ	energy dissipation function
ϕ	generalized dependent flow parameter
ψ	stream function, newt-sec/m^2
Ω	empirical length parameter
ω	normalized stream function
ω_s	water vapor mixing ratio at saturation

1. INTRODUCTION

While turbulent boundary layers in the presence of heat and mass transfer are quite commonplace in engineering problems, great interest has developed in recent years to understand transport phenomena in thermally stratified boundary layers. Adequate knowledge in this area will be valuable in predicting the diffusion process of air pollutants in the lower atmosphere as well as in forecasting air-water circulation for weather conditions.

Many physical parameters are involved in atmospheric transport processes, such as wind, temperature, and concentration of the diffusing medium as well as the geographical terrain. Studies of atmospheric motions are hindered by the turbulence generated from the interactions of all these related parameters. Moreover, due to the random motion of the turbulence eddies, field measurements are often not sufficiently adequate for formulating any mathematical model.

Investigations of atmospheric boundary layers are often accomplished by wind tunnel simulations and numerical modeling. Many questions have been raised as to whether atmospheric turbulence can be realistically simulated in a wind tunnel. No reliable answer is readily available. The variation of the scale of turbulence throughout the atmosphere cannot be modeled in the wind tunnel. However, wind tunnel modeling has provided a means for controlling certain conditions, allowing important variables to be

collectively analyzed and used as a basis in formulating analytical models.

The planetary boundary layer consists of two distinct layers, each governed by its own particular set of flow parameters. The lower layer, in which most human activity takes place, depends upon friction forces and is analogous to turbulent boundary layer flow along a flat plate. The upper layer is driven predominantly by both Coriolis and pressure forces. When density stratification in the lower atmosphere is caused by temperature stratification, the flow is considered to be thermally stratified. In neutral stratification, the vertical gradient of temperature equals the adiabatic lapse rate, which corresponds approximately to a $1^{o}C$ decrease in temperature per 100 meters of height. Unstable stratification, or lapse condition, results when the temperature decreases faster than the adiabatic rate with height. Consequently, as a parcel of air rises, the air parcel becomse warmer than its environment, causing the density to decrease with the result that buoyancy accelerates it upward. Stable stratification, or inversion, occurs when the temperature increases faster than the adiabatic lapse rate with height. This causes the rising air to become cooler and more dense than its surroundings with the result that the air parcel tends to return to its original position. Due to the influence of these temperature gradients, the buoyancy forces on the flow regime therefore either increase the rate of turbulence diffusion in the

vertical direction, corresponding to lapse conditions, or impede turbulence diffusion, corresponding to an inversion. In most engineering heat transfer studies, stratification effects are negligible.

The source of concentration, or heat, can be either constant or variable, and is usually approximated by either a point or line source, located on the ground or at a specific height. Concentration may either be active, influencing the flow field by which it is transported, or passive, independent of the flow field by which it is transported. Most studies dealing with diffusion of pollutants have assumed the concentration to be passive. In dealing specifically with the case of marine fog studies, concentrations corresponding to liquid water content and water vapor content are considered active.

The objectives of this research have been to develop a suitable analytical model, using available empirical and mathematical information, to numerically predict heat, mass, and momentum transport for both wind tunnel experiments and field measurements. A numerical scheme was used which would allow for a wide range of applications suitable to both engineering and meteorological processes. This study is to verify the numerical method with available wind tunnel data and to apply this method to predict the formation of advection fog.

II. REVIEW OF THE LITERATURE

Numerous theories have developed in an effort to describe transport phenomena in the atmosphere. An adequate study of atmospheric processes can be accomplished by coupling experimental investigations with analytical theory. Presentation of the literature in this review is given as a logical progression consistent with this point of view.

A. Field Measurements

A considerable amount of experimental data has been taken on atmospheric diffusion from fixed sources in lower layers of the atmosphere, particularly the dispersion of gaseous pollutants into the atmosphere. Fay, et al (1) have complied a list of field data from various authors pertaining to different types of air pollution.

Observation of plumes ejected from smoke stacks has been analyzed by Briggs (2), who compared plume rise for buoyant plumes in both stable and neutral air for both calm and windy conditions. Hoult, et al (3) likewise observed plume rise trajectories in an effort to simulate laboratory measurements with empirical parameters. Haagen-Smit (4), analyzing the presence of smog in the Los Angeles area, correlated the effect of hydrocarbons and nitrogen oxides with crop damage, eye irritation, and rubber cracking. Wyngaard and Cote (5) made direct observations of surface stress and heat flux over a horizontally uniform site and compared dissipation and production of turbulence kinetic

energy for both stable and unstable conditions.

Field measurements have also been made over large geographical regions. Webb (6) studied diabatic mean velocity and temperature profile forms taken from field data made at O'Neill, Nebraska and from Kerang and Hay, Australia and formulated constants used in the log-linear law for flow in both stable and unstable conditions. Priestly (7) and Lumley and Panofsky (8) document a considerable number of field measurements concerning diabatic mean profiles for heights up to tens of meters. Haugen, et al (9) used data from Project Prairie Grass for investigating values of parameters appearing in Sutton's (10) diffusion models. Sutton (11) likewise documents a number of experiments concerning field measurements.

The oceans of middle and high latitude have a large maximum frequency of fog in the summer season because of advection of warm air over cold water. Because very few advection fogs of this kind occur over land, little study is available in the literature. However, recent investigations of the microphysical and micrometeorological properties of sea fog have been made by the Calspan Corporation (see "Project Sea Fog") using shipboard procedures. Observations and measurements of drop size distributions and visibility were made throughout the life cycle of fogs.

Sea-air interaction produces the environment of moisture and sea salt particles in the lower atmospheric boundary over the ocean surface. Numerous observations of the

sea-air interface have been made by Kraus (12). Wind and temperature data were obtained by Deacon (13), from observations over the sea, in an effort to calculate roughness parameters for the sea surface. Hidy (14) reviewed a substantial number of articles by various authors in an effort to analyze air-sea interaction phenomena in the atmospheric boundary layer. Field measurements dealing with the microphysics of the marine atmosphere are discussed in detail by Roll (15).

Unfortunately, these field studies are difficult to compare with one another due to the random nature of the atmosphere. Mean wind velocity and temperature gradients change significantly in a very short time and cannot be controlled during the long periods of sampling. Moreover, field studies usually require considerable effort and expense from the investigator.

B. Wind Tunnel Simulation

Perhaps the most important factor regarding wind tunnel modeling of the atmospheric boundary layer is that the experiment can be controlled under specific conditions, allowing many flow variables to be isolated and studied. The greatest deterent to wind tunnel modeling is the difference in the physical nature of turbulence between the atmosphere and the wind tunnel. However, many of the flow parameters are synonymous. Reynolds number, Richardson number, Prandtl number, and Schmidt number can be readily applied to either the wind tunnel or the atmospheric boundary layer. The

surface boundary conditions and certain turbulent characteristics can be similarly related.

Specifically an atmospheric wind tunnel must develop a very thick boundary layer and be capable of creating a wide range of Richardson numbers, i.e., temperature and velocity gradients. The requirements of such modeling have been reported by Cermak, et al (16). Chuang and Cermak (17), Plate (18), and Plate and Lin (19) showed that velocity profiles in a meteorological tunnel were similar to those observed in the atmospheric surface layer. Schon and Mery (20) have likewise shown a method for artificially simulating a neutral atmospheric surface layer using wind tunnel techniques. Presently there exist facilities for meteorological wind tunnels at Colorado State University, New York University, Calspan Corporation Laboratories, The Ecole Centrale Lyonnaise, and several others.

Poreh and Cermak (21) studied the diffusion of ammonia gas from a line source at ground level for ambient velocities of 2.74, 3.66, and 4.87 m/sec (9, 12, and 16 ft/sec) in a neutral atmosphere. The downstream diffusion pattern was divided into four separate zones: initial, intermediate, transition, and final. Poreh intorduced a similarity parameter, λ, defined as the distance from the wall where the concentration is equal to 50 per cent of the wall value. Within the intermediate zone, λ was found to be approximately equal to the horizontal distance from the source, X_s, to the 0.8 power, $\lambda \simeq X_s^{.8}$, and the maximum ground

concentration was found to vary as $C_{max} \propto X_s^{-.9}/U_\infty$. Velocity distribution was found to follow the 1/7 power law. The intermediate zone was defined as that region where $.37<\lambda/\delta<.64$, δ being the boundary layer thickness.

Quraishi (22) experimentally investigated the diffusion of ammonia gas from a line source located at ground level and elevated positions under neutral conditions. Flexible roughness elements were fixed on the floor of the wind tunnel test section consisting of plastic strips fastened to wooden strips. Free stream ambient velocity was 6.10 m/sec (20 ft/sec). The concentration field was divided into three zones according to distance from the source and were found to follow three different universal functions. It was found that as the elevation of the source increased, the concentration at ground level for a short distance from the source was lower than for a ground level source, increasing to a peak value and then decreasing asymptically as though for a source at the boundary. Both longitudinal and lateral turbulence intensities and Reynolds shear stress were measured using hot-wire anemometry.

Davar (23) used a continuous point source with a turbulent boundary layer over a smooth neutral boundary and studied the characteristics of diffusion plumes at an ambient air velocity of 1.83 m/sec (6 ft/sec). He varied the source height over a range of 0 to .127 meters (5 inches), using anhydrous ammonia as a tracer gas. Bhaduri (24) likewise used a continuous point source with a turbulent

boundary layer over fixed wooden strips in neutral stability and ambient air velocity of 3.81 m/sec (12.5 ft/sec). Elevation of the source varied from 0 to .0254 meter (1 inch).

Schon and Mery (20) used the method of injecting air upstream of a boundary layer in order to simulate a neutral atmospheric surface layer. A comparison was made with other laboratory data obtained by using a shear screen device to artifically thicken the flow regime. Although mean velocity profiles were similar, the velocity fluctuations did not represent those of a neutral boundary layer, as in the case of the air injection method. Good agreement was found to exist between the laboratory and atmospheric data for fluctuating spectra. Turbulence intensities in three directions were measured along with Reynolds shear stress at four different locations for an ambient velocity of 6.5 m/sec. Comparison of turbulence intensity in the simulated tunnel with that in the real atmosphere showed the turbulence characteristics in the tunnel to be less intense by 5-10 per cent.

Arya (25) experimentally investigated the structure of a stably stratified thick boundary layer. Unfortunately no mass diffusion experiments were made, but measurements of mean velocity, temperature, turbulence intensities in three directions, Reynolds shear stress, heat fluxes and turbulent spectra were made at two locations downstream of the leading edge of the test section. In the logarithmic law of the wall, empirical constants for mean velocity and temperature

were found to be valid for both atmospheric data as well as wind tunnel data. The ratio of the turbulent exchange coefficient of heat to that of momentum was found to be 0.75, which is in general agreement with Fleagle and Businger (26). The small scale structure of turbulence remained unaffected by stability, however the magnitude of turbulence production and dissipation reduced significantly as stability increased.

Chaudhry and Meroney (27) studied the downwind diffusion of a passive gas in a stably stratified turbulent shear layer. A micrometeorological wind tunnel was used in which the air was heated and the wind tunnel floor cooled. Concentration characteristics were compared with atmospheric observations and showed favorable agreement. A summary of wind tunnel diffusion experiments conducted at Colorado State University was given for the period prior to their report.

Malhotra (28) investigated the diffusion of ammonia from a ground level point source within a two dimensional boundary layer for both neutral and unstable conditions for ambient velocities of 1. 83, 1.98, and 2.74 m/sec (6, 6.50, and 9 ft/sec). A synthetic line source was obtained by numerically integrating the point source data. The concentration distribution for both neutral and unstable conditions were found to follow identical universal dimensionless curves. A comparison between heat diffusion data of Wieghardt (29) and mass diffusion data showed that universal distribution curves were similar for both point and line sources located on the surface of an isothermal boundary

layer.

Wieghardt (29) measured the temperature distribution from a point and line source of heat on the bottom of a turbulent boundary layer. Measurements were made at ambient velocities of 5.40 to 30.9 m/sec at various downstream locations from the faint source of heat. Line source data showed that λ^*, the similarity parameter for heat analogous to that for concentration could be related by $\lambda^* = \text{const.} X_s/(U_\infty X_s/\nu)^{.2}$, where X_s is the horizontal distance from the source and ν the kinematic viscosity. An empirical relation was likewise derived for the wall temperature as a function of U_∞, δ, X_s, and the strength of the heat source per unit length. Malhotra (28) found that the results of Wieghardt (29) were similar in behavior to the mass diffusion data of Poreh (30).

While wind tunnel diffusion data exist in detail and show good qualitative agreement with observations in the atmosphere, the scale of turbulence and range of variables still differ. Inconclusive results exist as to the variation of exchange coefficients for heat and mass from experimental data. A wider range of flow conditions, coupled with types of sources and driving mechanisms, have yet to be analyzed. Although these criteria are substantial detriments to wind tunnel simulation, data can be obtained which may contribute to an understanding of basic mechanisms associated with atmospheric diffusion and turbulent flow phenomena.

C. Anayltical Models

Mathematical analysis of the turbulent transport processes are discussed extensively by Rao, et al (31) and Monin and Yaglom (32). Based upon their studies, transport phenomena occurring in the atmosphere can be classified into three distinct categories, dependent upon the method used to describe the diffusion mechanism: 1) exchange coefficient approach, 2) turbulence kinetic energy approach, and 3) statistical theory.

1. Exchange Coefficient Hypothesis

The equations governing turbulent flow, while similar in form to laminar equations, involve the added complexity of turbulent flux terms and prove to be very cumbersome in obtaining realistic solutions to actual flow phenomena. Boussinesq (33), assuming that turbulent fluxes are directly proportional to mean gradients of independent variables, introduced the concept of an eddy coefficient. He replaced the double correlation terms appearing in the turbulent equations by an eddy coefficient term times a mean gradient tensor. Following the procedure described by Malhotra (28), the conservation equation for concentration, C, can be written in terms of mean variables as

$$\rho\{\frac{\partial C}{\partial t} + \frac{\partial}{\partial X_j}(U_j C)\} = \frac{\partial}{\partial X_j}\{D_c \frac{\partial C}{\partial X_j} - \rho\overline{u_j' c'}\} \qquad (2\text{-}1)$$

where the overbar denotes time averaged quantity, the prime denotes fluctuating component, and D_c the molecular diffusion coefficient. The fluctuating term for mass flux is

related to the mean concentration gradient through the eddy coefficient, ε_c, such that

$$\rho\overline{u_j'c'} = -\varepsilon_c\frac{\partial C}{\partial X_j} \tag{2-2}$$

The eddy coefficient is not considered a real property of the fluid but is effective only is there is some flow of the fluid. The problem therefore becomes apparent when attempting to describe the eddy coefficient in terms of realistic variables.

Equation (2-1) may be written as

$$\frac{\partial C}{\partial t} + \frac{\partial}{\partial X_j}(U_j C) = \frac{\partial}{\partial X_j}\{(D_c + \varepsilon_c)\frac{\partial C}{\partial X_j}\} \tag{2-3}$$

The exchange coefficient of concentration, K_c, is defined as $K_c = D_c + \varepsilon_c$. The concentration equation is therefore rewritten as

$$\frac{\partial C}{\partial t} + \frac{\partial}{\partial X_j}(U_j C) = \frac{\partial}{\partial X_j}(K_c\frac{\partial C}{\partial X_j}) \tag{2-4}$$

The concept of expressing the mass fluctuations in terms of the exchange coefficient of concentration, K_c, is commonly referred as the "K-theory" by meteorologists. Numerous closed solutions have been obtained using equation (2-4) assuming the exchange coefficient to be either constant, varying with height, or based upon the phenomenological mixing length theory.

Models dealing specifically with the exchange coefficient of concentration may be simply described by the Fickian diffusion model, power-law models, and Calder's

diffusion model, as described in detail by Rao, et al (31). These models lead to empirical relations in which the exchange coefficients are constant throughout the boundary layer, or a function specifically of height and friction velocity, u*. Despite their apparent usefulness, their drawback lies in the fact that the exchange coefficients vary as a function of the scale of turbulence throughout the atmosphere. This was pointed out by Richardson (34) in comparing values for molecular diffusion with diffusion during atmospheric storms. Moreover, equating the exchange coefficients of heat and momentum to the diffusion coefficient results in a expression mathematically desirable but not realistic in accounting for the effect of surface roughness or thermal stratification.

a. Mixing Length Theory

The mixing length concept has been used by many due to its relative simplicity in obtaining solutions adequate for engineering problems. Meteorologists have long assumed that the surface layer of the atmosphere can be regarded as a constant flux layer. The eddy coefficient of concentration is assumed to vary linearly with height and to depend upon the initial value of the friction velocity, u*, at the surface - analogous to the mixing length concept.

Introduction of the mixing length concept was originally made by Prandtl (35), who experimentally observed momentum exchange in turbulent flows. He concluded that the exchange coefficient of momentum for plane flows could

be written as a product of a mixing-length parameter and the cross stream gradient of the mean velocity, and assumed the mixing length proportional to the width of the mixing region. In theory, a lump of fluid carried a constant amount of momentum determined by the difference in mean velocity between adjacent parallel planes. Prandtl (36) later revised his concept by including additional terms containing the second order derivative of the mean velocity in the stream direction and a length parameter.

Taylor (37), developing a theory similar to Prandtl (35), assumed that vorticity might be considered a transferable quantity for two-dimensional flow. The eddy coefficient differed from Prandtl's model by a factor of 2. Further extension of the vorticity-transport theory to three dimensional flow tended to sacrifice accuracy for simplicity.

Von Karman (38) likewise made the assumption that the value of the mixing length is determined by local flow conditions described in terms of quantities determined by these local conditions. Unreasonable results occurred, however, where the second derivative of the mean flow, appearing in the denominator, became zero, i.e., the eddy coefficient of momentum became infinite. Hinze (39) points out that this particular model does not appear to offer many advantages over Prandtl's simpler assumption, while all three theories lack the ability to describe the transport of turbulence in detail.

Van Driest (40), using a modification of the mixing

length theory, was concerned with a layer in which the shear stress was everywhere equal to that at the wall. He assumed that the eddy coefficient of momentum decayed exponentially to laminar viscosity near the wall, but became proportional to the distance from the wall in the center region of the boundary layer.

Patankar (41) slightly modified van Driest's relation by replacing the wall shear stress with the local shear stress in the fluid. The Reynolds stress term is defined by Prandtl's hypothesis as

$$-\rho\overline{u_1' u_3'} = \rho \ell^2 \left|\frac{\partial U_1}{\partial X_3}\right| \frac{\partial U_1}{\partial X_3} \qquad (2\text{-}5)$$

where ρ is the fluid density, ℓ the mixing length, X_3 the vertical distance normal to the direction of flow, and $|\partial U_1/\partial X_3|$ the absolute value of the cross-stream velocity gradient. Combining the laminar viscosity and employing the assumptions of van Driest (40), the exchange coefficient of momentum was written as

$$K_m = \mu + \rho\eta^2 X_3^2 \left[1 - \exp\{-X_3\sqrt{\tau\rho}/(\mu A_+)\}\right]^2 \left|\frac{\partial U_1}{\partial X_3}\right| \qquad (2\text{-}6)$$

where A_+ and η are constants, μ is the laminar viscosity, and τ is the local shear stress. The exponential term is seen to be effective only in the region near the wall and tends to dampen the eddy motion of the fluid as the flow approaches the wall.

Cebeci, et al (42) formulate an expression for the eddy coefficient based upon van Driest's (40) hypothesis

and similar to that originated by Patankar (41), using modified empirical constants and reintroducing the wall shear into the exponential term. Two expressions for the eddy coefficient were used to account for the inner viscous sublayer region and the turbulent viscosity in the outer region of flow. Cebeci and Mosinskis (43), in a later work, again modify their expression for the eddy coefficient in order to account for the effect of mass transfer in the inner region of flow.

A number of mathematical models have been developed by meteorologists based upon a somewhat analogous form of the mixing length concept in accounting for the exchange coefficients. Nearly all assume that the exchange coefficient for momentum, heat, and concentration are identical, and that they are a function of vertical height and either velocity or temperature gradient, in the case of thermal stratification.

Using the application of dimensional analysis in formulating turbulent diffusion phenomena, Monin and Obukhov (44) assumed that the flow in an atmospheric boundary layer could be completely determined by the friction velocity, u*, and a stability length scale, L, defined as

$$L = \frac{u^{*3}}{k\left(\frac{g}{T_m}\right)\left(-\frac{q}{\rho C_p}\right)} \qquad (2\text{-}7)$$

where k is the von Karman constant, q the turbulent heat flux, ρ the density of air, C_p the specific heat, g the

acceleration of gravity, and T_m the mean absolute temperature of the surface layer. A temperature scale was likewise defined for a steady, horizontally homogenoeus flow as

$$t^* = - \frac{q}{\rho C_p k u^*} \qquad (2\text{-}8)$$

Ellison (45), considering flow over an infinite rough plate, assumed that shear stress and heat flux remain constant with height. Neglecting diffusion terms, Ellison replaced double correlations in the turbulence equations with decay times such that, in the absence of production terms, these quantities would begin to diminish. Ratios for momentum and heat exchange coefficients were obtained as a function of these decaying time terms, friction velocity, and flux Richardson number. Townsend (46) analyzed flow in a stably stratified fluid far from boundary interaction by assuming homogeneous flow in the direction of shear and inhomogeniety in the direction of flow. Dissipation terms were expressed as a function of two length scales.

Yamamoto and Shimanuke (47), using a numerical solution for a two-dimensional diffusion equation, obtained an expression for K_c based upon a general velocity distribution from the similarity theory of Monin and Obukhov (44) and a fourth order equation to describe the variation of X_3/L. Later work by Yamamoto and Shimanuke (48), in extending the above treatment to three dimensional diffusion from a point source, assumed the lateral exchange coefficient of concentration to be a function of u*, k, and empirical functions determined

from the observation of the lateral spread of smoke at various stability conditions.

Estoque (49), numerically modeling transport phenomena in the atmosphere, assumed that the planetary boundary layer consisted of three distinct strata: a soil layer; a surface layer in which the vertical fluxes of heat, momentum, and moisture were constant with height; and an overlying transition layer where the influence of turbulent transfer processes gradually decrease with height. The exchange coefficient was assumed to be a function of the gradient Richardson number, the surface roughness, and the average potential temperature gradient. The exchange coefficient was assumed to decrease linearly with height in the transition layer. Unfortunately the numerical model neglected the effect of horizontal advection and, coupled with the attempt to describe the turbulent mixing process in the transition layer with a linearly decreasing exchange coefficient, resulted in unrealistic characteristics of the boundary layer.

Fisher and Caplan (50) attempted to predict the formation of fog and stratus using a slightly modified version of Estoque's exchange coefficient. An upper and lower value was imposed upon the coefficient to prevent exaggerated values. The exchange coefficient of momentum was assumed to be equal to the coefficients of heat and water vapor. Although results appeared reasonably valid for simple cases, the biggest defect of the model was the failure to make the exchange coefficient an internal parameter of the model.

A more recent model involving the potential temperature gradient and based primarily upon the Fisher and Caplan (50) model was made by Mack, et al (51). The exchange coefficient, while a function of local stability, was deduced from the Monin-Obukhov (44) similarity theory and a fourth order equation for X_3/L. A modification of the exchange coefficient was necessary to prevent extreme discontinuity near the upper boundary of the surface layer.

Blackadar (52), in describing the momentum exchange coefficient in a neutral boundary layer, used Heisenberg's (53) hypothesis of energy dissipation and mixing length related by

$$K_m = \Sigma^{1/3} \ell^{4/3} \rho \qquad (2\text{-}9)$$

with ℓ, the mixing length, defined by

$$\ell = kX_3(1 + kX_3/\Omega)^{-1} \qquad (2\text{-}10)$$

where Ω is an empirical length parameter and k the von Karman constant. The energy dissipation term is given as

$$\Sigma = K_m\{(\frac{\partial U_1}{\partial X_3})^2 + (\frac{\partial U_3}{\partial X_3})^2\}\rho^{-1} \qquad (2\text{-}11)$$

Using these above relationships, Blackadar obtained as a general statement for the exchange coefficient

$$K_m = \{(\frac{\partial U_1}{\partial X_3})^2 + (\frac{\partial U_3}{\partial X_3})^2\}^{\frac{1}{2}}(\frac{kX_3}{1 + kX_3/\Omega})^2\rho \qquad (2\text{-}12)$$

The advantage of this model over previous relations for K_m is the fact that at small heights, the mixing length increases linearly with height and reaches a fixed value at

upper limits of the atmospheric surface layer. Zdunkowski and Trask (54), investigating the effect of nocturnal temperature changes over various soil types for analyzing the stability of radiation fog, used a variation of Blackadar's (52) exchange coefficient generalized by Wu (55) to account for thermal stability. Results using this form of exchange coefficient showed a numerical discontinuity occurring in the upper region of the boundary layer and a modification of the model was necessary in order to extrapolate the momentum exchange coefficient to zero.

b. Rate Equation Hypothesis

An analytical approach to mass diffusion in a two-dimensional thermally stratified boundary layer is given by Rao, et al (31) based on an extension of the nonlocal phenomenological differential theory developed by Nee and Kovasnay (56). A rate equation is assumed to govern the momentum exchange coefficient, $K_m^* = \nu + \varepsilon_m/\rho$, in a thermally stratified boundary layer as

$$U_1\frac{\partial K_m^*}{\partial X_1} + U_3\frac{\partial K_m^*}{\partial X_3} = \frac{\partial}{\partial X_3}\left(K_m^*\frac{\partial K_m^*}{\partial X_3}\right) + A(K_m^* - \nu)\frac{\partial U_1}{\partial X_3} - \frac{BK_m^*(K_m^* - \nu)}{X_3^2}$$

$$- E\frac{R_i}{\sigma_{h_t}}(K_m^* - \nu)\frac{\partial U_1}{\partial X_3} \qquad (2\text{-}13)$$

where R_i is the gradient Richardson number, σ_{h_t} is the turbulent Prandtl number, and the three empirical constants A, B, and E are given as A = 1., B = 1., and E = 1. The generation or decay of turbulence due to the effect of buoyancy is represented by the last term in equation (2-13).

Although more complicated than the mixing length hypothesis, simulataneous solution of the rate equation with the equations of motion results in a theory which overcomes the effect of localness given by the older phenomenological theories and allows the past history of the flow to influence the solution.

2. Turbulence Kinetic Energy Approach

A more realistic approach to the modeling of the eddy coefficient concept is the suggestion made by Kolmogorov (57) that the eddy coefficient in a turbulent flow might be expressed as a function of the local kinetic energy of turbulence, Q, in which Q is defined as: $Q=\frac{1}{2}(\overline{u_i' u_i'})$. As a result, a number of empirical models have been developed in an attempt to close the turbulence kinetic energy equation with the governing equations of motion.

a. One-equation Models

Using the hypothesis by Kolmogorov (57) and Prandtl (36) of coupling the kinetic energy of turbulence with a characteristic length scale, ℓ, Patankar and Spalding (58) defined the exchange coefficient of momentum as

$$K_m = \mu + \ell \rho Q^{\frac{1}{2}} \qquad (2\text{-}14)$$

where μ is the dynamic viscosity and ρ the density of the fluid. This relation was also used by Glushko (59). The term, $\ell \rho Q^{\frac{1}{2}}$, was used only where the flow was fully turbulent, a condition expressed by a "local Reynolds number of turbulence" given as

$$R_t = \ell \rho Q^{\frac{1}{2}}/\mu \qquad (2\text{-}15)$$

Wolfshtein (60), using the Kolmogorov turbulence kinetic energy hypothesis, obtained numerical solutions for Couette flow with turbulence augmentation, pressure gradient, and turbulent duct flow. The characteristic length scales were defined as functions of X_3 and the Reynolds number of turbulence, R_t. The dissipation of turbulence kinetic energy was defined by

$$D_Q = \frac{.416\rho Q^{3/2}}{\ell_D} \qquad (2\text{-}16)$$

where

$$\ell_D = X_3\{1 - \exp(-.263R_t)\} \qquad (2\text{-}17)$$

An extension of this particular model was made by Wolfshtein (61) in using the turbulence kinetic energy equation to obtain steady two-dimensional solutions of the elliptic governing equations for a turbulent impinging jet. In both cases, the length scale was set equal to the distance from the wall for regions near the wall. Use of the Kolmogorov model was further emphasized by Gosman, et al (62) in analyzing heat and mass transfer in two-dimensional recirculating flows. A differential equation similar to the equation for turbulence kinetic energy was introduced to account for the length scale. A generalized set of equations was given which could be adjusted to any particular flow geometry or condition.

Bradshaw, et al (63), using a linear relationship to relate the turbulent shear stress to the turbulence kinetic energy, as suggested by Nevzglajdov (64), assumed that

$$-\rho\overline{u_i' u_j'} = a_1 \rho Q \tag{2-18}$$

where a_1 is an empirical constant, ρ the fluid density, and Q the turbulence kinetic energy, defined by Bradshaw as $Q = \overline{(u_i' u_i')}$. By converting the turbulence kinetic energy into a shear stress equation, a hyperbolic set of equations was developed to account for the mean momentum, continuity, and shear stress. Numerical integrations of these equations were obtained by using the method of characteristics. The resulting equation for shear stress was written as a function of three empirical parameters, a_1, L_Q, and G, which depend on the shape of the shear stress profile and are defined as

$$\left.\begin{aligned} a_1 &= \tau/\rho Q \\ L_Q &= (\tau/\rho)^{3/2}/D_Q \\ G &= \left(\frac{\overline{p'w'}}{\rho} + Qw'\right)\Big/\left(\frac{\tau_m}{\rho}\right)^{\frac{1}{2}} \frac{\tau}{\rho} \end{aligned}\right\} \tag{2-19}$$

where D_Q is given as

$$D_Q = \nu\left(\frac{\partial U_i}{\partial X_j}\frac{\partial U_i}{\partial X_j}\right) \tag{2-20}$$

Based upon the measurements of Klebanoff (65), a_1 was found to be equal to 0.15. The relations for L_Q and G were given as empirical functions related to Q and τ_m, the maximum shear stress in the profile. Evaluation of this model in analyzing measurements of the turbulent structure in

equilibrium boundary layers was later discussed by Bradshaw (66) to account for the influence of pressure gradients.

Using the linear relation suggested by Nevzglajdov (64) and the initial work of Bradshaw, et al (63), Harsha and Lee (67) correlated some existing experimental data in jets and wakes and concluded that a reasonable degree of similarity existed between free turbulence and fully developed boundary layers for the constant a_1. Byrne (68) investigated the influence of mass injection and pressure gradient on two-dimensional turbulent boundary layers using the turbulence kinetic energy equation as one of the governing equations of motion with the linear model of Nevzglajdov (64). The dissipation term in the turbulence kinetic energy equation was defined by

$$D_Q = a_2 \rho Q^{3/2} / \delta \tag{2-21}$$

where

$$\left.\begin{aligned} a_2 &= 1.8 && X_3 > X_{3\tau m} \\ a_2 &= 1.8 \frac{X_{3\tau m}}{X_3} && X_3 < X_{3\tau m} \end{aligned}\right\} \tag{2-22}$$

and $X_{3\tau m}$ is the location of the maximum shear point. The value of 1.8 was determined by numerical experiments in conjunction with the earlier work of Lee and Harsha (69). A similar study was made by Lee, et al (70) using turbulence energy to study the transfer of heat, mass, and momentum in an incompressible self preserved turbulent boundary layer

along a flat plate for both accelerating and decelerating flows with suction and blowing. Comparison of results with atmospheric wind tunnel data of Arya (25) and Malhotra (28) indicated that the prospects of using the turbulence model of Nevzglajdov (64) in analyzing atmospheric boundary layers were good.

By relating the turbulent shear stress to the local value of turbulence kinetic energy, Glushko (59) simultaneously solved the continuity, momentum, and turbulence kinetic energy equations, using an expression containing an empirical function related to the local value of turbulence kinetic energy, Q, and a universal function related to distance from the wall. The production and dissipation of turbulence kinetic energy were defined as a function of $Q^{\frac{1}{2}}$, characteristic mixing length, and μ, the dynamic viscosity of the fluid. The total diffusion of turbulence kinetic energy was assumed to be related to the gradient of turbulence kinetic energy, based on the turbulence measurements of Klebanoff (65).

b. Two-equation Models

Recent interest has developed in the use of turbulence models in which one or more turbulence quantities are found from the solution of two or more transport equations. Jones and Launder (71) proposed a two-equation model based on the simultaneous solution of the turbulence kinetic energy and a turbulence dissipation rate. The equation for turbulence kinetic energy was written as

$$\rho U_j \frac{\partial Q}{\partial X_j} = \frac{\partial}{\partial X_3}\{(\mu + \frac{\varepsilon_m}{\sigma_k})\frac{\partial Q}{X_3}\} + \varepsilon_m(\frac{\partial U_1}{\partial X_3})^2 - \rho D_Q - 2\mu(\frac{\partial Q}{\partial X_3})^{\frac{1}{2}} \quad (2\text{-}23)$$

and the equation for turbulence dissipation rate as

$$\rho U_j \frac{\partial D_Q}{\partial X_j} = \frac{\partial}{\partial X_3}\{(\mu + \frac{\varepsilon_m}{\sigma_{D_Q}})\frac{\partial D_Q}{\partial X_3}\} + C_{1Q}\frac{D_Q}{Q}\varepsilon_m(\frac{\partial U_1}{\partial X_3})^2 - \frac{C_2\rho D_Q^2}{Q}$$

$$+ 2\frac{\mu\varepsilon_m}{\rho}(\frac{\partial^2 U_1}{\partial X_3^2})^2 \quad (2\text{-}24)$$

where D_Q is the dissipation of turbulence kinetic energy for both equations, $\sigma_k = 1.0$, $\sigma_{D_Q} = 1.3$, $C_1 = 1.45$, $C_2 = 2.0$, and ε_m the eddy coefficient of momentum, given as

$$\varepsilon_m = C_\mu \rho Q^2 / D_Q \quad (2\text{-}25)$$

where

$$C_\mu = .09 \exp.\{-2.5/(1+R_t/50)\} \quad (2\text{-}26)$$

with R_t being the turbulent Reynolds number. The dissipation equation is seen to parallel the turbulence kinetic energy equation. Each equation assumes that diffusional transport proceeds at a rate proportional to the product of the turbulent exchange coefficient and the gradient of the property in question; the generation and decay terms are likewise similar.

Gibson and Spalding (72) formulated a two equation model for turbulence kinetic energy introducing a partial differential equation for F, a variable having dimensions

of frequency squared, along with an equation for turbulence kinetic energy, Q. The equations for Q and F are written as follows:

$$\rho U_j \frac{\partial Q}{\partial X_j} = \frac{\partial}{\partial X_3}\left(\frac{K_m}{\sigma_k}\frac{\partial Q}{\partial X_3}\right) + \varepsilon_m\left(\frac{\partial U_1}{\partial X_3}\right)^2 - C_D \rho Q F^{\frac{1}{2}} \qquad (2\text{-}27)$$

$$\rho U_j \frac{\partial F}{\partial X_j} = \frac{\partial}{\partial X_3}\left(\frac{K_m}{\sigma_F}\frac{\partial F}{\partial X_3}\right) + C_1 \varepsilon_m \left(\frac{\partial^2 U_1}{\partial X_3^2}\right)^2 - C_2 \rho F^{\frac{3}{2}}$$

$$+ C_3 \rho F^{\frac{1}{2}}\left(\frac{\partial U_1}{\partial X_3}\right)^2 \qquad (2\text{-}28)$$

where C_D, C_1, C_2, and C_3 are empirical constants. The exchange coefficient of momentum, K_m, is given as

$$K_m = \mu + \varepsilon_m$$

$$\varepsilon_m = C_\mu \rho Q F^{-\frac{1}{2}} \qquad (2\text{-}29)$$

where ε_m is the eddy coefficient of momentum and C_μ a constant. The dissipation exchange coefficient is related to the momentum exchange coefficient K_m through the empirical parameters σ_k and σ_F. The constants in the turbulence model are obtained empirically.

Launder, et al (73) analyzed the performance of three distinct classes of turbulence models: 1) eddy coefficient models - length scale found from a partial differential equation of transport, 2) eddy coefficient models - length scale found by algebraic formulae, and 3) shear stress models in which the shear stress is the dependent variable of a partial differential conservation equation. Two

models were discussed within each class and a comparison made with twenty three different test cases and experimental data. The turbulence models which determine the length scale of turbulence from the transport equation for energy dissipation rate were found to give more correct predictions over a wider range of flow conditions than models using algebraic relations for the length scale.

c. Second Order Closure Model

An invariant second order closure model was developed by Donaldson (74) in an effort to numerically predict the dispersion of pollutants in a thermally stratified atmosphere. While mathematically more accurate than the previously discussed models, the second order closure method is considerably more complicated, and requires a number of empirical constants.

Following the technique used by Reynolds (75), the equations for the properties of a turbulent atmospheric shear layer are expressed as the sum of mean values of the variables plus fluctuating components corresponding to these mean values. As an example, the equation of motion, after time averaging, becomes

$$\rho\frac{\partial\bar{U}_i}{\partial t} + \rho\bar{U}_j\frac{\partial\bar{U}_i}{\partial X_j} = -\frac{\partial\bar{P}}{\partial X_j} + \frac{\rho g\bar{T}}{T_m} + \frac{\partial}{\partial X_j}\left(\mu\frac{\partial\bar{U}_i}{\partial X_j} - \rho\overline{u_i'u_j'}\right) \qquad (2\text{-}30)$$

where the overbar indicates the average value of that quantity while the prime denotes instantaneous fluctuation. The Reynolds stress term is introduced from the turbulent motion as $\rho\overline{u_i'u_j'}$. An equation for the velocity fluctuation can be

obtained by subtracting equation (2-30) from the unaveraged momentum equation. Multiplication of the resulting equation by u_k' and time averaging produces the equation

$$\rho\overline{u_k'\frac{\partial u_i'}{\partial t}} + \rho(\bar{U}_j\overline{u_k'\frac{\partial u_i'}{\partial X_j}} + \overline{u_j'u_k'}\frac{\partial \bar{U}_i}{\partial X_j} + \overline{u_k'u_j'\frac{\partial u_i'}{\partial X_j}}) = -\overline{u_k'\frac{\partial p'}{\partial X_i}}$$

$$+ \frac{\rho g_i\overline{u_k't'}}{T_m} + \mu\overline{u_k'\frac{\partial^2 u_i'}{\partial X_j\partial X_j}} \qquad (2\text{-}31)$$

Interchanging i and k in equation (2-31) and adding the resulting equation to (2-31) gives the equation for the Reynolds stress correlation

$$\rho\frac{\partial\overline{u_i'u_k'}}{\partial t} + \rho U_j\frac{\partial\overline{u_i'u_k'}}{\partial X_j} = -\rho\overline{u_i'u_j'}\frac{\partial U_k}{\partial X_j} - \rho\overline{u_k'u_j'}\frac{\partial U_i}{\partial X_j} - \rho\frac{\partial}{\partial X_j}(\overline{u_i'u_j'u_k'})$$

$$-\frac{\partial}{\partial X_i}(\overline{p'u_k'}) - \frac{\partial}{\partial X_k}(\overline{p'u_i'}) + \overline{p'(\frac{\partial u_i'}{\partial X_k} + \frac{\partial u_k'}{\partial X_i})} + \frac{\rho}{T}(g_i\overline{u_k't'}$$

$$+ g_k\overline{u_i't'}) + \mu(\frac{\partial^2\overline{u_i'u_k'}}{\partial X_j\partial X_j} - 2\frac{\partial\overline{u_i'}\partial\overline{u_k'}}{\partial X_j\partial X_j}) \qquad (2\text{-}32)$$

where the overbars have been removed from the mean quantities for simplicity. If the same scheme is applied to the energy equation, an equation for the heat flux term, $\rho\overline{u_i't'}$, can be obtained similar to equation (2-32). Since $\overline{t'^2}$ arises in the transformed energy equation, an equation for this second order correlation can be obtained by multiplying the equation for the temperature fluctuation, t', with 2t', resulting in an equation similar to equation (2-32). Application of the Reynolds scheme to the concentration equation likewise produces equations for $c'u_i'$ and $\overline{c'^2}$ analogous to

those for shear and energy. An additional term $\rho\overline{c't'}$ appears in the concentration flux equation which represents the production of concentration transport in the direction of gravitational acceleration due to fluctuations in temperature. Closure of the set equations is completed by deriving an equation for $\rho\overline{c't'}$ in the same manner.

The complete set of equations, based upon the second order closure model, is given by Donaldson (74) as: 1) conservation of mass, 2) conservation of momentum, 3) conservation of energy, 4) conservation of species (concentration), 5) equation for $\rho\overline{u_i'u_k'}$, 6) equation for $\rho\overline{u_k't'}$, 7) equation for $\overline{t'^2}$, 8) equation for $\rho\overline{u_k'c'}$, 9) equation for $\rho\overline{c't'}$, and 10) an equation for $\rho\overline{c'^2}$.

The triple correlation terms appearing in the turbulence flux equations were reduced to second order correlations by introducing a scalar length, Λ_α, and a scalar velocity, q given as

$$q_s = \sqrt{u_m'u_m'} \qquad (2\text{-}33)$$

As an example, the triple correlation appearing in equation (2-32), $\overline{u_i'u_j'u_k'}$, is redefined as

$$\overline{u_i'u_j'u_k'} = -\Lambda_\alpha q_s\left\{\frac{\partial}{\partial X_i}(\overline{u_j'u_k'}) + \frac{\partial}{\partial X_j}(\overline{u_i'u_k'}) + \frac{\partial}{\partial X_k}(\overline{u_i'u_j'})\right\} \qquad (2\text{-}34)$$

where the minus sign insures diffusion from regions of high turbulent intensity to regions of low intensity. The triple correlation, $\overline{u_j'u_k't'}$, occurring in the equation for $\rho\overline{u_k't'}$, is modified to

$$\overline{u_j' u_k' t'} = - \Lambda_\alpha q_s \{ \frac{\partial}{\partial X_j} (\overline{u_k' t'}) + \frac{\partial}{\partial X_k} (\overline{u_j' t'}) \} \qquad (2\text{-}35)$$

By analogy with equation (2-34), the remaining triple correlations are redefined as a function of length scale, scalar velocity, and double correlation gradients.

It is apparent that in order to perform the numerical calculations involving the second order correlations, it is necessary to determine the various length scales, Λ_α, corresponding to each particular double correlation equation. Relations for the length scales were initially formulated by Donaldson (74) in analyzing boundary layer flows by assuming $\Lambda_\alpha = C_\alpha \delta$, where C_α is an empirical constant and δ is the boundary layer thickness. An equation for Λ_α, similar to those for the second order correlation terms, was suggested by Donaldson (74) in an effort to more realistically account for the variation of Λ_α. This concept, however, was not discussed in detail.

Numerical results proved to be quite realistic and provided some interesting results regarding the contribution of the double correlation flux terms appearing in the governing equation to the main motion of the flow. However, comparison with existing data does not show the second order closure method in its present state to be significantly better than some existing eddy transport models; this could perhaps be due to the simplication procedure in describing the length scales. Similar application of the second order closure

method was discussed by Weinstein (76) in analyzing fog formation. Unfortunately, the model was not compared with any experimental data and the numerical predictions not carried out in detail.

d. General Circulation Models

Clearly two-dimensional simulation of turbulence is not applicable to the three-dimensional nature of the atmosphere. While the use of two-dimensional concepts in describing the physical nature of turbulence has produced fairly accurate approximations with experiments, the two-dimensional descriptions are valid only under certain restrictions.

A number of investigations have been made in an effort to numerically simulate three-dimensional flow while retaining two-dimensional modeling techniques, using an exchange coefficient hypothesis. A review of these methods will not be given here.

A general numerical technique was developed by Patankar and Spalding (77) for the calculation of transport processes in three-dimensional parabolic flows. Because of the basic assumptions regarding boundary layer flow, the three-dimensional procedure was related principally to the two-dimensional work developed earlier by Patankar and Spalding (58) and Gosman, et al (62). Although dealing specifically with general flow equations, inclusion of the turbulence terms into the general scheme along with a closure model for the second order turbulent flux terms was not investigated.

A considerable amount of research has been undertaken at

the National Center for Atmospheric Research, NCAR, dealing with three-dimensional simulation of turbulence in an effort to predict global circulation phenomena. A numerical study of three-dimensional turbulent channel flow was made by Deardorff (78), in which the time dependent equations of motion were closed by using a subgrid scale averaging technique, SGS , to account for the exchange coefficient of momentum, K_m. This method used an averaging operator which was applied to the governing equations in order to filter out subgrid scale motion. The exchange coefficient, K_m, was related to a length interval, Δ, as

$$K_m = (\zeta\Delta)^2\{\frac{\partial U_i}{\partial X_j}(\frac{\partial U_i}{\partial X_j} + \frac{\partial U_j}{\partial X_i})\}^{\frac{1}{2}}\rho \qquad (2\text{-}36)$$

where ζ is equal to 0.10. Although clearly analogous to a mixing length hypothesis, application of this meteorological approach to three-dimensional plane Poiseuille flow proved to be successful in predicting general shapes and detailed flow patterns, but did not compare favorably with measured mean velocity profiles. Profiles were obtained for turbulence intensities and Reynolds shear stress along with energy balances for the production, diffusion, and dissipation terms appearing in the turbulence kinetic energy equation. Results clearly showed the cascading nature of turbulence, particularly the transport of momentum towards the boundaries.

Recent work by Kasahara and Washington (79) has lead to numerical simulation of the atmosphere to include the

effects of orography, radiation, and surface temperature. The earth's surface was divided into three regions: oceanic regions, snow and ice free continents, and snow-ice regions where surface temperature is at or below the freezing point. The atmosphere was divided into 6 increment layers, each layer being 3 km in height. Exchange coefficients were solved by the SGS method to account for the horizontal diffusion of momentum, water vapor, and heat. Unfortunately, the surface boundary layer level was given as boundary conditions with minor alterations due to the presence of mountains. Complimentary work by Deardorff (80) in parameterizing the surface boundary layer for use in this general circulation model, has been recently developed in an effort to include boundary fluxes of momentum, heat and stability conditions. Such large scale modeling of the earth's general circulation shows promising results in numerically forecasting weather and climate conditions. A comprehensive review of meteorological efforts to account for the closure of the governing equations of turbulence is given by Lilly (81).

While investigations into the three-dimensional character of atmosphere turbulence are still rather primitive, exhaustive studies are currently being made concerning the nature of turbulence and the formulation of more accurate theories pertaining to three-dimensional modeling. For three-dimensional atmospheric turbulence, present-day computer technology does not permit a straightforward mathematical analysis to be made as yet.

3. Statistical Theory

The exchange coefficient hypothesis and turbulence kinetic energy hypothesis are based upon an Eulerian description of the fluid motion, i.e., the flow is viewed passing a fixed point in space such that a variable, say U, can be described by $U(x_i t)$, with x_i being the spatial coordinates. Transport phenomena, however, is difficult to interpret accurately in Eulerian terms. A more convenient method is to use the Lagrangian description of the flow, i.e., following the motion of fixed "fluid particles" beginning at some specified time rather than the velocities of the fluid at some specified point, x_i. Following the analysis presented by Monin and Yaglom (35), a "fluid particle" is regarded as an identifiable volume of fluid having dimensions which are very large compared to the average distance between molecules, but with linear dimensions so small that the velocity and pressure inside the volume are essentially constant. This allows the volume to be governed by the equations of fluid mechanics. The Lagrangian description relates to the motions of these individual fluid elements which produce, in sum, the entire flow phenomena. While physically more natural than the Eulerian description, the use of Lagrangian form turns out to be much more awkward analytically. Although the use of viscous Lagrangian equations in turbulent theory is still a matter for the future, some progress has been made in formulating expressions for the mechanism of turbulent diffusion.

The Lagrangian characteristics are described by Monin and Yaglom (35) for an incompressible fluid as $X_i(x_i,t)$ which describes, for any time t, the coordinate X_i of all the "fluid particles" given by the values of some parameter x_i. The velocity corresponding to one of these point elements can be related to the Eulerian velocity as

$$u_i\{X_i(x_i,t),t\} = \frac{\partial X_i(x_i,t)}{\partial t} \qquad (2\text{-}37)$$

Transformation from Eulerian to Lagrangian equations requires the replacement of (x_i,t) variables by (X_i,t) and $u_i(X_i,t)$ to $X_i(x_i,t)$. Likewise, $x_i = X_i(x_i,t)$, which describe all possible trajectories of the fluid particles at all possible points x_i. This allows the "fluid particles", actually mathematical points flowing with the fluid, to describe the fluid motion by a family of trajectories, each differing by x_i. The incompressible Navier-Stokes equation is transformed by Monin and Yaglom (32) from

$$\frac{\partial u_i}{\partial t} + u_j\frac{\partial u_i}{\partial X_j} = -\frac{1}{\rho}\frac{\partial P}{\partial X_j} + \frac{\partial}{\partial X_j}(\nu\frac{\partial u_i}{\partial X_j}) \qquad (2\text{-}38)$$

to the equation

$$\frac{\partial^2 X_i}{\partial t^2} = -\frac{1}{\rho}(X_j,X_k,P) + \nu\{X_2,X_3,(X_2,X_3,\frac{\partial X_i}{\partial t})\}$$
$$+ \{X_3,X_1,(X_3,X_1,\frac{\partial X_i}{\partial t})\} + \{X_1,X_2,(X_1,X_2,\frac{\partial X_i}{\partial t})\} \qquad (2\text{-}39)$$

with the unknown variables being $X_i(x_i,t)$ and $P(x_i,t)$, $i = 1, 2, 3$.

The statistical description of turbulence arises from

the Lagrangian variables being described by a probability distribution, such that

$$X_i(x_i,t) = x_i + \int_0^t u_i\{X_i(x_i,T),T\}dT \qquad (2\text{-}40)$$

Subsequent sets of variables produce joint probability distributions, giving rise to Lagrangian autocorrelations, and space-time correlation tensors, i.e., see Lumley and Panofsky (8), which describe the variances of the "fluid particles" as a function of time. Integration of the spatial correlation coefficient gives the scale of turbulence, or characteristic size of the eddies. For homogeneous turbulence the variances are equal, reducing the equations to simple mathematical relations.

Present-day statistical theories of turbulent diffusion in the atmosphere are based primarily on the works of Taylor (82), Frenkiel (83) and Sutton (11), all of whom assume homogeneous and isotropic conditions for the statistical properties of turbulence. Frenkiel (83) and Sutton (10) similarly assumed that mean concentrations within a diffusion cloud were distributed according to a three-dimensional Gaussian law from an instantaneous point source. Unfortunately, application of this particular approach to boundary layer flow phenomena proved to be quite difficult.

Gifford (84) applied the concepts of Lagrangian similarity with the Monin-Obukhov theory in investigating turbulent diffusion from a point source in a thermally stratified boundary layer at ground level. Prediction of a centerline

of marked particles released from a fixed source, and axial concentration values using field observations obtained during Project Prairie Grass, showed successful agreement between theory and field data. Klug (85) points out, however, that the Lagrangian theory implies that the vertical and lateral spreads of concentration are determined by the same feature, irrespective of stratification, while experimental data show that the variation of point source concentration does not occur with change in stability. Batchelor (86), using Lagrangian similarity, assumed that the velocity of a marked particle was dependent only upon u* and time after release from ground level, and successfully obtained ground concentrations for a fixed source in a neutral atmosphere.

Due to the absence of reliable methods for measuring Lagrangian statistical characteristics of turbulence, particularly the correlation coefficients, along with the restriction of the theory to homogeneous turbulence, makes this theory difficult to apply to transport phenomena in the atmosphere at the present time. Further mathematical refinement of this approach, coupled with more sophisticated experimental methods, could eventually lead to a complete understanding of the basic mechanisms of turbulent transport.

III. THEORETICAL ANALYSIS

The basic reason for seeking analytical solutions to turbulence problems is to provide insight into the mechanisms of turbulence with mathematical and economic conciseness. Unfortunately, analytical treatment of the basic field equations is complicated by the irregularity of motion due to the cascading nature of turbulence. However, certain conclusions can be drawn from previous efforts in attempting to describe turbulent processes in the atmosphere.

A large amount of experimental data exists on atmospheric diffusion from both field and wind tunnel measurements. Due to the irregularity of the field data, meteorological wind tunnel modeling has provided adequate information pertinent to analytically investigating transport phenomena in an atmospheric boundary layer. A considerable degree of similarity has been found to exist between the atmospheric surface layer and aerodynamic flow over a flat plate.

Because of this similarity to turbulent flow over a flat plate, a number of mathematical models have been developed; most have been based upon a Prandtl mixing length hypothesis. Nearly all meteorological methods assumed that exchange coefficients were synonymous with the momentum exchange coefficient and a function of friction velocity, von Karman constant, and either velocity or temperature gradient. Modification of these models was necessary near the

upper limit of the atmospheric boundary layer to realistically account for the variation of the exchange coefficients. The effect of advection on solution to atmospheric flow phenomena was usually neglected.

A parabolic solution of the governing equations is simple and easily adaptable in dealing with various boundary layer problems. The numerical finite difference method of Patankar and Spalding (58) has been shown to be very effective in accurately predicting various flow phenomena with a minimum of computational effort; specifically attractive was the ability of the boundary layer height to be allowed to develop and act as the upper boundary condition for the numerical model. The method was also found to be easily modified to accept any number of dependent variables.

The influence of buoyancy in a thermally stratified atmosphere is significant in atmospheric boundary layers, but does not become important in most engineering situations. Meaningful investigations of transport phenomena in the atmospheric boundary layer can only be accomplished by realistically modeling the actual conditions.

Simultaneous solution of turbulence kinetic energy with the governing equations of motion appears to be a more sensible approach than mixing length concepts for analyzing turbulent exchange processes. Based upon the Kolmogorov hypothesis of a turbulence kinetic energy-shear stress correlation, various phenomenological models have been developed which appear to effectively close the governing

equations and adequately account for the history of the flow.

A. Approach

Much of the analysis to be presented here has been previously developed. Modification of existing theories was kept to a minimum in order to maintain the flexibility of the technique for extension to a wide range of flow problems. Basically the method must: (i) maintain generality in dealing with a wide range of problems, (ii) use a minimum of empiricism, (iii) be capable of long term objectivity, i.e., not easily outdated, (iv) retain its ability to be easily modified for any specific hypothesis, and (v) be computationally inexpensive.

The computational scheme developed by Patankar and Spalding (58) has been chosen along with the Nevzglajdov (64) model for the shear stress as modified by Lee and Harsha (69). The turbulence kinetic energy is introduced into the set of governing equations and simultaneously solved with the momentum, continuity, and concentration. Under the assumption that no reverse flow exists, the general elliptic equations are truncated to parabolic form. The Patankar-Spalding method allows a set of equations to be easily introduced into the program and solved with a high degree of computational efficiency.

Boundary layer flow in this work will be considered as any flow in which there exists a predominant direction of flow; shear stresses, heat fluxes, and diffusional fluxes

are caused only by gradients in the direction normal to the direction of flow; and upstream conditions can influence downstream flow properties but not vice versa. Modification of these generalized conditions for atmospheric boundary layer flows requires several minor alterations to the governing set of equations; however, many of the assumptions used by Byrne (68) in analyzing non-equilibrium boundary layers have been used.

B. Basic Equations

The conservation equations for two dimensional, steady turbulent boundary layers are: continuity, momentum, energy, turbulence kinetic energy, and concentration or species. The derivation of these equations will not be given here but can be found in detail in Byrne (68) and Patankar (41).

The coordinate system used throughout this study employs the orthogonal coordinates x and z, x being the distance along which the boundary layer is developing and z the distance normal to the direction of flow. Figure 1 shows the coordinate system which will be used. The symbols used throughout this chapter are defined in the Nomenclature.

The equation of continuity expresses the fact that for a unit volume there exists a balance between masses entering and the masses leaving per unit time and change in density. Steady state turbulent flow leads to the equation for continuity, given by Schlichting (87), as

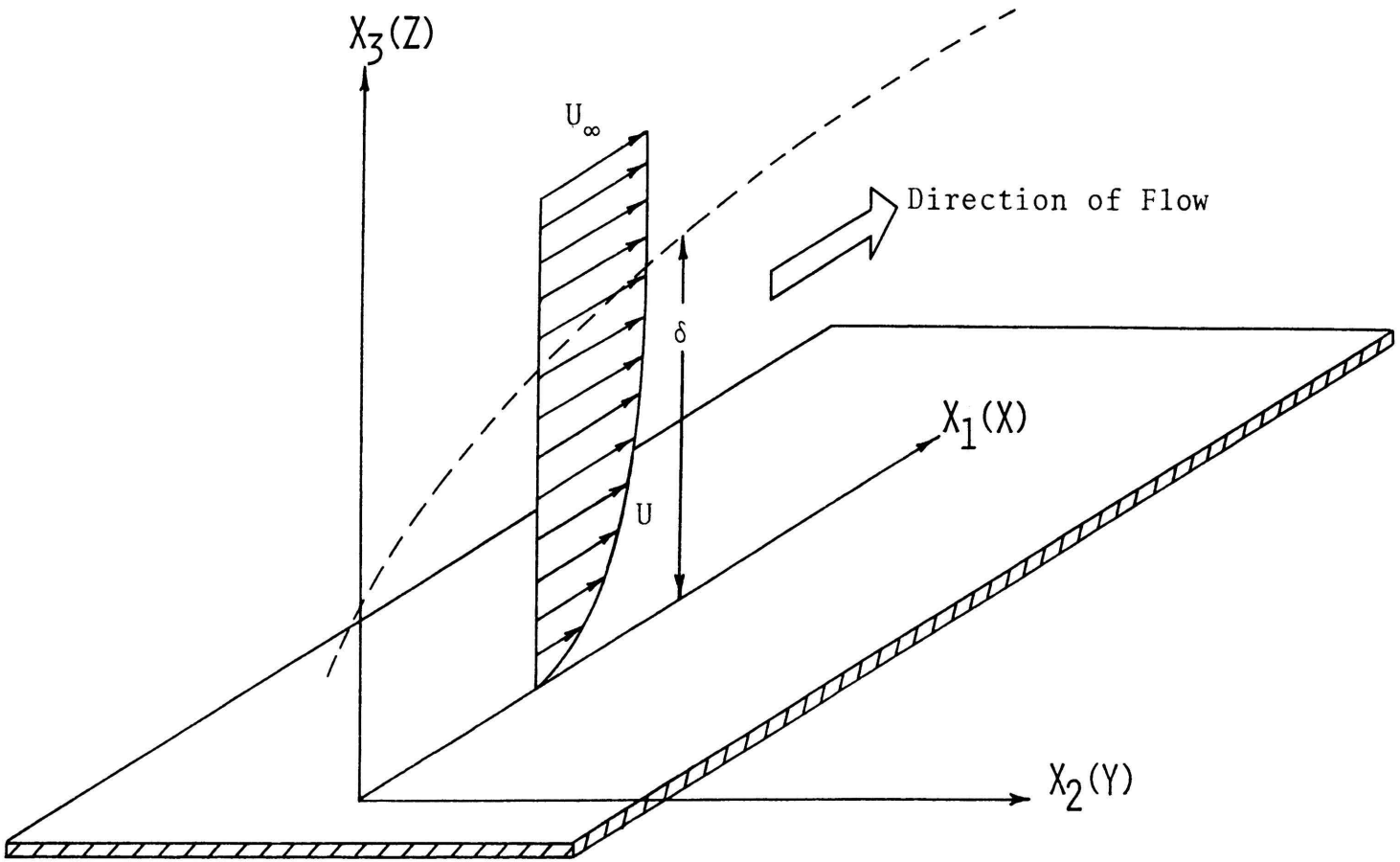

Figure 1. The Atmospheric Boundary Layer

$$\frac{\partial}{\partial X_i}(\rho U_i) = 0 \qquad (3\text{-}1)$$

The momentum equation is obtained from the Navier-Stokes equations, using the method of Reynolds (75) in which instantaneous velocities are divided into mean and fluctuating components. If time averages are taken, the momentum equation can be written as

$$\rho U_j \frac{\partial U_i}{\partial X_j} = \frac{\partial}{\partial X_j}(\mu \frac{\partial U_i}{\partial X_j} - \rho \overline{u_i' u_j'}) - \frac{\partial P}{\partial X_i} + F_i \qquad (3\text{-}2)$$

where $\rho \overline{u_i' u_j'}$ is the turbulent contribution to the shear stress, known as the Reynolds stress term.

The conservation of species n, or concentration equation, is normally written in the form

$$\rho U_j \frac{\partial C^n}{\partial X_j} = \frac{\partial}{\partial X_j}(\mu \frac{\partial C^n}{\partial X_j} - \rho \overline{u_i' c'}) + S^n \qquad (3\text{-}3)$$

where S^n is the rate of generation of the chemical species n. The concentration equation is written in terms of this generalized species equation since a fluid may consist of more than one constituent. The source term S^n must be correctly defined for each particular concentration, i.e., when dealing specifically with the atmosphere, a species equation for water vapor content contains a latent heat of vaporization or condensation source term while an equation for liquid water content contains an additional term to account for the terminal fallout of water drops (51). Pollutant diffusion has been assumed to be passive in this study ($S^n = 0$); a test case involving the formation of fog,

using water vapor content and liquid water content, is assumed to be active since the release of latent heat influences the flow field.

Recent use of the turbulence kinetic energy as a governing equation by several investigators has lead to an understanding of its development and its significance in effectively describing the nature of turbulent flow. Current state of the art seems directed toward tying the turbulence kinetic energy equation to a suitable empirical model for the eddy coefficient of momentum. While in most engineering situations the effect of buoyancy is normally neglected in the turbulence kinetic energy equation, the effect of buoyancy in atmospheric boundary layers must be included.

The atmosphere is taken as being a perfect gas of constant composition. Using the hypothesis of Arya (25) and Plate (19), the density will be regarded as being non-uniform but with the fluid being incompressible, i.e., changes in density are due to changes in temperature and not due to change in pressure. The variations in ρ can be neglected if the temperature gradients are small.

The dynamic behavior of the flow is described by means of the equations of motion for U_i and U_j. Subtracting the average values from these equations produces two equations for the fluctuating components, u_i' and u_j'. Multiplying the equation for u_i' by u_j' and the equation for u_j' by u_i', adding the two equations, and time averaging, produces an equation

for $\overline{u_i' u_j'}$. A contraction of this equation produces the turbulence kinetic energy, Q, normally defined as $Q = \frac{1}{2}(\overline{u_i' u_i'})$.

The form of the turbulence kinetic energy most often found in the literature is written as

$$U_i \frac{\partial Q}{\partial X_i} = -\frac{\partial}{\partial X_i} \overline{u_i'(\frac{p'}{\rho} + Q)} - \overline{u_i' u_j'} \frac{\partial U_j}{\partial X_i} + \nu \frac{\partial}{\partial X_i} \overline{u_j'(\frac{\partial u_i'}{\partial X_j} + \frac{\partial u_j'}{\partial X_i})}$$

$$- \nu \overline{(\frac{\partial u_i'}{\partial X_j} + \frac{\partial u_j'}{\partial X_i}) \frac{\partial u_j'}{\partial X_i}} + \frac{\overline{u_j' t'} g}{T} \delta_{j3} \qquad (3\text{-}4)$$

in which the term $(g/T)\overline{u_j' t'}\delta_{j3}$ reflects the effect of buoyancy, obtained from the body force source term, F_i, existing only in the vertical direction. Buoyancy is normally referred to as a production term in which fluctuating components of velocity and heat draw energy from the mean motion. Consequently, if the heat flux is upward, this term serves as a source of energy while if the flux is downward, the term acts as an energy sink.

For a medium with a non-uniform temperature distribution, turbulent mixing causes temperature fluctuations to occur, in addition to velocity fluctuations. As a consequence, the presence of these velocity and temperature fluctuations generate supplementary heat flux terms analogous to the Reynolds stresses. The energy equation is expressed here in terms of the static enthalpy, where $dh = c_p dT$. The form most commonly found is given as

$$\rho U_j \frac{\partial h}{\partial X_j} = \frac{\partial}{\partial X_j}(\frac{\alpha}{C_p} \frac{\partial h}{\partial X_j} - \rho \overline{u_i' h'}) + \overline{\mu \Phi} + U_j \frac{\partial P}{\partial X_j} + R \qquad (3\text{-}5)$$

where $\overline{\mu\Phi}$ represents the instantaneous dissipation of kinetic energy into heat, usually expressed as

$$\overline{\mu\Phi} = (\mu\frac{\partial U_i}{\partial X_j} - \rho\overline{u_i' u_j'})\frac{\partial U_i}{\partial X_j} \tag{3-6}$$

and R the heat added instantaneously by radiation. The potential temperature is normally used when describing temperature distribution throughout the atmosphere. This is related to the static temperature as

$$\frac{\partial \theta}{\partial X_3} \simeq \frac{\partial T}{\partial X_3} + \frac{g}{c_p} \tag{3-7}$$

where g/c_p is defined as the adiabatic lapse rate. Since excessive heights were not considered in analyzing wind tunnel simulation studies, the potential temperature gradient was represented by

$$\frac{\partial \theta}{\partial X_3} \simeq \frac{\partial T}{\partial X_3} \simeq \frac{1}{c_p}\frac{\partial h}{\partial X_3} \tag{3-8}$$

Equation (3-7) was used by Pepper and Lee (88) in numerically modeling the formation of advection fog. In this case, the adiabatic lapse rate was important since minute changes in temperature could produce significant variations in moisture content.

C. Closure

Because of the addition of the fluctuating terms, the governing equations in their present form are not amenable to solution. In an effort to obtain solutions to these fluctuating terms, Boussinesq (33) introduced the concept of an eddy coefficient. Specifically, this involved the

assumption that the turbulence flux terms could be directly related to corresponding mean gradients. Although physically somewhat inexact, solutions for turbulent flow at least become possible.

Dealing with the momentum equation, the advantage of defining an eddy coefficient for momentum, ε_m, is that if ε_m can be numerically determined, this apparent form of shear stress can be substituted into the momentum equation, reducing the number of dependent variables. This was performed by Boussinesq (33) in which

$$-\rho\overline{u_i' u_j'} = \varepsilon_m D_{ij} = \varepsilon_m \left(\frac{\partial U_i}{\partial X_j} + \frac{\partial U_j}{\partial X_i}\right) \qquad (3\text{-}9)$$

where D_{ij} is known as the deformation tensor of the fluid due to shear stress. Although $-\rho\overline{u_i' u_j'}$ is not a stress term but an inertia term, coming from the convective part of the momentum equation, it is normally referred to as a stress component because it enters into the equation in the same way as the laminar stress term.

A nearly complete survey of existing empirical models for the eddy coefficient of momentum was made by Harsha (89) for analyzing engineering problems. Similar investigations by Harsha and Lee (67) using data for two-dimensional jets and wakes showed that a linear correlation existed between the turbulent shear stress and the turbulence kinetic energy, as was previously suggested by Nevzglajdov (64), such that

$$-\rho\overline{u_i' u_j'} = a_1 \rho Q \qquad (3\text{-}10)$$

where $a_1 = 0.3$.

Based upon this hypothesis, available meteorological wind tunnel data and the data of Klebanoff (65) for flow over a flat plate were used to ascertain the validity of using a linear relation between the shear stress and the turbulence kinetic energy. The models to be discussed are the Prandtl mixing length, the Kolmogorov model, and the Nevzglajdov relationship. The first model is well known and involves only a mixing length concept; the other two deal specifically with the kinetic energy-shear stress relationship.

1. Prandtl Mixing Length Model

The Prandtl mixing length model is given by the relation

$$- \rho\overline{u_1' u_3'} = \rho \ell^2 \left|\frac{\partial U_1}{\partial X_3}\right| \frac{\partial U_1}{\partial X_3} \qquad (3\text{-}11)$$

where ℓ has the dimension of length and is determined experimentally for each particular case. The experimental data of Schon and Mery (20) and Klebanoff (65) is shown in Figure 2 with $\tau/\rho U_\infty^2$ as the ordinate and the nondimensional gradients $\{\partial(U_1/U_\infty)/\partial(X_3/\delta)\} \cdot |\partial(U_1/U_\infty)/\partial(X_3/\delta)|$ as the abscissa, where U_∞ is the free stream velocity and δ is the boundary layer thickness. The Prandtl mixing length can best be represented by letting $\ell = .16\delta$. The disarray of data points indicates that the mixing length value requires modification for each particular problem.

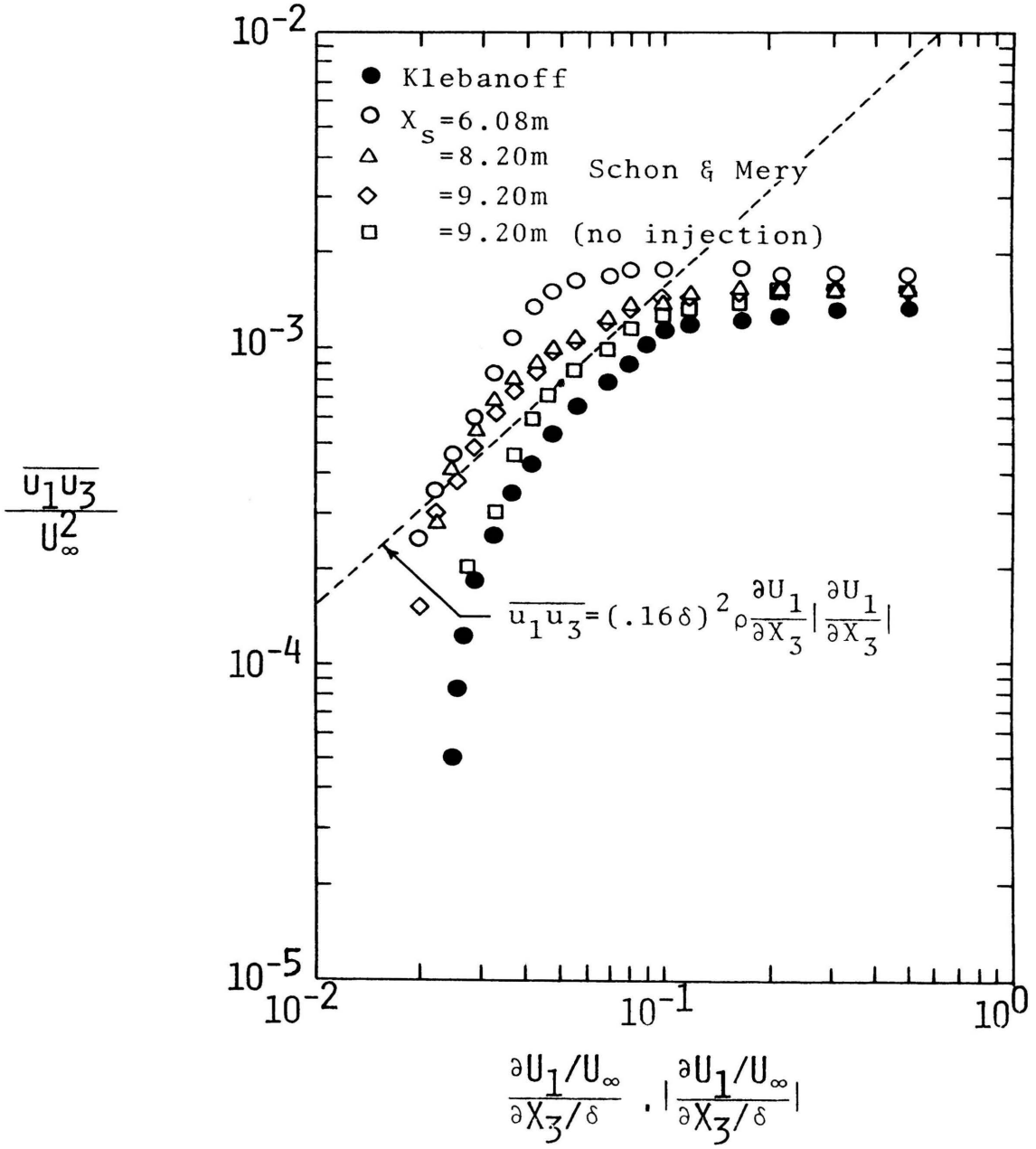

Figure 2. The Prandtl Mixing Length Model

2. Kolmogorov Model

Based upon the suggestion made by Kolmogorov (64), the turbulent shear stress can be related to the turbulence kinetic energy by the relation

$$-\rho\overline{u_i' u_j'} = \ell_k Q^{\frac{1}{2}} \frac{\partial U_1}{\partial X_3} \tag{3-12}$$

where Q is the turbulence kinetic energy defined as

$$Q = \tfrac{1}{2}\overline{(u_i' u_i')} \tag{3-13}$$

and ℓ_k is similar to the Prandtl mixing length. The log-log plot of the non-dimensional turbulent shear stress versus $(Q^{\frac{1}{2}}/U_\infty)\{\partial(U_1/U_\infty)/\partial(X_3/\delta)\}$ is shown in Figure 3. There is a decisive advantage in using the kinetic energy over the Prandtl mixing length model in that the general trend of data appears to approach a somewhat constant linear relation similar to that obtained by Tai (90) for Klebanoff's (65) data

$$\ell_k = .52\delta \tag{3-14}$$

This is understandable since the Klebanoff (65) and Schon and Mery (20) data were obtained under neutral conditions, i.e., without thermal stratification. Equation (3-14) represents the data reasonably well only in the region where $(Q^{\frac{1}{2}}/U_\infty)\{\partial(U_1/U_\infty)/\partial(X_3/\delta)\}$ is small.

A slight modification of this model was used by Wolfshtein (60) such that

$$-\rho\overline{u_1' u_3'} = .22\ell_\mu \rho Q^{\frac{1}{2}} \frac{\partial U_1}{\partial X_3} \tag{3-15}$$

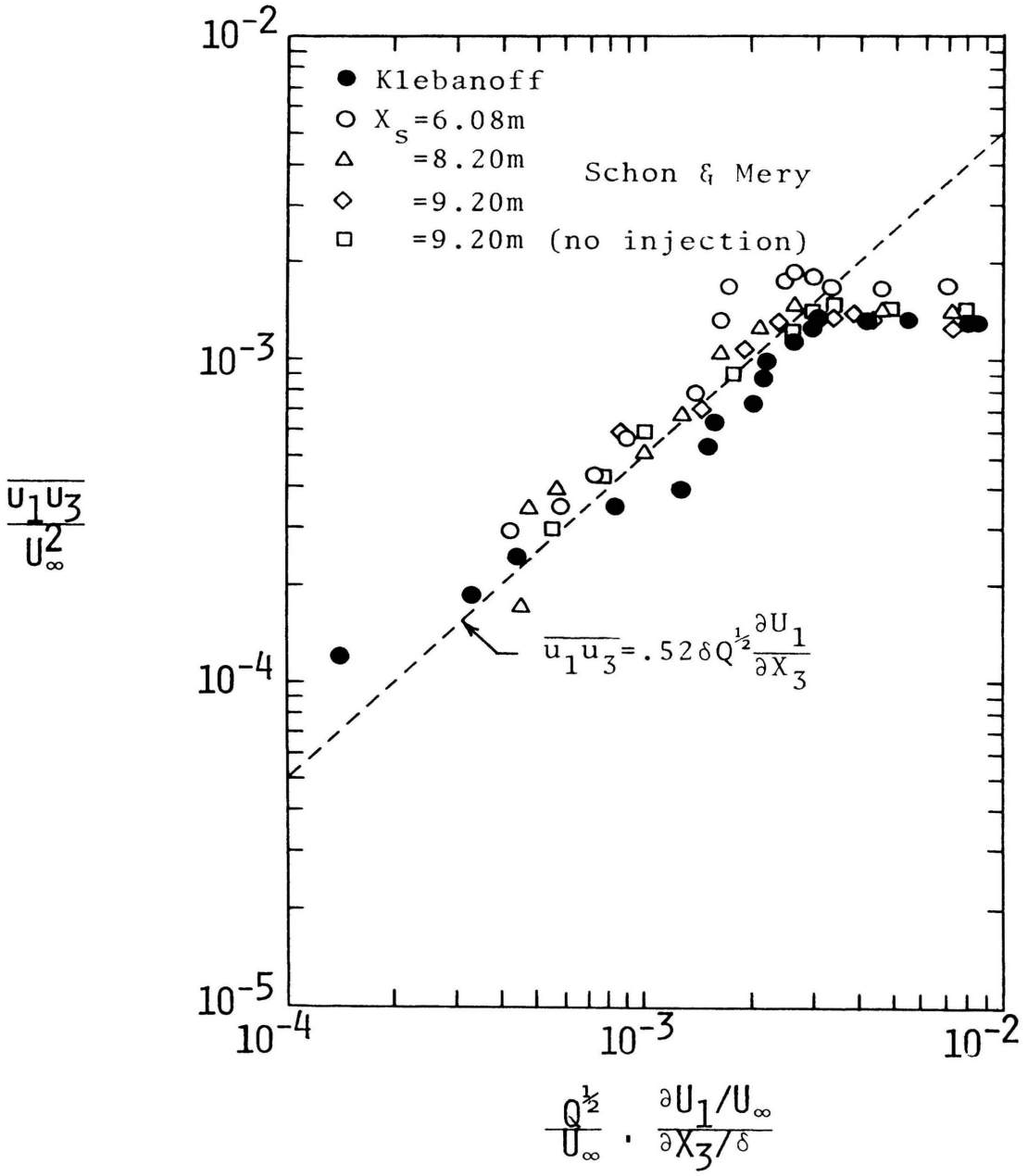

Figure 3. The Kolmogorov Model

where

$$\ell_\mu = X_3\{1 - \exp(-.016R_t)\} \tag{3-16}$$

with

$$R_t = \frac{Q^{\frac{1}{2}}\rho X_3}{\mu} \tag{3-17}$$

being the "turbulent" Reynolds number. A similar expression for the length scale was used by Wolfshtein (60) in formulating an empirical model for the dissipation of turbulence kinetic energy, D_Q. Further modifications of the Kolmogorov concept were used in several two-equation eddy coefficient models (71,72).

3. Nevzglajdov Model

The Nevzglajdov model, given by equation (3-10), uses the rather simple relation that the shear stress is linearly proportional to the turbulence kinetic energy through the constant a_1. As shown in Figure 4, the correlation between the non-dimensional shear and turbulence kinetic energy is best satisfied by the 45^o straight line where $a_1 = 0.3$ for the neutral case, which is identical to the value obtained previously by Harsha and Lee (67) and Byrne (68). This relation represents a comparatively wider range of accuracy than equation (3-11) or equation (3-12) and will be used in this study.

It is interesting to note that the model develops discrepancies near the wall and at the outer edge of the boundary layer. Because the shear becomes very low near the

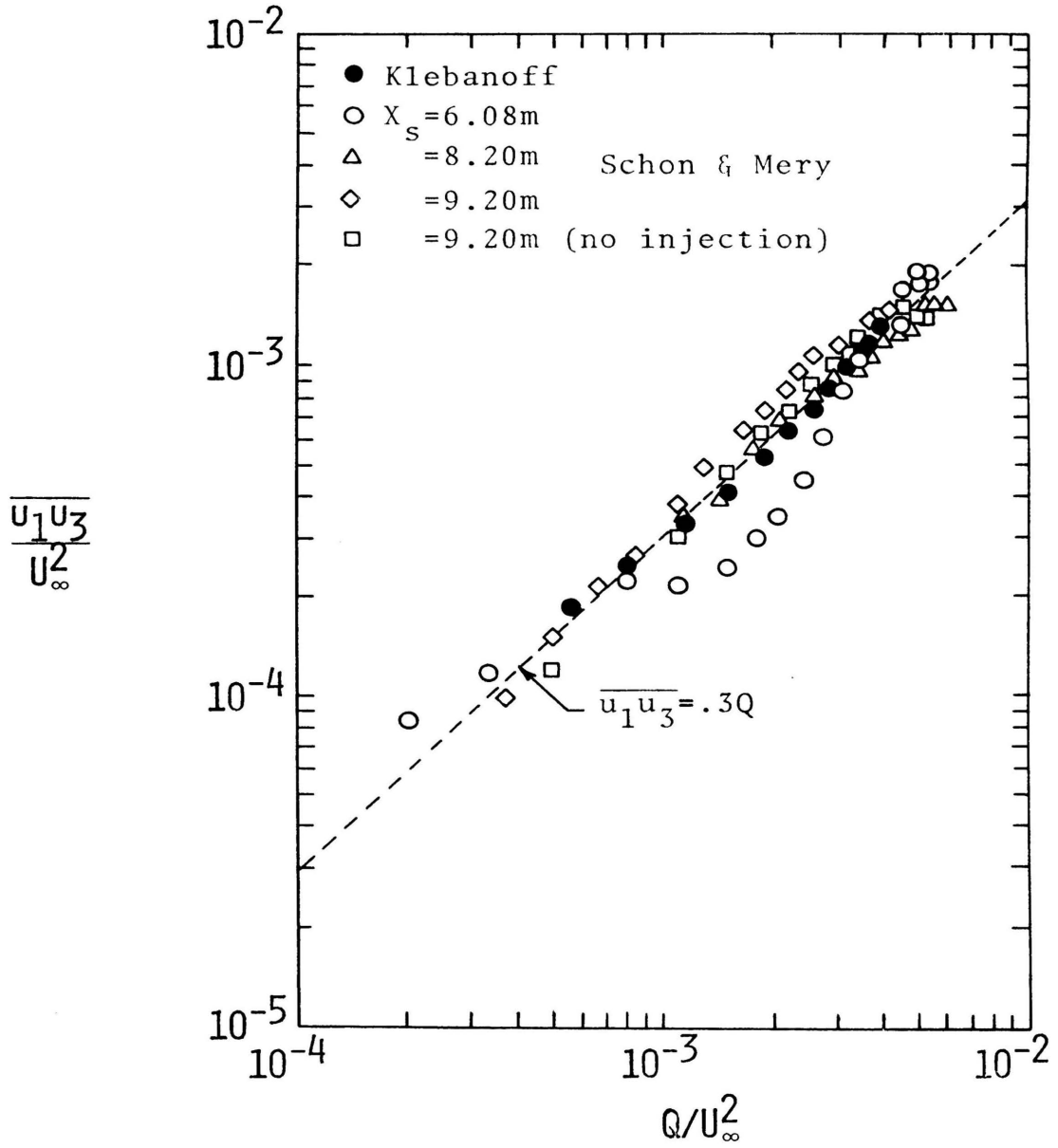

Figure 4. The Nevzglajdov Model

outer portion of the boundary layer, the inaccuracy of the model in predicting the shear force in this region is insignificant in influencing the balance of momentum. As pointed out by Byrne (68), the greatest difficulty in using this model comes from the region of high shear flow near the wall, where the shear forces approach a maximum value at the wall while the turbulence kinetic energy approaches zero, or in a region where the shear stress is zero while the turbulence kinetic energy is not, such as near an axis of symmetry in free mixing. Lee and Harsha (69) modified the proportionality constant, a_1, for the latter case by assuming that

$$a_1 = .3\left(\frac{\partial U_1}{\partial X_3}\right) / \left|\frac{\partial U_1}{\partial X_3}\right|_{max} \qquad (3\text{-}18)$$

where $\left|\partial U_1/\partial X_3\right|_{max}$ is the mean velocity gradient at the point of maximum shear, in the region between the axis of symmetry and the point of maximum shear. For the region between the maximum velocity gradient and the external boundary of the mixing region, the relation

$$a_1 = .3\left(\frac{\partial U_1}{\partial X_3}\right) / \left|\frac{\partial U_1}{\partial X_3}\right| \qquad (3\text{-}19)$$

was used. These relations did not prove very successful, however, in dealing with wall generated turbulence (68).

In this study, equation (3-10) is assumed to be valid throughout the entire boundary layer. This results in a fictitious value for the kinetic energy at the wall, although in reality the turbulence kinetic energy is known to

be zero. In the lower 10-15 per cent of the boundary layer, the turbulence kinetic energy approaches a maximum value, then sharply reduces to zero in the laminar sublayer region. As a consequence, the model modifies this region of intense turbulence such that a maximum value occurs at the wall, corresponding to a maximum wall shear, when dealing specifically with zero pressure gradient cases. A non-dimensional turbulence kinetic energy profile is plotted from the data obtained by Klebanoff (65) in Figure 5. The approach then is to use available turbulence kinetic energy values except near the wall (10-15 per cent) and to substitute a "slip" value consistent with equation (3-10) using a law of the wall formulation.

The concentration flux term, $-\rho\overline{u_i' c'}$, appearing in equation (3-3), is related to the mean concentration gradients, following the method by Boussinesq (33), as

$$-\rho\overline{u_i' c'} = \varepsilon_c\left(\frac{\partial C^n}{\partial X_j} + \frac{\partial C^n}{\partial X_i}\right) \qquad (3\text{-}20)$$

where ε_c is the eddy coefficient of concentration. Substantial difficulty still exists, however, in accounting for the newly obtained eddy coefficient relation for concentration. Using the turbulent Schmidt number, σ_{c_t}, the eddy coefficient of concentration can be related to ε_m, the eddy coefficient of momentum, as

$$\varepsilon_c = \frac{\varepsilon_m}{\sigma_{c_t}} \qquad (3\text{-}21)$$

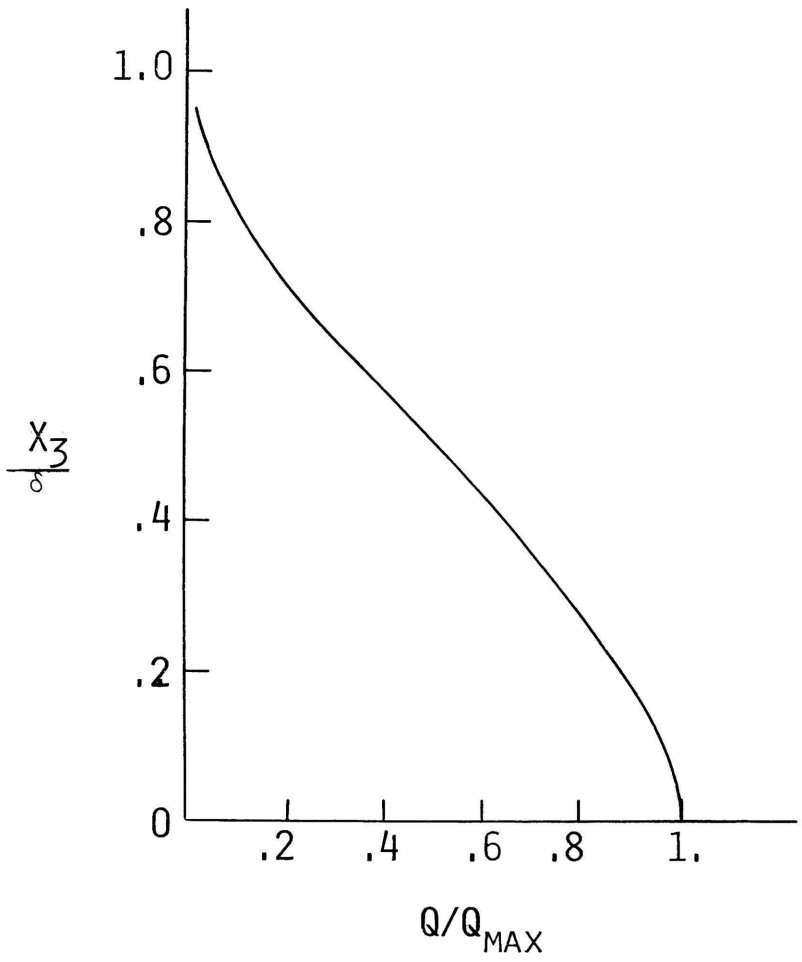

Figure 5. Distribution of Turbulence Kinetic Energy in a Turbulent Boundary Layer Measured by Klebanoff

Likewise, use of this procedure in describing the turbulence flux term, $-\rho\overline{u_i'h'}$, appearing in the energy equation, results in

$$-\rho\overline{u_i'h'} = \varepsilon_h\left(\frac{\partial h}{\partial X_j} + \frac{\partial h}{\partial X_i}\right) \qquad (3\text{-}22)$$

where ε_h is the eddy coefficient of heat. Introduction of the turbulent Prandtl number, σ_{h_t}, yields

$$\varepsilon_h = \frac{\varepsilon_m}{\sigma_{h_t}} \qquad (3\text{-}23)$$

producing an expression synonymous with that for concentration.

The turbulence kinetic energy equation, equation (3-4), contains several double correlation flux terms, in addition to gradient forms of the fluctuation velocity. Three important terms are seen to arise which require simplification; these are: $-\partial\{\overline{u_i'(p'/\rho + Q)}\}/\partial X_i$, $-g\overline{u_j't'}\delta_{j3}/T$, and the gradient fluctuation terms containing the kinematic viscosity, ν.

a. Diffusion

The term containing the pressure and velocity fluctuation gradients, known as the convective diffusion term, shows no similarity in relation to local or overall flow conditions. Naudascher (91) and Hinze (39) make a simplification by assuming the combined terms to be proportional to the local gradient of turbulence kinetic energy, since it leads to a mathematically simple form which appears to be physically plausible. Consequently,

$$-\frac{\partial}{\partial X_i}\overline{u_i'\left(\frac{p'}{\rho}+Q\right)} = \frac{\partial}{\partial X_i}\left(\varepsilon_Q \frac{\partial Q}{\partial X_i}\right) \qquad (3\text{-}24)$$

where ε_Q is the eddy coefficient for turbulence kinetic energy. Lee and Harsha (69) introduce the empirical function, σ_k, such that

$$\varepsilon_Q = \frac{\varepsilon_m}{\sigma_k} \qquad (3\text{-}25)$$

This results in the need of calculating only the eddy coefficient of momentum, ε_m, throughout the set of equations by a suitable phenomenological model. For most cases, ε_m is different for each flow condition and cannot be regarded as being constant for any given flow.

The empirical constant, σ_k, appearing in equation (3-25), was chosen as being similar to the turbulent Prandtl number and given a value, $\sigma_k = .7$. Lee, et al (92) found this relation to be reasonable for two-dimensional wakes. Byrne (68) found that solutions were relatively insensitive to the value of σ_k and concluded that the diffusion of turbulence kinetic energy is insignificant in boundary layer development. Gibson and Spalding (72) use a value of $\sigma_k = 1.0$ for their two-equation model of turbulence, indicating that the eddy coefficient for momentum is synonymous with the diffusional transport coefficient for turbulence kinetic energy for high Reynolds number flow. For want of a better value, σ_k in this study is assumed to be represented by $\sigma_k = .7$.

b. Production

The buoyancy term, $-\rho g\overline{u_i' t'}/T$, can be redefined as a function of ε_h, the eddy coefficient of heat, such that

$$\frac{-\rho g\overline{u_3' t'}}{T} = \frac{\varepsilon_h g}{c_p T}\left(\frac{\partial h}{\partial X_3}\right) \tag{3-26}$$

Further simplification yields

$$\frac{\varepsilon_h g}{c_p T}\left(\frac{\partial h}{\partial X_3}\right) = \frac{g}{T}\,\frac{\varepsilon_m}{\sigma_{h_t}}\left(\frac{\partial T}{\partial X_3}\right) \tag{3-27}$$

The additional double correlation term, $-\rho\overline{u_i' u_j'}$, appearing in equation (3-4), is termed the production of turbulence kinetic energy due to the transfer of energy from the mean motion to the fluctuating motion and is normally expressed as

$$-\rho\overline{u_1' u_3'}\,\frac{\partial U_1}{\partial X_3} = \varepsilon_m\left(\frac{\partial U_1}{\partial X_3}\right)^2 \tag{3-28}$$

The Richardson number is used as a gross parameter to describe the stability of the atmospheric boundary layer, signifying the effect of buoyancy on turbulent motion. The flux Richardson number is defined as the ratio of the two production terms, equations (3-26) and (3-28),

$$R_f = \frac{g\overline{u_3' t'}}{T} \Big/ \overline{u_1' u_3'}\,\frac{\partial U_1}{\partial X_3} \tag{3-29}$$

This relation gives an indication of the importance of buoyancy as compared to production due to turbulent stresses. The production by shear stresses adds primarily to the longitudinal component of turbulence, while buoyancy acts only in the vertical direction. The flux Richardson

number therefore acts as a local measure of the anisotropy of the turbulence, i.e., both buoyancy and shear cause turbulence to become less homogeneous.

Because the flux Richardson number requires the simultaneous measurements of both heat and momentum flux, a more useful quantity to use in analyzing stability is the gradient Richardson number, R_i, defined as

$$R_i = \frac{\frac{g}{T}\left(\frac{\partial T}{\partial X_3}\right)}{\left(\frac{\partial U_1}{\partial X_3}\right)^2} \tag{3-30}$$

The flux Richardson number, R_f, is related to R_i by

$$R_f = \frac{\varepsilon_h}{\varepsilon_m} R_i \tag{3-31}$$

As Plate (18) points out, it is important to note that both Richardson numbers are not synonymous. The flux Richardson number describes the effect of local stability on turbulence. The gradient Richardson number determines stability in a stratified fluid without perturbations of turbulence, i.e., it is identified as the ratio of the buoyancy to inertia forces and serves as a measure of the onset of turbulence in the fluid.

Using equations (3-26), (3-28), and (3-30), the two production terms can be combined to give

$$\frac{\rho g \overline{u_3' t'}}{T} - \rho \overline{u_1' u_3'} \frac{\partial U_1}{\partial X_3} \equiv \varepsilon_m \left(\frac{\partial U_1}{\partial X_3}\right)^2 \left(1 - \frac{R_i}{\sigma_{h_t}}\right) \tag{3-32}$$

in which the gradient Richardson number, R_i, accounts for

the production of turbulence due to buoyancy.

c. Dissipation

The dissipation of turbulence kinetic energy appears in equation (3-4) as the term

$$D_Q = -\nu\overline{\frac{\partial u_j'}{\partial X_i}\left(\frac{\partial u_i'}{\partial X_j} + \frac{\partial u_j'}{\partial X_i}\right)} \tag{3-33}$$

The viscous terms, appearing in equation (3-4), can be re-written as

$$\nu\frac{\partial}{\partial X_i}\overline{u_j'\left(\frac{\partial u_i'}{\partial X_j} + \frac{\partial u_j'}{\partial X_i}\right)} - \nu\overline{\left(\frac{\partial u_i'}{\partial X_j} + \frac{\partial u_j'}{\partial X_i}\right)\frac{\partial u_j'}{\partial X_i}} = \nu\left(\frac{\partial^2 Q}{\partial X_i \partial X_i} - \overline{\frac{\partial u_j'}{\partial X_i}\frac{\partial u_j'}{\partial X_i}}\right) \tag{3-34}$$

with $D_Q = -\nu\left(\overline{\partial u_j' \partial u_j'/\partial X_i \partial X_i}\right)$ and $Q = \frac{1}{2}\overline{(u_j' u_j')}$.

Because of the difficulty involved in measuring the dissipation rate, D_Q, as it appears in equation (3-33), an auxiliary relation is used based upon dimensional analysis. Following the suggestions of Patankar and Spalding (58), Byrne (68) defines the dissipation term as

$$D_Q = a_2 \rho Q^{3/2}/\delta \tag{3-35}$$

where δ is the boundary layer thickness and a_2 an empirical constant defined, for $X_3/\delta > .25$, as

$$\begin{aligned} a_2 &= 1.8 && X_3 > X_{3\tau m} \\ a_2 &= \frac{1.8 X_{3\tau m}}{\delta} && X_3 \leq X_{3\tau m} \end{aligned} \tag{3-36}$$

where $X_{3\tau m}$ is the location of maximum shear; when no shear peak occurred for $X_3/\delta \geq .25$, a_2 was calculated from

$$a_2 = 1.8 \qquad X_3 > \delta/4$$

$$a_2 = \frac{1.8\delta}{4Z} \qquad X_3 \leq \delta/4 \tag{3-37}$$

The empirical value of 1.8 was heuristically chosen after comparing with the free mixing work of Lee and Harsha (69) and Bradshaw's (66) boundary layer model. This value was also used in this study.

D. Governing Equations

Assuming two-dimensional, steady, boundary layer flow, the tensor form of the basic equations can be expressed as the orthogonal set of coordinates, x and z, shown in Figure 1. Further modification of these equations can be made by using boundary layer assumptions, resulting in parabolic partial differential equations. The end result of this simplification process produces a set of equations which can be easily solved by numerical means. The pertinent equations and corresponding assumptions used to numerically simulate atmospheric boundary layer flow are written as follows:

1. Conservation of Mass

$$\frac{\partial}{\partial X}(\rho U) + \frac{\partial}{\partial Z}(\rho W) = 0 \tag{3-38}$$

where U is the velocity parallel with the x direction and W the cross stream velocity in the z direction.

2. Conservation of Momentum

Since the boundary layer is assumed to develop predominantly in the x direction, only the longitudinal momentum equation is needed to describe the flux of momentum. Equation (3-2) is therefore reduced, with the help of equation

(3-9), to

$$\rho U\frac{\partial U}{\partial X} + \rho W\frac{\partial U}{\partial Z} = \frac{\partial}{\partial Z}\{(\mu + \varepsilon_m)\frac{\partial U}{\partial Z}\} - \frac{dP}{dX} \qquad (3\text{-}39)$$

or

$$\rho U\frac{\partial U}{\partial X} + \rho W\frac{\partial U}{\partial Z} = \frac{\partial}{\partial Z}(K_m\frac{\partial U}{\partial Z}) - \frac{dP}{dX} \qquad (3\text{-}40)$$

where $K_m = \mu + \varepsilon_m$. This allows K_m to adjust to either laminar or turbulent flow.

3. Conservation of Species

The concentration equation can be written in boundary layer form as

$$\rho U\frac{\partial C^n}{\partial X} + \rho W\frac{\partial C^n}{\partial Z} = \frac{\partial}{\partial Z}\{(\frac{\mu}{\sigma_{c_l}} + \frac{\varepsilon_m}{\sigma_{c_t}})\frac{\partial C^n}{\partial Z}\} + S^n \qquad (3\text{-}41)$$

where σ_{c_l} is the laminar Schmidt number and S^n the rate of production of concentration by chemical reaction. Introducing the exchange coefficient of momentum, the concentration equation becomes

$$\rho U\frac{\partial C^n}{\partial X} + \rho W\frac{\partial C^n}{\partial Z} = \frac{\partial}{\partial Z}(\frac{K_m}{\sigma_c}\frac{\partial C^n}{\partial Z}) + S^n \qquad (3\text{-}42)$$

where σ_c is the mixed Schmidt number, which reduces to the laminar Schmidt number in the sublayer region or to the turbulent Schmidt number in the outer region of flow.

4. Turbulence Kinetic Energy

It is a simple matter to rewrite the turbulence kinetic energy equation into a general, parabolic two-dimensional form. The form of the turbulence kinetic energy equation most often used in the literature is written

as

$$\rho U\frac{\partial Q}{\partial X} + \rho W\frac{\partial Q}{\partial Z} = \frac{\partial}{\partial Z}\left(\frac{K_m}{\sigma_k}\frac{\partial Q}{\partial Z}\right) + \varepsilon_m\left(\frac{\partial U}{\partial Z}\right)^2\left(1 - \frac{R_i}{\sigma_h}\right) - D_Q \qquad (3\text{-}43)$$

where D_Q is defined by equation (3-35). When the flow is unstable, the gradient Richardson number is negative. This leads to an increase in the production of turbulence through the increasing effect of buoyancy, i.e., increasing instability diminishes the effect of shear until the shear becomes insignificant in driving the flow field. At this point, the flow is influenced entirely by buoyancy and becomes a free-convection flow. This increase in turbulence production accounts for the rapid dispersion of pollutants under lapse conditions.

For stable flows, the gradient Richardson number is positive. This causes a decrease in the production of turbulence since buoyancy tends to draw energy from the turbulence. Under inversion conditions, the temperature increases with height such that the buoyancy forces impede turbulent mixing in the vertical direction, causing turbulent diffusion to proceed slowly.

In neutral stratification, the temperature remains constant with height, causing the gradient Richardson number to vanish. Under actual conditions, the vertical gradient of temperature is equal to the adiabatic lapse rate; however, in this study the former condition for neutrality is assumed.

5. Conservation of Energy

The conservation of stagnation enthalpy is introduced at this point instead of static enthalpy in order to simplify the governing energy equation. This permits a much wider range of flow situations to be solved with no alteration of the resulting equation.

The total energy of the fluid consists of thermal energy due to heat transfer, the turbulence kinetic energy due to the velocity fluctuations, the chemical energy due to species production, and the kinetic energy due to the friction generated by the mean flow. The total enthalpy of the fluid can be written as being composed of these four components:

$$H = h + \frac{U^2}{2} + Q + \sum_n h^n C^n \qquad (3\text{-}44)$$

where h is the static enthalpy, U the mean velocity, Q the turbulence kinetic energy, h^n the enthalpy of production of species n, and C^n the concentration of species n. If chemical reactions do not occur, the production of energy appearing in the summation term can be neglected. The equation for static enthalpy is obtained from equation (3-5) and equation (3-6) as

$$\rho U\frac{\partial h}{\partial X} + \rho W\frac{\partial h}{\partial Z} = \frac{\partial}{\partial Z}\{(\frac{\alpha + \varepsilon_h}{C_p})\frac{\partial h}{\partial Z}\} + \varepsilon_m(\frac{\partial U}{\partial Z})^2 + U\frac{dP}{dX} + R \qquad (3\text{-}45)$$

where α is the thermal conductivity of the fluid, ε_h is the eddy coefficient of heat transfer, and R the radiation term. Following the procedure discussed by Lin (93), the ratio of

the eddy coefficient of friction to that of heat transfer can be expressed as

$$\sigma_h = \frac{c_p K_m}{\alpha + \varepsilon_h} \tag{3-46}$$

where σ_h is designated as the mixed Prandtl number, which reduces to the molecular Prandtl number for the sublayer region at the surface and to the turbulent Prandtl number in the outer region of the turbulent boundary layer. Introduction of the stagnation enthalpy along with the kinetic energy of turbulence and chemical energy of the species alters the static enthalpy equation to

$$\rho U\frac{\partial H}{\partial X} + \rho W\frac{\partial H}{\partial Z} = \frac{\partial}{\partial Z}\left[\frac{K_m}{\sigma_h}\{\frac{\partial H}{\partial Z} + (\sigma_h - 1)\frac{\partial}{\partial Z}(\frac{U^2}{2}) + (\frac{\sigma_h}{\sigma_k} - 1)\frac{\partial Q}{\partial Z} + \sum_n (\frac{\sigma_h}{\sigma_c} - 1)h^n\frac{\partial C^n}{\partial Z}\}\right] + S^n - D_Q + P_Q + R \tag{3-47}$$

where σ_k is the empirical constant for the turbulence kinetic energy, σ_c the mixed Schmidt number, S^n the production of chemical species n due to chemical reaction, D_Q the dissipation of turbulence kinetic energy, and P_Q the production of turbulence kinetic energy given as

$$P_Q = \varepsilon_m(\frac{\partial U}{\partial Z})^2(1 - \frac{R_i}{\sigma_h}) \tag{3-48}$$

The stagnation enthalpy equation, equation (3-47), can be simplified by neglecting the additional source terms on the right-hand side to an equation containing only advection and diffusional terms, using an order of magnitude analysis.

Conversion of the stagnation enthalpy to static or potential temperature can be easily made by use of the thermodynamic relation: $c_p = \partial h/\partial T$.

The radiation term, R, appearing in equation (3-47), is included in the energy equation to account for long-wave radiation from the surface of the earth. Following the hypothesis of Plate (18), the effect of radiation on temperature distribution is usually small when the humidity in the atmosphere is low. In addition, the effect of radiative heat fluxes over land is ignored since it is usually negligible and complicates the energy equation. However, when dealing with flow over water surfaces, the atmospheric air is normally more moist, allowing the long-wave radiation to become trapped in the lower regions of the atmosphere. This is due to an increase in the absorption characteristics of air as moisture content increases. As a result, the effect of radiation cannot be neglected over water. In this study, the radiation source term, R, was neglected for all test cases except for the case of advection fog formation over the ocean.

The radiation term, R, was modeled after the relation for radiative flux divergence given by Mack, et al (51) as

$$R = \beta'\sigma T^4(0)\,1.6K_w\rho C^n \exp\{-1.6K_w\rho \int_{z_o}^{z} t C^n(z')dz'\} \qquad (3\text{-}49)$$

where $\beta' = .25$, the fraction of blackbody radiation from the earth's surface at temperature $T(0)$, σ is the Stefan-Boltzmann constant, K_w the mean mass absorption coefficient

of fog for infrared radiation, C^n the liquid water mixing ratio, and z_t the top of the fog. In spite of this simple treatment, results obtained by Mack, et al (51) showed that this relation did simulate the net upward radiation flux at the surface.

E. Boundary Conditions

Solutions to the boundary layer equations depend upon information available from initial profiles and along boundaries, or solid surfaces. This information is normally given as values or as gradients of dependent variables. Particularly important in dealing with turbulent boundary layers over wall boundaries are those boundary conditions specifying flow in the vicinity of the wall. Usually very steep gradients of velocity and other variables exist near a wall along with a decreasing of the eddy coefficient to a laminar viscosity relation. Because of ensuing difficulties associated with this phenomenon, many proposals have been made in the literature regarding exchange coefficients near walls. As a result, a universal law of the wall has been formulated in this study to account for turbulence kinetic energy at the wall along with Couette flow relations to account for the remaining dependent variables.

1. Law of the Wall

The equivalent law of the wall for velocity in a thermally stratified flow field is used to calculate the friction velocity, u*, at the wall, which in turn is used to calculate the wall shear stress and wall turbulence kinetic

energy value. This relationship is not used as a wall constraint for the mean velocity but is used expressly for the purpose of approximating a fictitious "slip" value for the kinetic energy in order to validate equation (3-10); the velocity, along with the stagnation enthalpy and concentration, are based upon Couette flow analysis.

Based upon the Monin-Obukhov (44) similarity theory, a non-dimensional wind shear can be written as

$$\phi(\S) = \frac{kZ}{u^*} \frac{\partial U}{\partial Z} \tag{3-50}$$

where $\S = Z/L$, with L being defined by equation (2-5), u^* the friction velocity, and k being the von Karman constant, defined by k = .41. For the case of a neutral atmosphere, $\S \to 0$, equation (3-50) can therefore be rewritten as

$$\frac{\partial U}{\partial Z} = \frac{u^*}{kZ} \phi(0) \tag{3-51}$$

where $\phi(0) = 1$. Representing $\phi(\S)$ in a Taylor series and eliminating second order terms, since § is assumed to be small, equation (3-51) is expressed as

$$\frac{\partial U}{\partial Z} = \frac{u^*}{kZ}\left(1 + \frac{\beta^* Z}{L}\right) \tag{3-52}$$

where β^* is a constant determined from experiments. Introducing non-dimensional coefficients

$$u^+ = \frac{U}{u^*}$$

$$Z^+ = \frac{Zu^*}{\nu} \tag{3-53}$$

equation (3-52) becomes

$$\frac{\partial(u^+u^*)}{\partial(Z^+\nu/u^*)} = \frac{u^{*2}}{k\nu Z^+}\left(1 + \frac{\beta^*\nu Z^+}{Lu^*}\right) \qquad (3\text{-}54)$$

The diffusion of fluid particles is assumed to proceed linearly over a short distance, Z. Since the region of interest is sufficiently close to the wall, simplification produces

$$\frac{du^+}{dZ^+} = \frac{1}{kZ^+}\left(1 + \frac{\beta^*\nu Z^+}{Lu^*}\right) \qquad (3\text{-}55)$$

Integration of equation (3-55) yields

$$u^+ = \frac{1}{k}\left(\ln z^+ + \frac{\beta^* Z}{L}\right) + C_1 \qquad (3\text{-}56)$$

where k is the von Karman constant, β^* an empirical constant, L the stability length given by Lumley and Panofsky (8) as

$$L = \frac{\sigma_h u^*(\partial U/\partial Z)T}{kg(\partial T/\partial Z)} \qquad (3\text{-}57)$$

and C_1 determined from experiments as being equal to 4.9.

A modification of equation (3-57) was made by Lee, et al (70) to account for pressure gradients and mass injection. Using the data obtained by Julien, et al (94) and Thielbahr, et al (95), equation (3-56) was rewritten as

$$u^+ = \frac{1}{k}\left\{\ln Z^+ + \beta_1 K_p + \beta_2 Z^+ k\frac{(\rho W)_B}{(\rho U)_\infty} + \beta_3 \frac{R_i}{\sigma_h} Z^+ \frac{\partial U^+}{\partial Z^+} + 2.05\right\} \qquad (3\text{-}58)$$

where the subscripts B and ∞ designate the blowing and free stream conditions respectively, W the cross stream velocity normal to U, σ_h the mixed Prandtl number, R_i the gradient Richardson number, and the β coefficients given as

$$\left.\begin{aligned} \beta_1 &= 1.45 \times 10^5 \\ \beta_2 &= 40. \\ \beta_3 &= \begin{cases} 5.2 & \text{stable} \\ 0 & \text{neutral} \\ 4.5 & \text{unstable} \end{cases} \end{aligned}\right\} \qquad (3\text{-}59)$$

The values for β_3 are deduced from Webb's (6) results for stratified atmospheric flow. The local pressure-gradient parameter, β_1, is derived from an analysis of the flow at the outer edge of the boundary layer where

$$\rho_\infty U_\infty \frac{dU_\infty}{dX} = -\frac{dP}{dX} \qquad (3\text{-}60)$$

Multiplying both sides by $\nu/\rho_\infty U_\infty^3$,

$$\frac{\nu}{U_\infty^2}\frac{dU_\infty}{dX} = -\frac{dP}{dX}\frac{\nu}{\rho_\infty U_\infty^3} \qquad (3\text{-}61)$$

or

$$K_p = \frac{\nu}{U_\infty^2}\frac{dU_\infty}{dX} \qquad (3\text{-}62)$$

where K_p is assumed to cover a particular range of constants for accelerating or decelerating flows. The blowing fraction, β_2, is based principally upon the data of Julien (96) and Julien, et al (94).

It should be remembered that this law of the wall formulation is used only to provide a means for determining the shear stress at the wall, under condition of thermal stratification, which in turn is used in creating an acceptable turbulence kinetic energy wall boundary condition as given

by equation (3-10). A Couette flow analysis has not been developed for the turbulence kinetic energy using this model because of instabilities in using equation (3-10); the mean velocity, U, and the remaining dependent variables can be effectively treated as being one-dimensional near the wall.

2. Couette Flow Relations

Because of the success obtained by Patankar (41) in regarding the near wall region as being one-dimensional, a similar hypothesis has been used in this study. The primary reason for using this concept is that the flow problem reduces to the solution of ordinary rather than partial differential equations. Consequently, these equations can be expressed in terms of algebraic relationships that can be used as asymptotes or boundary conditions for the partial differential equations. This results in a substantial savings in computational time with a minimum loss of accuracy. More conventional forms of finite difference techniques require an excessive amount of computational effort and storage capacity in order to overcome instability normally generated within this narrow region.

Since the velocity, U, is small and the x-wise convection negligible near a wall, the governing equations can be written as one-dimensional conservation equations expressed by

$$\rho W \frac{\partial U}{\partial Z} = \frac{\partial \tau}{\partial Z} - \frac{dP}{dX} \qquad (3\text{-}63)$$

$$\rho W \frac{\partial H}{\partial Z} = \frac{\partial J_H}{\partial Z} \tag{3-64}$$

$$\rho W \frac{\partial C}{\partial Z} = \frac{\partial J_C}{\partial Z} \tag{3-65}$$

where the source terms are neglected in the stagnation enthalpy and concentration equations. The flux relations, J_H and J_C, are defined as

$$J_H = \frac{K_m}{\sigma_h}\{\frac{\partial H}{\partial Z} + (\sigma_h - 1)\frac{\partial U^2/2}{\partial Z} + (\frac{\sigma_h}{\sigma_k} - 1)\frac{\partial Q}{\partial Z}\}$$

$$J_C = \frac{K_m}{\sigma_c}\frac{\partial C}{\partial Z} \tag{3-66}$$

The one-dimensional equations can be integrated to give

$$\tau = \tau_w + \dot{m}_w U + Z\frac{dP}{dX} \tag{3-67}$$

$$J_H = J_{H_w} + \dot{m}_w(H_w - H) \tag{3-68}$$

$$J_C = J_{C_w} + \dot{m}_w(C_w - C) \tag{3-69}$$

where the subscript w denotes wall value and $\dot{m}_w = \rho W_{wall}$. These relations can be reduced to simple expressions, following the non-dimensional procedure of Patankar (41), for shear stress, τ, and dependent variable flux, J, based upon shear stress and flux values at the wall.

In order to overcome the inaccuracy of the Nevzglajdov model in this region, an alternate exchange model must be used. The model proposed by van Driest (40), and later modified by Patankar (41), was found to provide adequate

results in describing the steep gradients of the dependent variables in the near wall region. The exchange coefficients near the wall are given by van Driest's (40) formula as

$$\frac{K_m}{\sigma_m} = \frac{\mu}{\sigma_1} + \frac{\rho\eta^2 Z^2}{\sigma_t}\left[1 - \exp\{-Z\sqrt{\tau\rho}/(\mu A_+)\}\right]^2 \left|\frac{\partial U}{\partial Z}\right| \qquad (3\text{-}70)$$

where σ_1 and σ_t denote laminar and turbulent Schmidt or Prandtl numbers respectively, σ_m is the mixed Schmidt or Prandtl number, and η and A_+ are constants. Subsequent nondimensionalizing and algebraic manipulation produces expressions for the gradients of velocity, concentration, and heat. This in turn leads to fictitious, or "slip", values for the dependent variables with regard to the boundary conditions. A false or "slip" value for the dependent variable is used in order to give a better representation for the interval near the boundary. This concept of employing fictitious values near the surface was initially designed by Patankar (41) in handling boundary conditions in which the gradients of the dependent variables were used at a boundary.

The velocity profile near the wall is assumed to vary according to the power law

$$U \propto |Z - Z_w|^{\beta} \qquad (3\text{-}71)$$

where the subscript w denotes the wall, or surface, and β the power law coefficient. Matching the slope at a point halfway between the wall and the first grid point along with

the velocity at the first grid point produces

$$U_{slip} = U_3/(1 + 2\beta) \tag{3-72}$$

A similar expression for ϕ can be obtained as

$$(\phi - \phi_w) \propto |Z - Z_w|^{\gamma} \tag{3-73}$$

where γ is the power law coefficient. The slip value of ϕ can be written as

$$\phi_{slip} = \phi_3\left(\frac{1 + \beta - \gamma}{1 + \beta + \gamma}\right) + \phi_w\left(\frac{2\gamma}{1 + \beta + \gamma}\right) \tag{3-74}$$

A slip value for the Z coordinate (physical dimension) can be obtained from equation (3-74) by letting $\gamma = 1$. This produces

$$Z_{slip} = Z_3\left(\frac{\beta}{2 + \beta}\right) + Z_w\left(\frac{2}{2 + \beta}\right) \tag{3-75}$$

A similar analysis can be obtained for a region near a free boundary.

The values of β and γ are found from the Couette flow relations, in conjunction with the van Driest (40) hypothesis, where

$$\beta = \left(\frac{Z}{U}\frac{\tau}{K_m}\right) \tag{3-76}$$

and

$$\gamma = \left(\frac{Z}{\phi - \phi_{slip}}\frac{J_\phi}{\frac{K_m}{\sigma_\phi}}\right) \tag{3-77}$$

From the Couette flow equations, equations (3-67), (3-68), and (3-69), the resulting expressions for β and γ become

$$\beta = \left\{\frac{(s + F + M)R}{K_m/\mu}\right\}_{slip} \tag{3-78}$$

and

$$\gamma = \left\{\frac{(S + M)R}{K_m/\mu\sigma_\phi}\right\}_{slip} \tag{3-79}$$

where

$$\left.\begin{aligned} s &= \tau_w/\rho U^2 \\ S &= J_w/\{\rho U(\phi_w - \phi)\} \\ R &= \rho UZ/\mu \\ F &= Z(dP/dX)/\rho U^2 \\ M &= \dot{m}_w/\rho U \end{aligned}\right\} \tag{3-80}$$

Couette flow relationships were derived by Wolfshtein (60) for turbulence flow, based on the Kolmogorov model. This hypothesis was found to be applicable to both the laminar sublayer and the fully turbulent region of one-dimensional flow. However, the turbulence kinetic energy equation could not be reduced to a simple first order equation; a numerical iterative method had to be used in conjunction with an excessive number of empirical constants to solve the second order equation. In describing the length scale, Wolfshtein used an expression similar to that used by van Driest (40). A comparison between this technique and the Couette flow-law of the wall technique employed in this study proved to be inconsequential.

3. Initial and Boundary Conditions

If the mean velocity profile is not given from measurements, a power law representation is employed such that

$$\frac{U}{U_\infty} = \left(\frac{Z}{\delta}\right)^{1/5.5} \tag{3-81}$$

where U_∞ is the free stream velocity and δ the boundary layer thickness obtained from measurements or arbitrarily estimated. This empirical relation gives a good approximation for the velocity profile in a fully developed boundary layer.

The initial temperature profile, which is easily converted to stagnation enthalpy, can be obtained from experimental data or specified by the semi-empirical relation

$$\frac{T_w - T}{T_w - T_\infty} = \left(\frac{Z}{\delta_t}\right)^{1/5.5} \tag{3-82}$$

where T_w is the temperature at the wall, T_∞ the free stream temperature, and δ_t the thermal boundary layer thickness. Because the two power law relations give a good average representation of the flow conditions over the whole boundary layer, meteorologists have employed the use of these equations extensively. Plate (18) correlated the exponent appearing in equation (3-81) with various surface roughness and types of terrain along with corresponding average boundary layer thicknesses.

The initial concentration profile is normally obtained from experimental data. If no data exists, or concentration is not considered, the concentration is initially assumed to

be zero everywhere. In the case of fog formation studies, species concentration is generated through the source term, S^n, for condensation and evaporation.

In the case of the turbulence kinetic energy, the initial profile is obtained from experimental data, which is usually scarce, or estimated from a non-dimensional turbulence kinetic energy profile based upon the flat plate data of Klebanoff (65), as shown in Figure 5. The turbulence kinetic energy near the wall has been modified in order to validate equation (3-10). Agreement between the measured data of Klebanoff (65) and the computational results obtained from equation (3-10) is very good within as close as 10 per cent of the wall region. The remaining 10 per cent is obtained by extrapolating the computed kinetic energy to the wall.

The boundary conditions are specified as follows:

Wall ($Z = 0$)

$U = 0$

$T = T_w$

$Q = \tau_w / a_1 \rho$

$\partial C / \partial Z = 0$

Free Stream ($Z \to \infty$)

$U = U_\infty$

$T = T_\infty$

$Q = 0$

$C = 0$

The concentration for a ground level source has a maximum value at the surface. Since the wall boundary condition implies that the vertical flux of concentration is zero, $\partial C/\partial Z = 0$, the concentration near the wall is obtained from a Couette flow relation for total flux specified at the surface.

F. Solution to the Finite Difference Equations

The numerical technique employed in this study is based principally upon the method developed by Patankar (41). The procedure allows an arbitrary number of non-linear parabolic partial differential equations to be simultaneously solved using an implicit technique and a variable grid size. Because of the simplicity of the method, combined with the use of variable grid size and the Couette flow wall functions, substantial savings in computer time for large scale calculations are achieved. In this study, the simultaneous solution of momentum, stagnation enthalpy, concentration, and turbulence kinetic energy required approximately 2½ minutes on an IBM 360/50 to solve three different cases of atmospheric flow (neutral, stable, and unstable) using a 25 point lateral grid. The general nature of the solution allows any number of different data sets to be run in succession with a minimum of computation.

Modifications to the Patankar (41) method were made by Harsha (89), Byrne (68), and Tai (90) in order to accommodate the Nevzglajdov model into the general numerical scheme. Patankar and Spalding (58) incorporated the Kolmogorov model

into Patankar's (41) original method in a similar manner. An additional modification to the original program was made by Harsha (89) in order to more accurately control the variation of grid size in free mixing studies; however, this proved to be limited to free mixing problems and could not be applied to wall turbulence situations.

1. Coordinate Transformations

To insure computational efficiency, the system of governing equations is converted from the physical coordinate system (X, Z) to the von Mises stream-function coordinate system (X, ψ). The stream function ψ is defined by the relations

$$\rho U = \frac{\partial \psi}{\partial Z}$$
$$-\rho W = \frac{\partial \psi}{\partial X} \qquad (3\text{-}83)$$

The X-direction momentum equation (3-40) can be transformed to

$$\frac{\partial U}{\partial X} = \frac{\partial}{\partial \psi}(K_m \rho U \frac{\partial U}{\partial \psi}) - \frac{1}{\rho U}\frac{dP}{dX} \qquad (3\text{-}84)$$

The stagnation enthalpy, turbulence kinetic energy, and concentration can be transformed in the same manner; their development will not be given here.

In order to limit the computation region to the outer edge of the boundary layer, i.e., within the region of significant gradients, a dimensionless stream function is defined as

$$\omega = \frac{\psi - \psi_I}{\psi_E - \psi_I} \tag{3-85}$$

where ψ_I is the stream line along the surface, or "internal" edge, and ψ_E the stream line on the outer edge of the boundary layer. Consequently, the value of ω varies as $0 \leq \omega \leq 1$. From equation (3-83),

$$\begin{aligned} -\frac{d\psi_I}{dX} &= \rho_I W_I = \dot{m}_I \\ -\frac{d\psi_E}{dX} &= \rho_E W_E = \dot{m}_E \end{aligned} \tag{3-86}$$

where $\dot{m}_I$ and $\dot{m}_E$ denote mass flow rate entrained through the boundaries. The X-momentum equation is therefore altered by equations (3-85) and (3-86) to

$$\frac{\partial U}{\partial X} + \left\{\frac{\dot{m}_I - \omega(\dot{m}_I - \dot{m}_E)}{\psi_E - \psi_I}\right\}\frac{\partial U}{\partial \omega} = \frac{\partial}{\partial \omega}\left\{\frac{\rho U K_m}{(\psi_E - \psi_I)^2}\frac{\partial U}{\partial \omega}\right\} - \frac{1}{\rho U}\frac{dP}{dX} \tag{3-87}$$

The remaining governing equations, equations (3-24), (3-35), and (3-39), can be similarly transformed so that all convert to a standard form which can be written as

$$\frac{\partial \phi}{\partial X} + (a + b\omega)\frac{\partial \phi}{\partial \omega} = \frac{\partial}{\partial \omega}\left(c\frac{\partial \phi}{\partial \omega}\right) + d \tag{3-88}$$

where

$$\begin{aligned} a &= \dot{m}_I/(\psi_E - \psi_I) \\ b &= (\dot{m}_E - \dot{m}_I)/(\psi_E - \psi_I) \\ c &= \rho U K_m/\sigma_\phi(\psi_E - \psi_I)^2 \end{aligned} \tag{3-89}$$

The values for ϕ, σ_ϕ, and d are given in Table I. The

TABLE I: COEFFICIENTS IN THE GENERALIZED PARABOLIC EQUATION

ϕ	σ_ϕ	d
U	1	$\frac{1}{\rho U}\frac{dP}{dX}$
H	σ_h	$\frac{1}{\rho U}(P_Q - D_Q + S^n + R)$
C^n	σ_c	$\frac{1}{\rho U}S^n$
Q	σ_k	$\frac{\rho U K_m}{(\psi_E-\psi_I)^2}\{(\frac{\partial U}{\partial \omega})^2 - \frac{R_i}{\sigma_h}\} - \frac{D_Q}{\rho U}$

general nature of equation (3-88) allows the governing equations to be solved using the same basic coefficients.

The coupling of the equations occurs in the coefficients c and d. The exchange coefficient is related to the turbulence kinetic energy while the source terms are related to the longitudinal momentum, thus securing closure of the equations.

2. Entrainment

Prediction of the entrainment rate of fluid between the longitudinal steps conserves a considerable amount of computation time by excluding the inviscid flow region. Consequently, the problem of entrainment arises when attempting to evaluate $\dot{m}_I$ and $\dot{m}_E$ in equation (3-89). Using the axial momentum equation applied along the edge of the boundary layer, the momentum equation can be expressed (60) as

$$\frac{dU}{dX} = -\frac{1}{\rho U}\frac{dP}{dX} \tag{3-90}$$

which is synonymous with the inviscid Bernoulli equation. If it is assumed that this relation holds just inside the boundary layer, equation (3-90) can be expressed as

$$\{\dot{m}_I + (\dot{m}_E - \dot{m}_I)\omega\}\frac{\partial U}{\partial \omega} = \frac{\partial}{\partial \omega}\{\frac{\rho U K_m}{(\psi_E - \psi_I)}\frac{\partial U}{\partial \omega}\} \tag{3-91}$$

where use has been made of equations (3-83) and (3-85). As $\omega \to 1$,

$$\dot{m}_E = \lim_{\omega \to 1} \frac{\partial}{\partial \omega}\{\frac{\rho_E U_E K_m}{(\psi_E - \psi_I)}\frac{\partial U}{\partial \omega}\}/\frac{\partial U}{\partial \omega} \tag{3-92}$$

Similarly, as $\omega \to 0$,

$$\dot{m}_I = \lim_{\omega \to 0} \frac{\partial}{\partial \omega} \left\{ \frac{\rho_I U_I K_m}{(\psi_E - \psi_I)} \frac{\partial U}{\partial \omega} \right\} / \frac{\partial U}{\partial \omega} \qquad (3\text{-}93)$$

If the exchange coefficient of momentum is assumed to be proportional near the boundaries to $\partial U/\partial Z$, the Prandtl mixing length model can be employed and the limits in equations (3-92) and (3-93) become finite.

An equation can be written for the entrainment rate, providing that the free boundary at the outer edge of the boundary layer obeys the mixing length hypothesis, using equations (3-92) and (3-11) as

$$\dot{m}_E = -2\rho_E \ell_E^2 \left| \frac{\partial^2 U}{\partial Z^2} \right|_E \qquad (3\text{-}94)$$

A similar expression can be obtained for the wall boundary entrainment rate. In the case of laminar flow, K_m does not vanish with $\partial U/\partial Z$ at the outer edge of the boundary layer. Consequently, an infinite entrainment rate occurs. This difficulty can be overcome by applying equation (3-91) away from the external boundary such that $0<\omega<1$; this procedure is explained by Patankar (41) in detail.

It is important to note that the entrainment across a free boundary is arbitrary; an entrainment rate has been similarly developed by Harsha (89) using the momentum integral to evaluate $(\psi_E - \psi_I)$ along with equation (3-92). The entrainment rates control the coefficients a, b, and c in equation (3-88) and influence the downstream integration step, along with $(\psi_E - \psi_I)$, given by equation (3-86). An

entrainment rate should be estimated which will produce an adequate amount of flow to account for all dependent variable gradients. Equation (3-94) has been used in this study because of its simplicity.

3. Finite Difference Procedure

The numerical technique employed in this study was originally developed by Patankar (41). Because of the widespread popularity of this method, a brief introduction to the formulation will be given here; the details can be found in references (68) and (41).

Figure 6 shows the numerical grid and nomenclature used in formulating the finite difference elements, where the subscripts U and D indicate upstream conditions and downstream conditions respectively. Since the generalized parabolic equation is non-linear with respect to ω, the equation is quasi-linearized by assuming that the dependent variable ϕ varies linearly with ω. Along the X-coordinate, the value of ϕ is ϕ_U except at $X = X_D$, where ϕ immediately assumes the value ϕ_D.

In order to formulate the difference equation, the derivatives of the dependent variables are evaluated as mean values integrated over the control volume, indicated in Figure 6 by the crosshatching. The dotted lines indicate midpoint locations with respect to ω. The principle gradients appearing in the convection terms in equation (3-88) can be expressed as

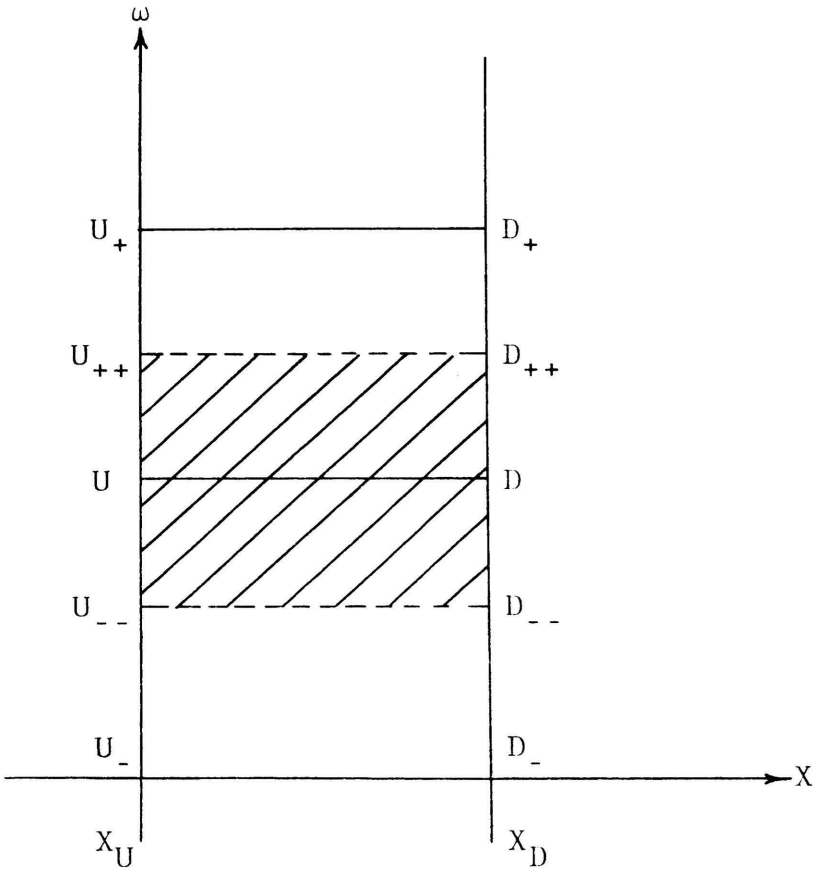

Figure 6. Finite Element Grid for X-ω Coordinates

$$\frac{\partial \phi}{\partial X} \simeq \frac{\int_{X_U}^{X_D} \int_{\omega_{D--}}^{\omega_{D++}} \frac{\partial \phi}{\partial X} \, d\omega dX}{(X_D - X_U)(\omega_{D++} - \omega_{D--})} \tag{3-95}$$

and

$$\frac{\partial \phi}{\partial \omega} \simeq \frac{\int_{\omega_{D--}}^{\omega_{D++}} \frac{\partial \phi}{\partial \omega} \, d\omega}{(\omega_{D++} - \omega_{D--})} \tag{3-96}$$

Assuming linear profiles between the grid points, equations (3-95) and (3-96) can be rewritten as

$$\frac{\partial \phi}{\partial X} \simeq \frac{1}{(X_D - X_U)(\omega_{D++} - \omega_{D--})} \{ \int_{\omega_{D--}}^{\omega_D} (\phi_D - \phi_U) d\omega + \int_{\omega_D}^{\omega_{D++}} (\phi_D - \phi_U) d\omega \} \tag{3-97}$$

and

$$\frac{\partial \phi}{\partial \omega} \simeq \frac{1}{(\omega_{D++} - \omega_{D--})} \left(\int_{\omega_{D--}}^{\omega_{D++}} d\phi \right) \tag{3-98}$$

Integration of equations (3-97) and (3-98), along with some algebraic manipulation, leads to the two expressions for the convection terms

$$\frac{\partial \phi}{\partial X} \simeq P_1(\phi_{D+} - \phi_{U+}) + P_2(\phi_D - \phi_U) + P_3(\phi_{D-} - \phi_{U-}) \tag{3-99}$$

where

$$P_1 \equiv \frac{\omega_{D+} - \omega_D}{4(X_D - X_U)(\omega_{D+} - \omega_{D-})}$$

$$P_2 \equiv \frac{3}{4(X_D - X_U)} \qquad (3\text{-}100)$$

$$P_3 \equiv \frac{\omega_D - \omega_{D-}}{4(X_D - X_U)(\omega_{D+} - \omega_{D-})}$$

and

$$(a + b\omega)\frac{\partial \phi}{\partial \omega} \simeq Q(\phi_{D+} - \phi_{D-}) + R_1\phi_{D+} + R_2\phi_D + R_3\phi_{D-} \qquad (3\text{-}101)$$

where

$$Q \equiv \frac{a}{\omega_{D+} - \omega_{D-}}$$

$$R_1 \equiv \frac{b}{4}\frac{\omega_{D+} + 3\omega_D}{\omega_{D+} - \omega_{D-}} \qquad (3\text{-}102)$$

$$R_2 \equiv -\frac{b}{4}$$

$$R_3 \equiv -\frac{b}{4}\frac{\omega_{D-} + 3\omega_D}{\omega_{D+} - \omega_{D-}}$$

The expression for the flux term in equation (3-88) can be expressed in a similar manner as

$$\frac{\partial}{\partial \omega}\left(c\frac{\partial \phi}{\partial \omega}\right) \simeq \frac{2}{\omega_{D+} - \omega_{D-}}\left(c_{uu_+}\frac{\phi_{D+} - \phi_{D-}}{\omega_{D+} - \omega_{D-}} - c_{uu_-}\right.$$

$$\left.\frac{\phi_D - \phi_{D-}}{\omega_D - \omega_{D-}}\right) \qquad (3\text{-}103)$$

Using the nomenclature of Patankar (41), equations (3-99), (3-101), and (3-103) can be expressed as

$$\frac{\partial \phi}{\partial X} + (a + b\omega)\frac{\partial \phi}{\partial \omega} \simeq g_1\phi_{D+} + g_2\phi_D + g_3\phi_{D-} + g_4 \qquad (3\text{-}104)$$

and

$$\frac{\partial}{\partial \omega}(c\frac{\partial \phi}{\partial \omega}) \simeq g_5(\phi_{D+} - \phi_D) - g_6(\phi_D - \phi_{D-}) \qquad (3\text{-}105)$$

where

$$\begin{aligned} g_1 &= P_1 + Q + R_1 \\ g_2 &= P_2 + R_2 \\ g_3 &= P_3 - Q + R_3 \\ g_4 &= -P_1\phi_{u+} - P_2\phi_u - P_3\phi_{u-} \\ g_5 &= 2c_{u++}/(\omega_{D+} - \omega_{D-})(\omega_{D+} - \omega_D) \\ g_6 &= 2c_{u--}/(\omega_{D+} - \omega_{D-})(\omega_D - \omega_{D-}) \end{aligned} \qquad (3\text{-}106)$$

The expressions for the g's are in terms of known values, i.e., upstream conditions at $X = X_U$.

The source term, d, may not be linear in ϕ over the interval $X_D - X_U$. Consequently, d is linearized according to the formula

$$d_D \simeq d_U + (\frac{\partial d}{\partial \phi})_U(\phi_D - \phi_U) \qquad (3\text{-}107)$$

As an example, the source term in the momentum equation, equation (3-87), can be evaluated from

$$d \simeq \frac{\int_{\omega_{D--}}^{\omega_{D++}} (d)_{X=X_D}\, d\omega}{\omega_{D++} - \omega_{D--}} \tag{3-108}$$

or

$$d \simeq \frac{1}{\omega_{D++} - \omega_{D--}} \int_{\omega_{D--}}^{\omega_{D++}} \{d_{X=X_U} + (\frac{\partial d}{\partial \omega})_{X=X_U}(U_{X=X_D} - U_{X=X_U})\}d\omega \tag{3-109}$$

Since $d = -(1/\rho U)(dP/dX)$, the momentum source term, after some algebra, becomes

$$d \simeq s_1 U_{D+} + s_2 U_D + s_3 U_{D-} + s_4 \tag{3-110}$$

where

$$\begin{aligned} s_1 &= \frac{P_1}{\rho_{U+} U_{u+}^2} \frac{dP}{dX}(X_D - X_U) \\ s_2 &= \frac{P_2}{\rho_U U_u^2} \frac{dP}{dX}(X_D - X_U) \\ s_3 &= \frac{P_3}{\rho_{U-} U_{u-}^2} \frac{dP}{dX}(X_D - X_U) \\ s_4 &= -2\frac{dP}{dX}(X_D - X_U)(\frac{P_1}{\rho_{U+} U_{u++}} + \frac{P_2}{\rho_U U_U} + \frac{P_3}{\rho_{U-} U_{U-}}) \end{aligned} \tag{3-111}$$

The complete difference equation can be compiled into one equation as

$$g_1\phi_{D+} + g_2\phi_D + g_3\phi_{D-} + g_4 = g_5(\phi_{D+} - \phi_D) - g_6(\phi_D - \phi_{D-}) + d_U + (\frac{\partial d}{\partial \phi})_U(\phi_D - \phi_U) \tag{3-112}$$

which conveniently reduces to

$$\phi_D = A\phi_{D+} + B\phi_{D-} + C \tag{3-113}$$

where

$$A = \frac{g_5 - g_1}{g_2 + g_5 + g_6 - (\partial d/\partial\phi)_U}$$

$$B = \frac{g_6 - g_3}{g_2 + g_5 + g_6 - (\partial d/\partial\phi)_U} \tag{3-114}$$

$$C = \frac{d_U - (\partial d/\partial\phi)_U\phi_U - g_4}{g_2 + g_5 + g_6 - (\partial d/\partial\phi)_U}$$

The particular significance of equation (3-113) is seen from the fact that the governing equations can all be reduced to an expression containing three unknowns in a particular order. Use of tri-diagonal successive substitution formulae, discussed by Richtmyer (97), allows the solution procedure to be computationally time dependent upon the number of equations to be solved, and not to its square as in the standard matrix-inversion technique.

The calculation of the stream function interval $\psi_E - \psi_I$, which is used in controlling the normal distance Z, to give the physical thickness of the boundary layer, is obtained from equation (3-86):

$$(\psi_E - \psi_I)_D = (\dot{m}_I - \dot{m}_E)_U(X_D - X_U) \tag{3-115}$$

where the entrainment rates are evaluated at the upstream locations.

Because the downstream step length is unknown in

equation (3-115), the next step length is calculated by assuming that a given fraction of the total mass flow is entrained from the upstream step, providing that the growth of the layer thickness is slow. Since the entrainment rates are defined, the step length can be expressed as

$$(X_D - X_U) = .05(\psi_E - \psi_I)_U/(\dot{m}_I - \dot{m}_E)_U \qquad (3\text{-}116)$$

with the value of .05 being empirically obtained by Patankar (41).

IV. RESULTS AND DISCUSSION

Because of the general nature of the numerical model described in the preceeding sections, a systematic progression of increasingly difficult flow situations has been analytically solved, using a minimum of modification. The particular technique employed in this model has been found in the past to adequately predict a wide range of turbulent boundary layer situations dealing specifically with engineering-type problems. Additional inputs into the present system include thermal stratification effects, surface temperature distribution, and concentration distributions associated with atmospheric diffusion phenomena. In the present investigation, all flow parameters have been assumed to be two-dimensional and steady state. Passive concentration fields are considered to be generated from continuous ground level line sources.

The calculations made in this study were first analyzed by comparing with theoretical models used to describe atmospheric boundary layer phenomena. While comparison with theory cannot be considered conclusive, it at least affords the theoretician an opportunity to ascertain the feasibility of his model. Once this is achieved, a more systematic appraisal of the model is necessary.

Further verification of the present model was made by using available experimental data. Comparisons with wind tunnel data were made under conditions similar to neutral,

stable, and unstable atmospheric boundary layers.

The last section to be discussed involves the formation of an advection fog occurring over a cold sea surface. While this study has intrinsic value, no available data exists with which the model can be properly evaluated. While several numerical models exist, each tends to predict somewhat irregular results. Using previous mathematical analysis based upon these schemes, the present model incorporates the effect of advection upon the formation of fog along with a more realistic model for the turbulent exchange coefficients.

A. Comparison With Theory

While many theoretical investigations have been conducted using various models to describe the exchange coefficients, very few provide enough information to adequately compare with the model used in this study. Successful results were obtained by Rao, et al (31) using a rate equation to govern the exchange coefficient of momentum in thermally stratified boundary layers. A comparison of the turbulence kinetic energy model with the rate equation was made in order to verify the ability of the numerical scheme to simulate atmospheric diffusion phenomena.

For the purpose of comparing theoretical results with those of the present analysis, calculations were made for a hypothetical atmospheric boundary layer based upon the flow configurations used by Rao, et al (31) in simulating the data of Poreh (30) and Malhotra and Cermak (98). Netrual, stable, and unstable stratifications were analyzed by

comparing prediction for velocity, temperature, and concentration.

1. Neutral Atmosphere

Rao, et al (31) used the experimental data of Poreh (30) to numerically simulate ground level line source diffusion in a neutral atmosphere. The initial velocity and concentration profiles used by Rao, et al (31) were likewise used in the present model as initial conditions.

The computed velocity profiles for the neutral case are shown in Figure 7 at four downstream locations, ranging from X_s = 2.74 meters to 10.8 meters, from the source of concentration. The source strength of concentration at X_s = 0 was equal to 0.66 mg/cm-sec. Both models appear to simulate relatively identical profiles. Slight discrepancies occur near the wall; however, this is felt to be due to the use of Couette flow relations in the turbulence kinetic energy model. A universal law of the wall formula is used in the rate equation model to describe the variation of mean velocity in the near wall region.

Using the concentration measured by Poreh (30) at X_s = .91 meter as initial conditions, both models show reasonable success in Figure 8a, 8b, and 8c in predicting the diffusion of concentration at the remaining downstream locations. The more signigicant underprediction by the turbulence kinetic energy model at X_s = 1.52 meters is caused by readjustment of the turbulence kinetic energy at the wall to comply with the Nevglajdov model and the initial u* value. While both

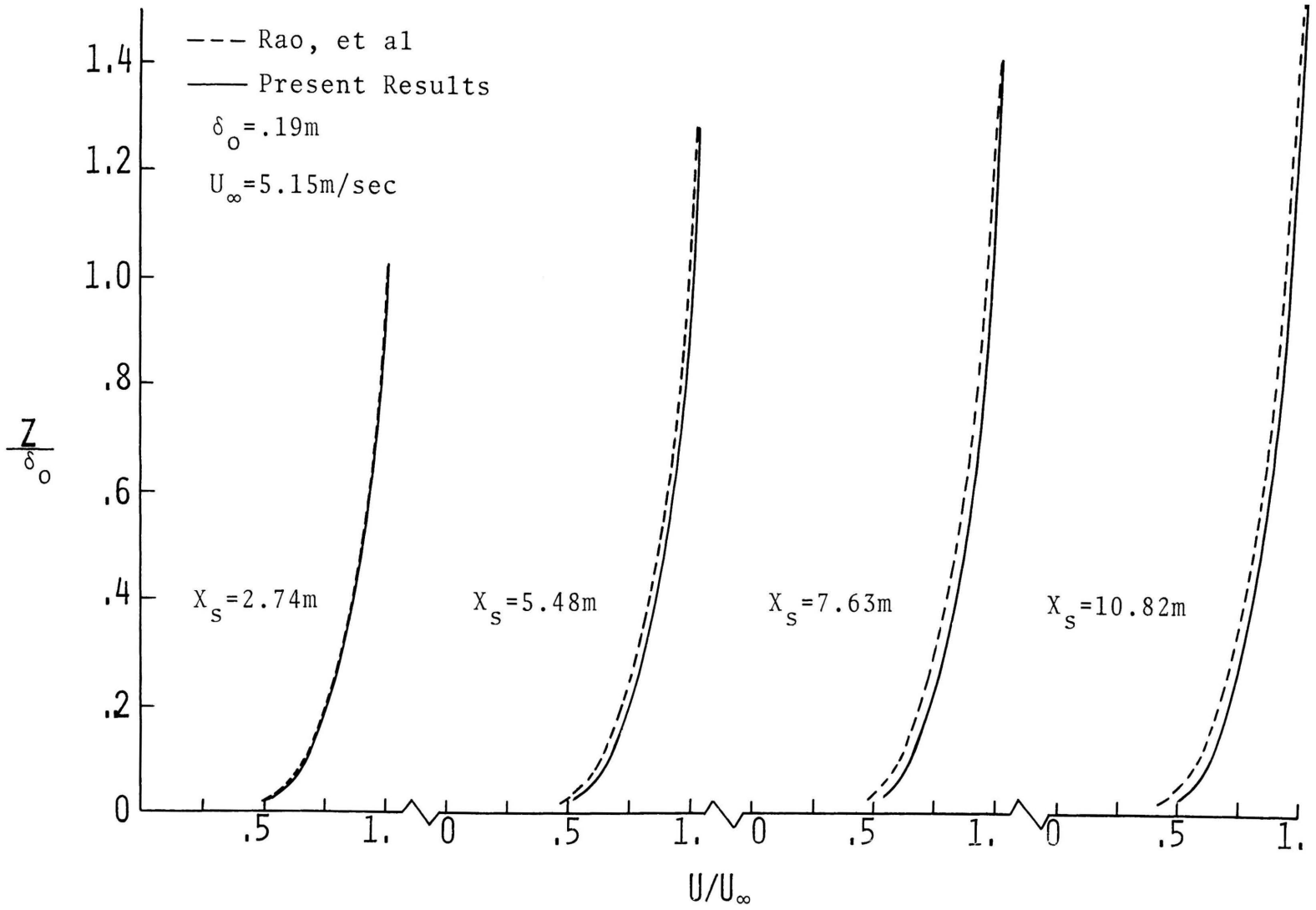

Figure 7. Comparison with Rate Equation Model in Predicting Velocity in a Neutral Atmosphere

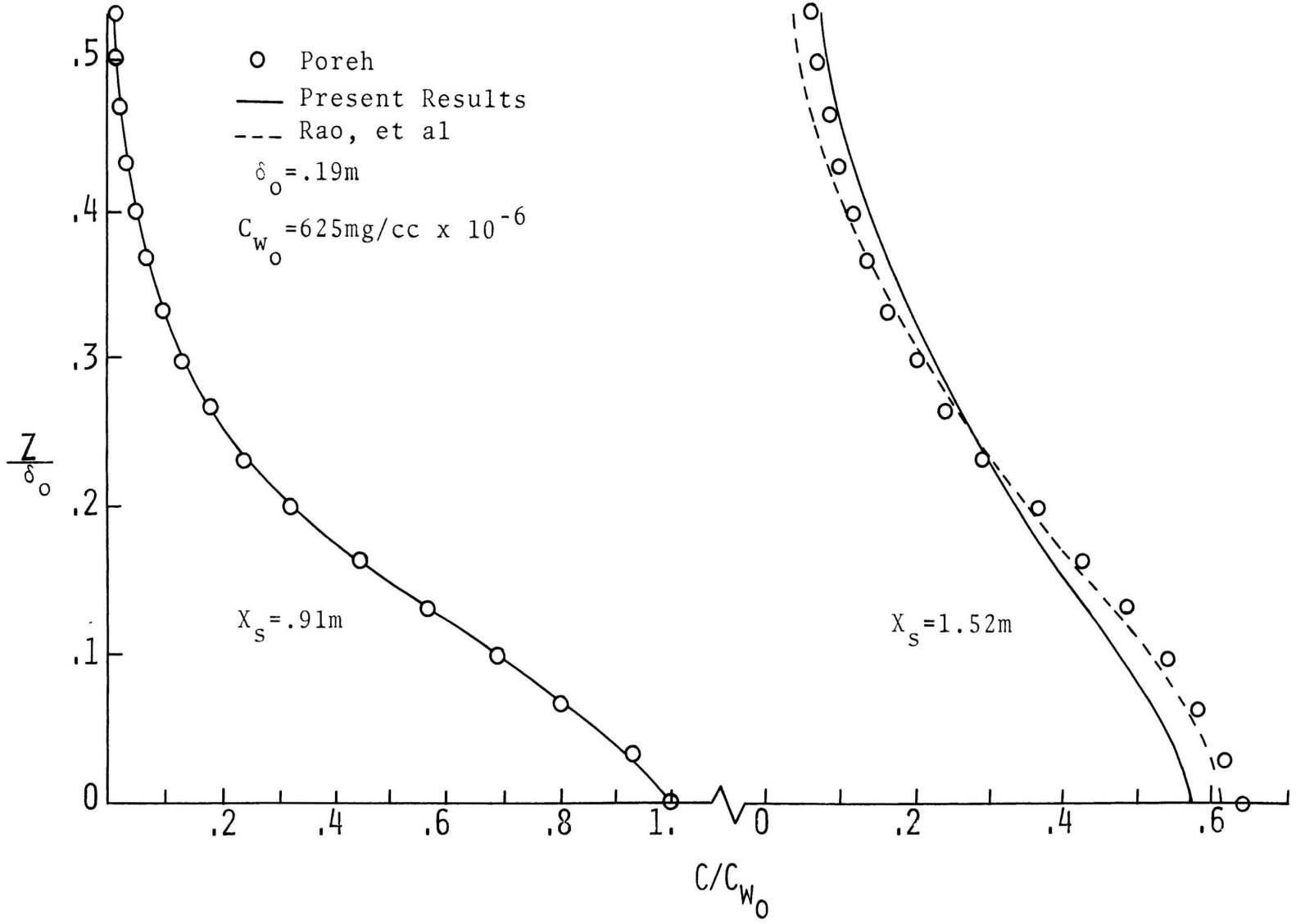

Figure 8a. Comparison with Rate Equation Model in Predicting Concentration Data in a Neutrally Stratified Turbulent Boundary Layer: X_s=.91 - 1.52 meters

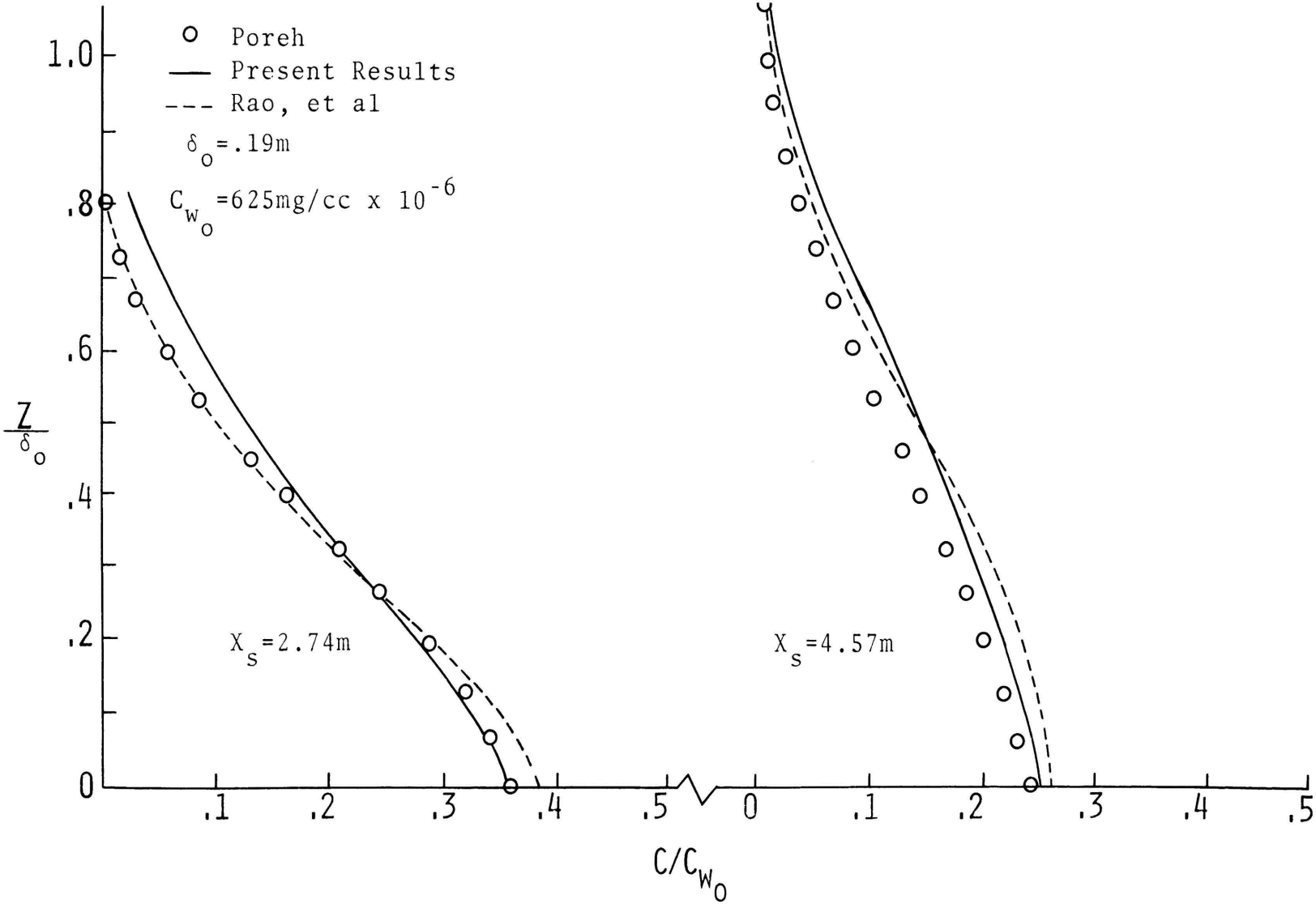

Figure 8b. Comparison with Rate Equation Model in Predicting Concentration Data in a Neutrally Stratified Turbulent Boundary Layer: X_s=2.74 - 4.57 meters

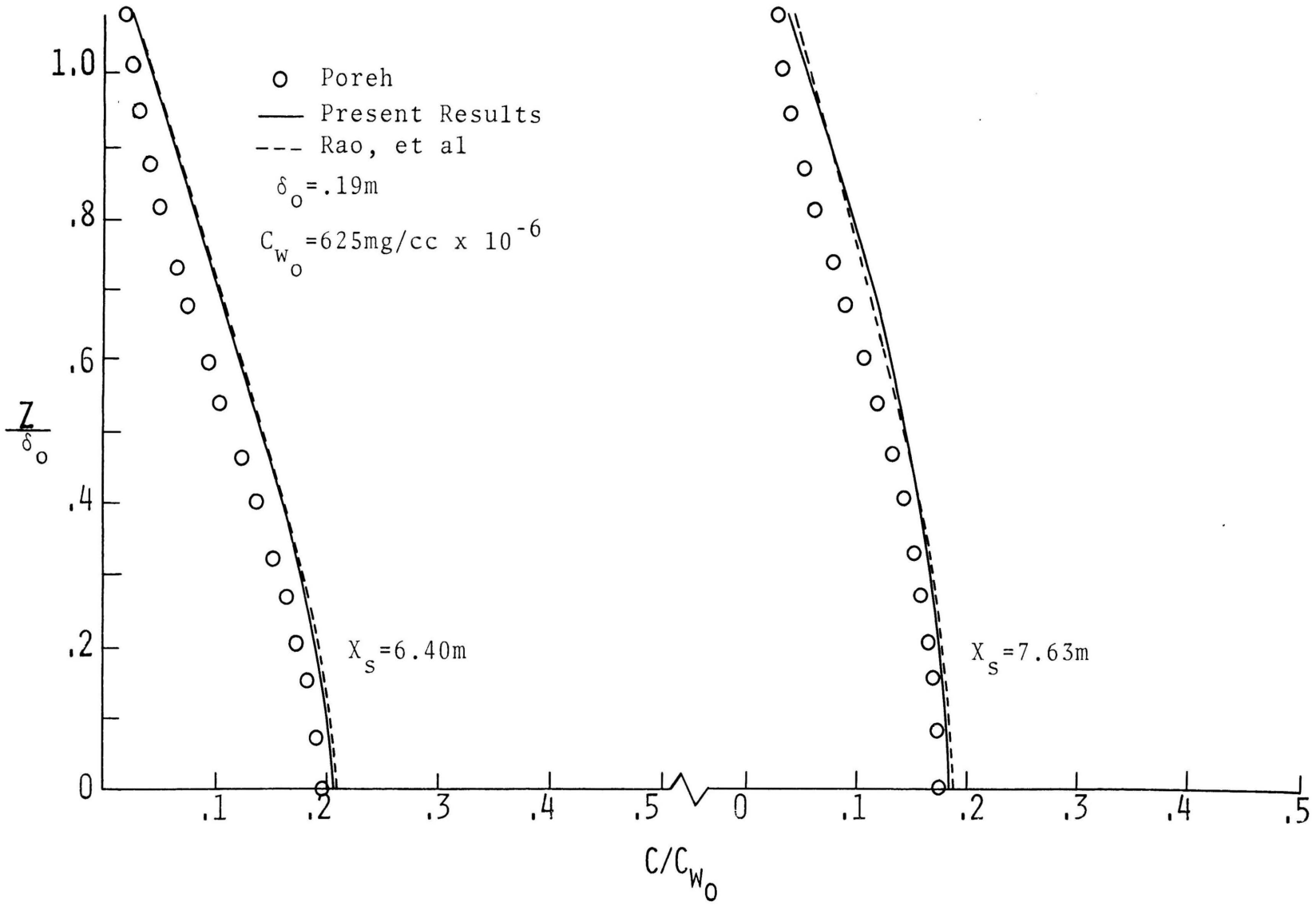

Figure 8c. Comparison with Rate Equation Model in Predicting Concentration Data in a Neutrally Stratified Turbulent Boundary Layer: X_s=6.40 - 7.63 meters

models begin to overpredict the concentration in the near wall region at X_s = 2.74 meters, the rate equation model is seen to be slightly more significant. Both models show their predicted concentration profiles to be almost identical at X_s > 6.40 meters.

2. Thermally Stratified Atmosphere

Flow conditions similar to those measured by Malhotra and Cermak (98) were used in the calculation of thermally stratified flows. The temperature of the wall and free stream were maintained at 277.45^{o}K and 322^{o}K respectively for stable stratification, and vice versa for unstable stratification. The concentration source strength was assumed to be equal to that used in the neutral case, C_s = .66 mg/cm-sec. The free stream velocity was likewise assumed to be the same as for the neutral case, U_∞ = 5.15 m/sec.

Comparisons of mean velocity profiles are shown in Figure 9 between the two models for the stable case. Both appear to predict nearly equal mean velocity distributions for the four locations, with only slight deviations in the near wall region of the boundary layer. Boundary layer growth and general shape of the profiles are essentially identical.

Figure 10 shows the non-dimensional temperature distribution as a function of Z/δ_o, where δ_o is the boundary layer thickness obtained from the initial velocity profile. Little variation is seen to exist between the profiles. The rate equation model and the turbulence kinetic energy

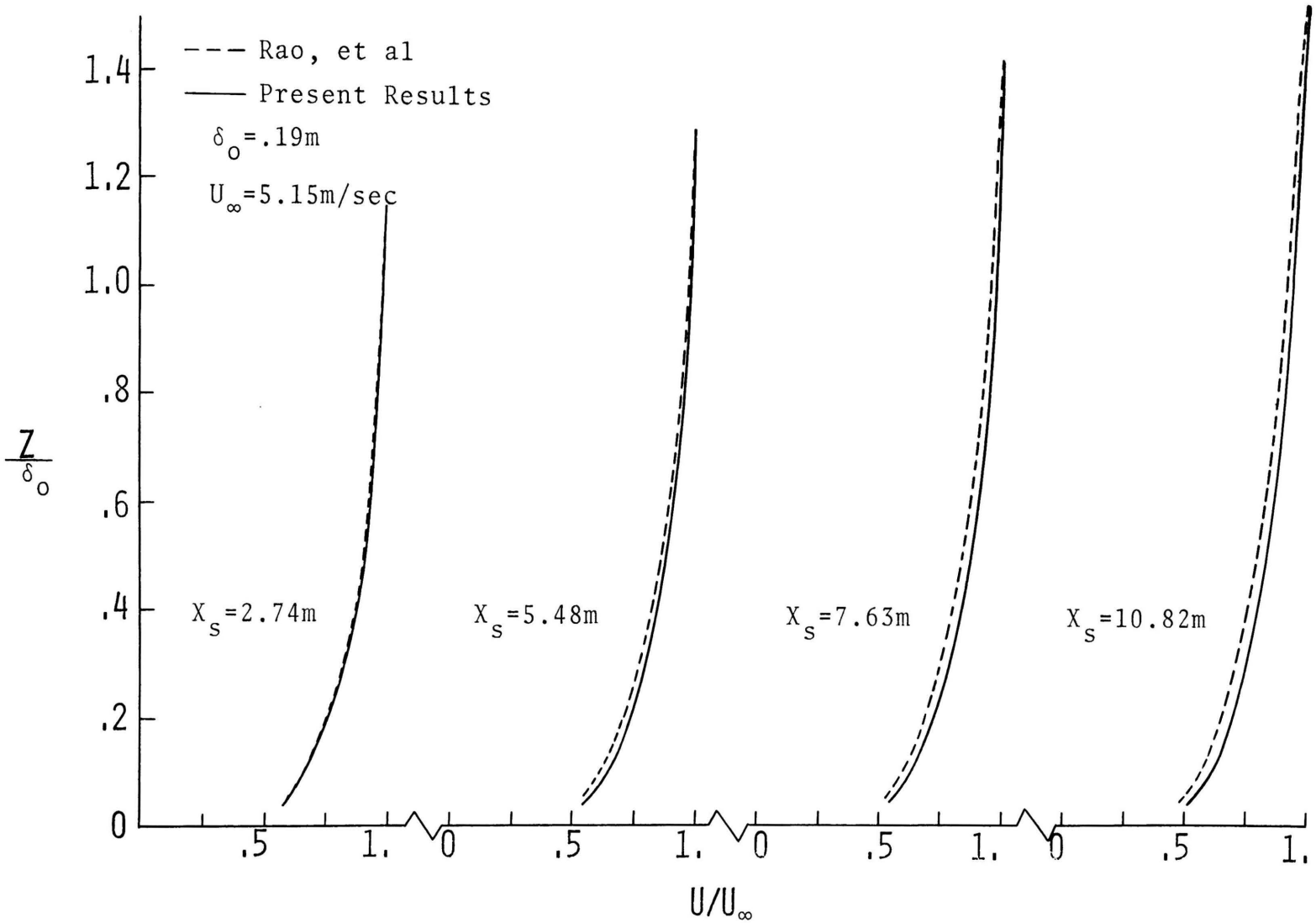

Figure 9. Comparison with Rate Equation Model in Predicting Velocity in a Stable Atmosphere

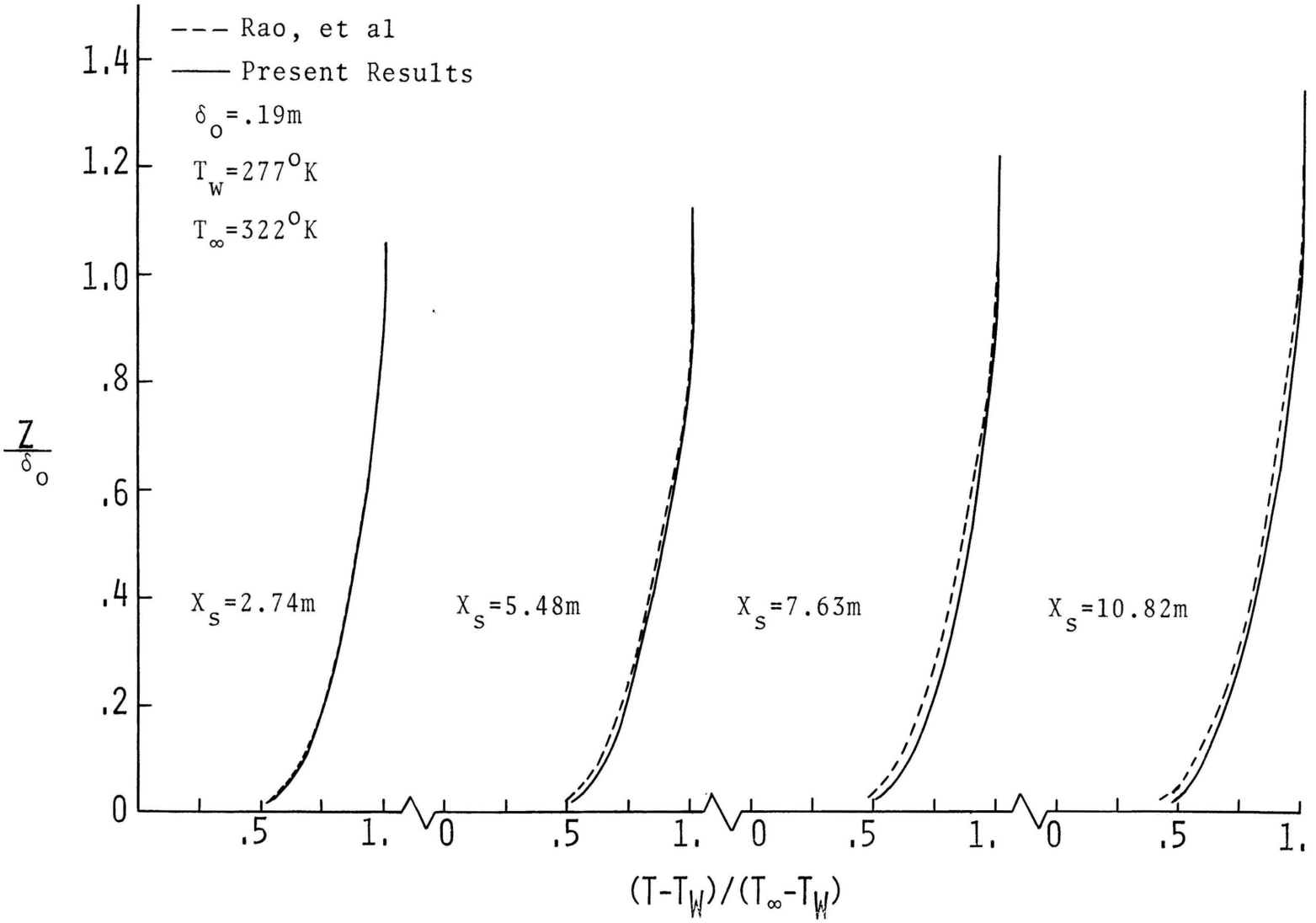

Figure 10. Comparison with Rate Equation Model in Predicting Temperature in a Stable Atmosphere

model both appear capable of predicting realistic temperature distributions characteristic of a stable atmosphere.

Mean velocity profiles predicted by the two models are shown in Figure 11 for an unstable condition. The distributions of mean velocity are seen to deviate slightly near the vicinity of the wall, but tend to become similar in value as the upper region of the boundary layer is approached. Boundary layer growth and thickness likewise appear to be equal.

Distributions of mean temperature in Figure 12 for the unstable case show similar deviations in the region near the wall for the velocity profiles, with subsequent alteration to nearly equal values in the upper region. This slight variation is attributed to the use of different mixed Prandtl numbers for the two models.

Concentration profiles are shown in Figures 13a and 13b for both unstable and stable conditions. The effect of buoyancy is seen to be quite significant in controlling the rate of diffusion of concentration. This is due principally to an increase of turbulence production in the unstable case, resulting in a more rapid dispersion of concentration, as compared to a decrease in production associated with a stable atmosphere. This can be seen in the turbulence kinetic energy equation, equation (3-43) where the gradient Richardson number, R_i, is negative for unstable conditions, and positive for stable conditions. Only minor variations are seen to exist in the predictions when using either model for the exchange coefficient. Readjustment of the

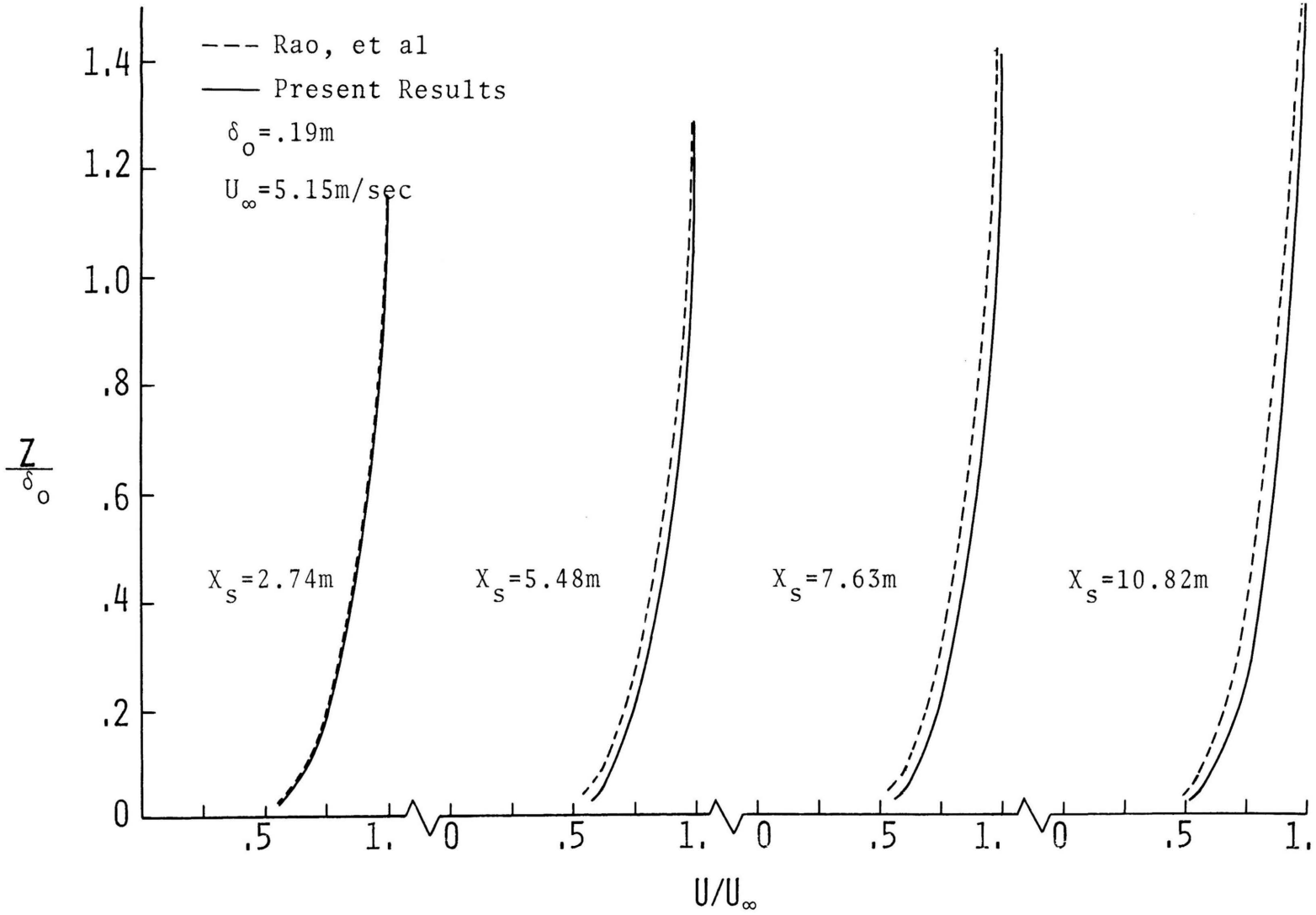

Figure 11. Comparison with Rate Equation Model in Predicting Velocity in an Unstable Atmosphere

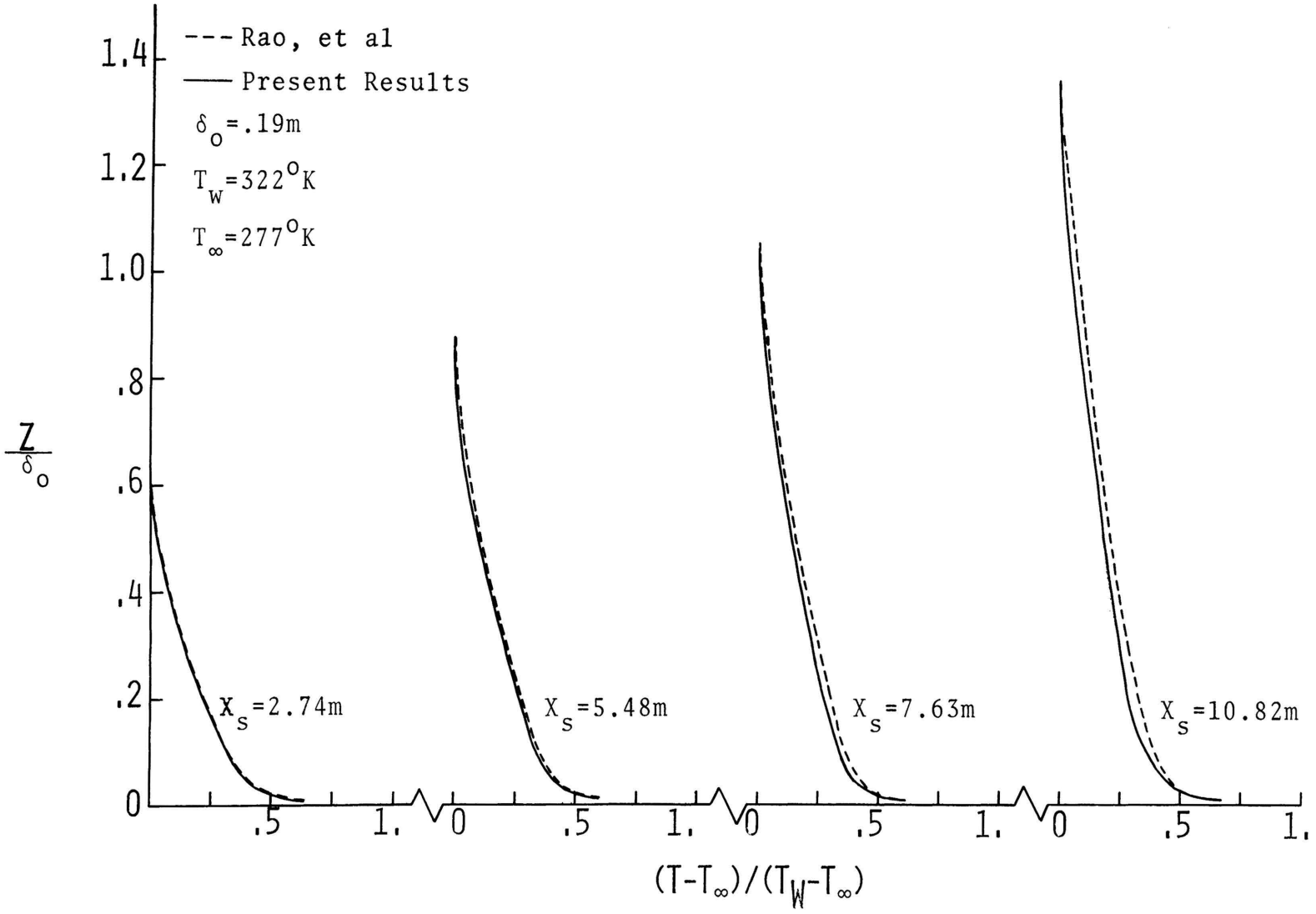

Figure 12. Comparison with Rate Equation Model in Predicting Temperature in an Unstable Atmosphere

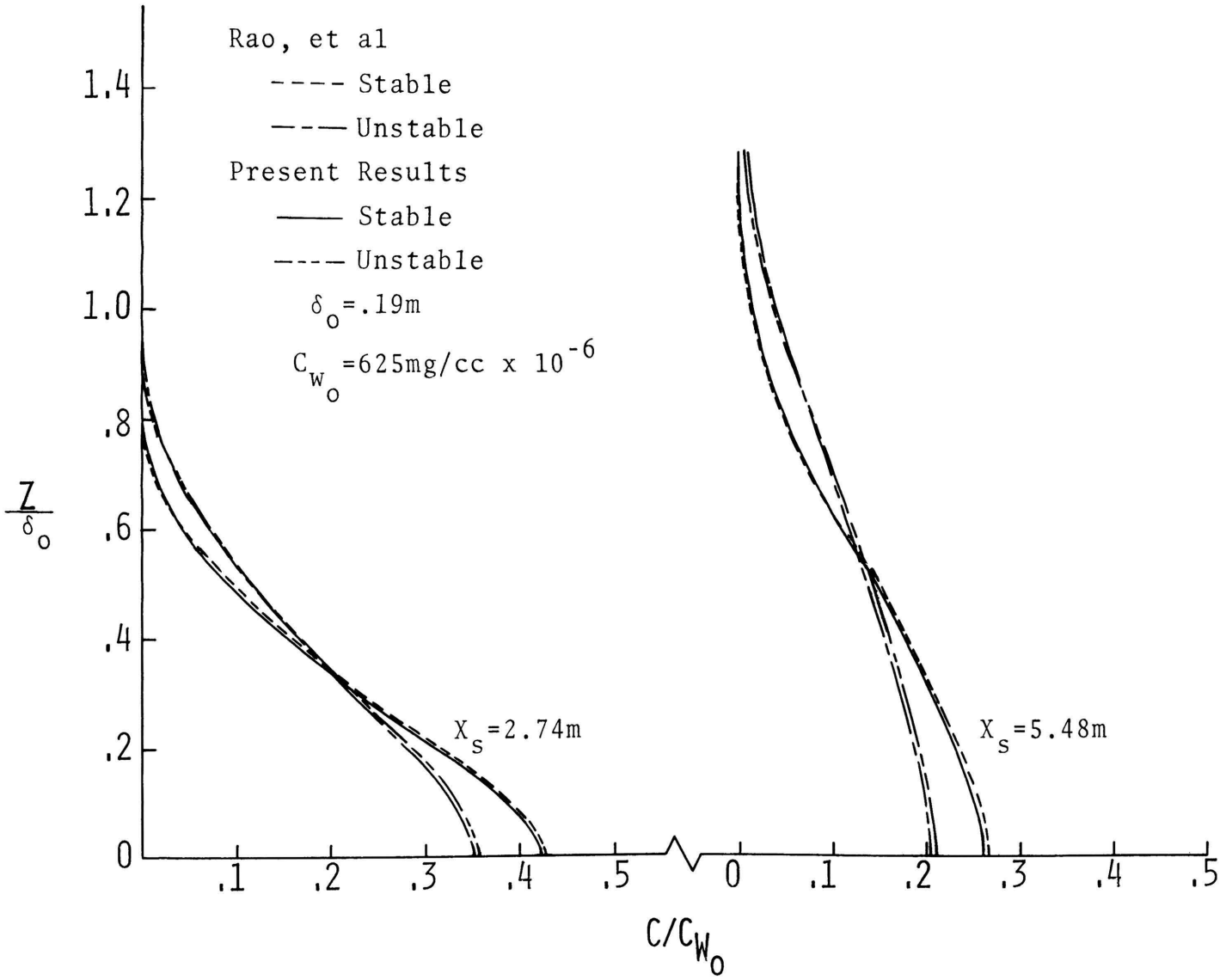

Figure 13a. Comparison with Rate Equation Model in Predicting Concentration Distribution in a Thermally Stratified Atmosphere: X =2.74 - 5.48 meters

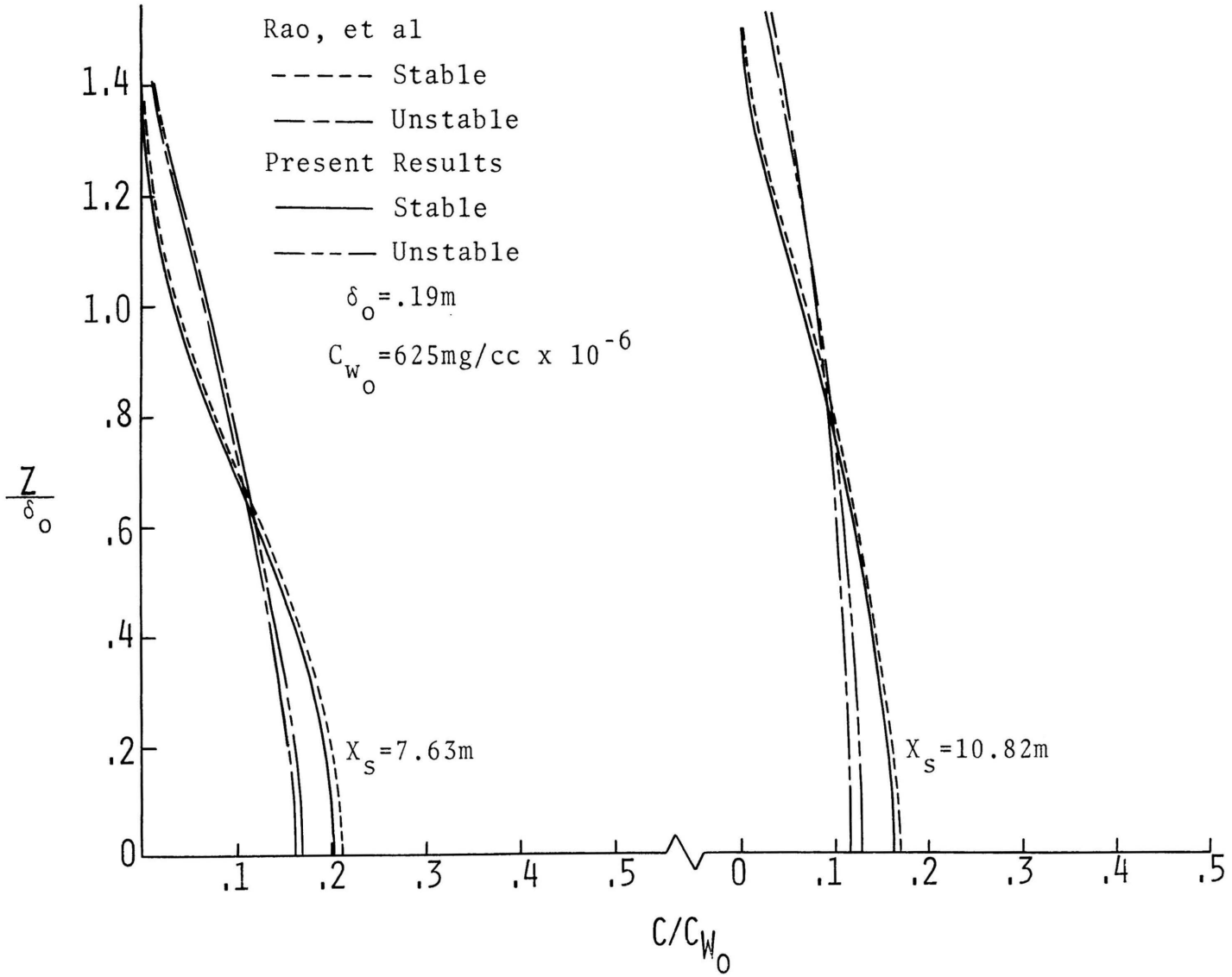

Figure 13b. Comparison with Rate Equation Model in Predicting Concentration Distribution in a Thermally Stratified Atmosphere: X_s=7.63 - 10.82 meters

mixed Schmidt number leads to slightly closer approximat-tions to the surface values for concentrations obtained from the rate equation model. However, since the adjustment provided only minor improvement, the concept of maintaining a constant mixed Schmidt number for all flow conditions seemed reasonable.

Significant differences in the predictions were expected because of the dissimilarity of the two models in describing the exchange coefficient of momentum. However, both produce almost exact results. The concept of using a very simple model related to the turbulence kinetic energy, as compared to the more complicated rate equation model, appears to be quite advantageous. However, additional verification of the model is needed. Consequently, a series of comparisons are made with wind tunnel data.

A summary of experimental investigations used in this study is given in Table II with regard to stratification conditions. The experimentally measured data are listed for each case.

B. Comparison With Experiment

A number of experimental tests have been made under neutral flow conditions in atmospheric wind tunnels, but only a few cases contain turbulence kinetic energy data pertinent to the eddy coefficient model employed here. Similar investigations of experimental work in thermally stratified flows disclose even less available data. While one case contained turbulence kinetic energy and shear

TABLE II: SUMMARY OF WIND TUNNEL EXPERIMENTS

Condition	Reference	Method of Simulation	Data Measured
Neutral	Schon & Mery	air injection	U,Q,τ
	Malhotra	initial rough surface	U,C
	Poreh & Cermak	long test section	U,C
Stable	Arya	long test section	U,T,Q,τ
Unstable	Reynolds, et al	*	U,T
	Malhotra	initial rough surface	U,T,C
	Wieghardt	*	U,T

*wind tunnels were not altered to simulate atmospheric boundary layers

stress data for stable conditions, it did not contain any concentration results. Unstable atmospheres, while investigated more extensively than the stable case, did not provide any turbulence data. The consequence of these investigations leads to the development of a numerical model which appears to be adequate in analyzing neutral atmospheric phenomena, but essentially unverified in thermally stratified flow. In those cases where turbulence kinetic energy is not present, an initial turbulence kinetic energy profile was assumed by using the friction velocity, u*, and the non-dimensional Klebanoff (65) turbulence kinetic energy profile, Figure 5. Verification of results could only be tested by comparing downstream velocity and turbulence kinetic energy profiles, if available, with the experimental data.

1. Neutral Atmosphere

Preliminary investigations were made in neutrally stratified flows by comparing the numerical results with the experimental work of Schon and Mery (20), Poreh and Cermak (21), and Malhotra (28).

The measurements made by Schon and Mery (20) were obtained by injecting air upstream of a boundary layer in order to artificially increase the layer thickness. At a certain distance downstream of the injection zone, the boundary layer was found to represent a natural boundary layer but with its thickness altered. Maintaining a free stream velocity of U_∞ = 6.50 m/sec, mean velocity, turbulence intensities, and Reynolds stress profiles were

reported for downstream locations ranging from 5 to 9 meters from the injection zone. The velocity profiles were found to nearly represent seventh root velocity distributions. Because of this similarity, the initial velocity distribution in the numerical prediction scheme was represented by the seventh root power relation at X_s = 5.08 meters. Figure 14 shows the comparison between the predicted velocity profiles and the experimental data. The agreement appears to be very good, particularly in terms of the boundary layer development and shape of the profiles.

The turbulence kinetic energy profiles are compared in Figure 15. A non-dimensional Klebanoff (65) profile, as shown in Figure 5, was used to generate the initial turbulence kinetic energy at X_s = 5.08 meters based upon an extrapolated wall value from Schon and Mery (20). An additional case was run using the measured data, but proved to be only slightly more accurate than the assumed profile for the three succeeding downstream locations. The initially assumed turbulence kinetic energy profile is considerably different from the measured data; this is due to the fact that the assumed profile is based upon a fully developed turbulent boundary layer profile. The measured data appears to still show the influence of injection at X_s = 5.08 meters, but begins to dampen rapidly at X_s = 6.08 meters, appearing to adjust to the numerically simulated profiles.

The turbulence kinetic energy is conserved throughout the entire boundary layer; therefore, the gain or loss of

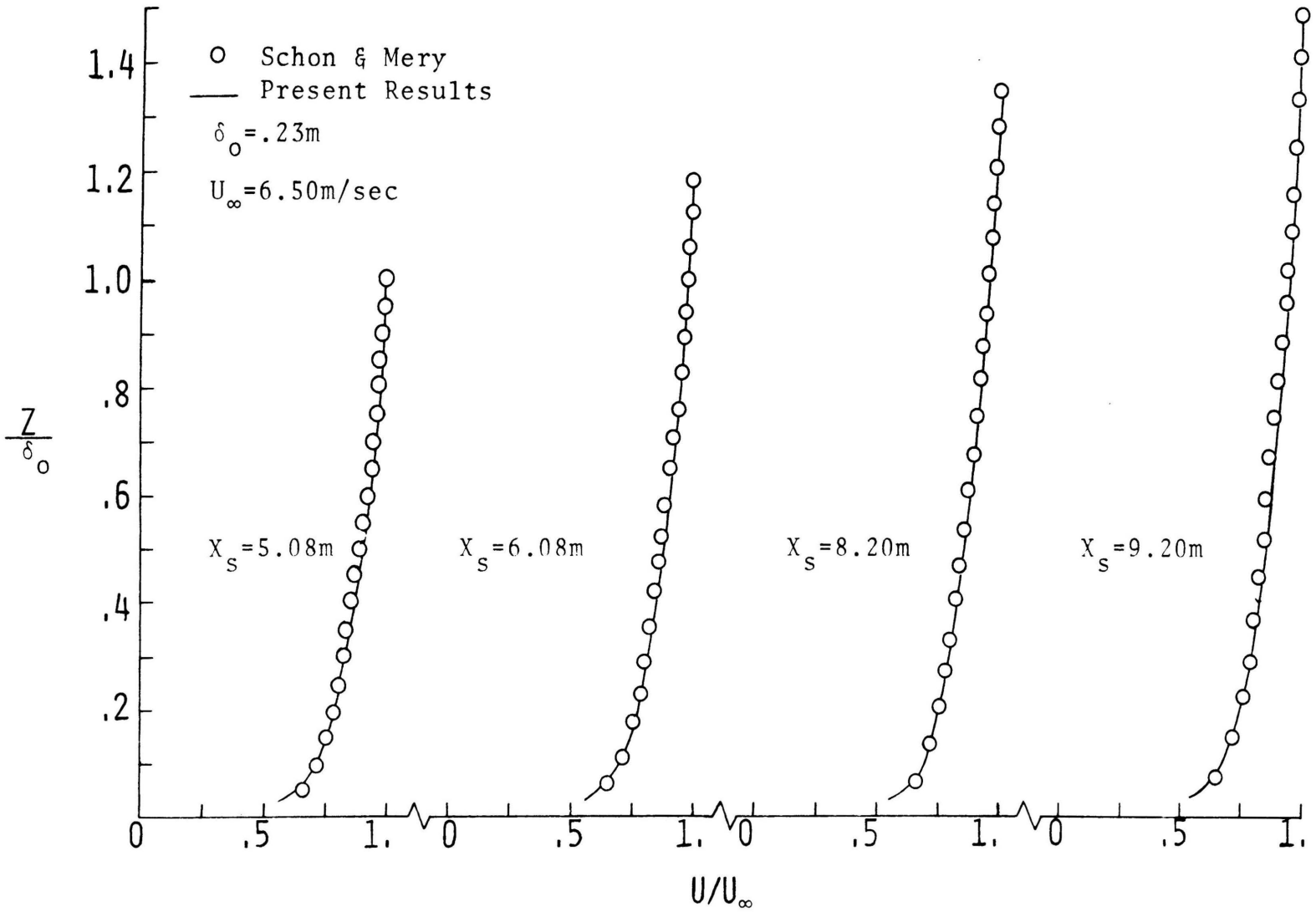

Figure 14. Comparison between Predicted Velocity and Experiment in a Neutrally Stratified Turbulent Boundary Layer

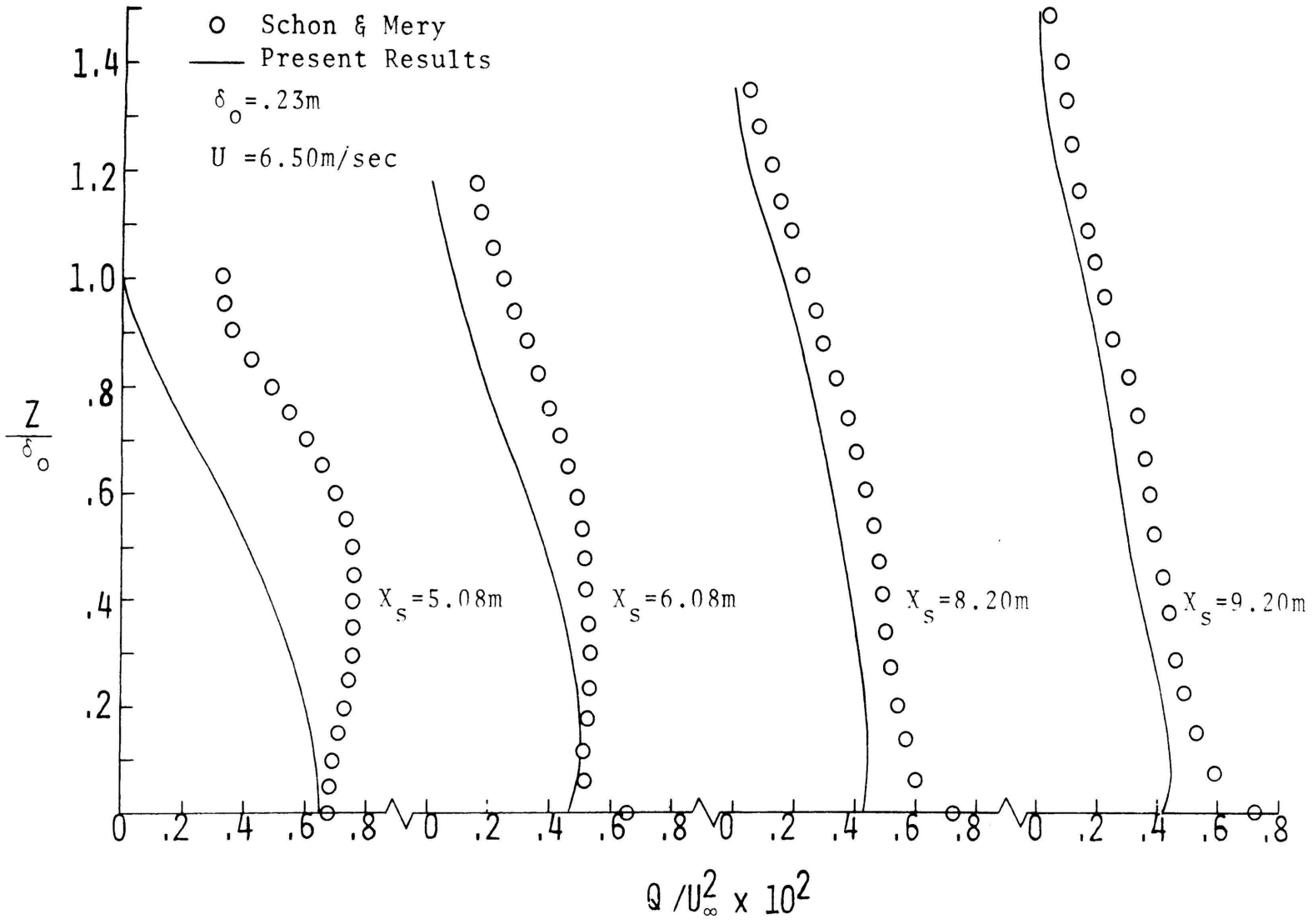

Figure 15. Comparison between Predicted Turbulence Kinetic Energy and Experiment in a Neutrally Stratified Turbulent Boundary Layer

turbulence kinetic energy by convection and diffusion, plus the gain due to production, must balance the loss due to dissipation. Figure 16 shows the energy balance for two downstream locations. A positive value of a quantity represents a gain of energy while a negative value denotes a loss. The main contribution to the energy balance is made by the production and dissipation terms as the wall region is approached. The unusually high values for the convection and diffusion at X_s = 6.08 meters is due to the initial starting conditions obtained from the non-dimensional Klebanoff (65) profile for turbulence kinetic energy. Farther downstream the contribution of convection and diffusion is negligible, except near the outer edge of the layer where the gain by turbulence diffusion counterbalances the loss by convection. This implies that a transfer of energy occurs by turbulence diffusion from the inner part of the boundary layer towards the outer part. This was similarly discussed by Hinze (39) in analyzing boundary layer flow along a smooth wall with zero pressure gradient.

The diffusion of passive concentration from a steady line source within a neutral, two-dimensional turbulent boundary layer was investigated using measurements reported by Poreh and Cermak (21) for mean velocity and mean concentration. The initial data obtained at X_s = .91 meter was used to produce profiles at four downstream locations ranging from 1.5 to 6.4 meters for an ambient velocity of 2.74 m/sec. The non-dimensional velocity profiles are shown

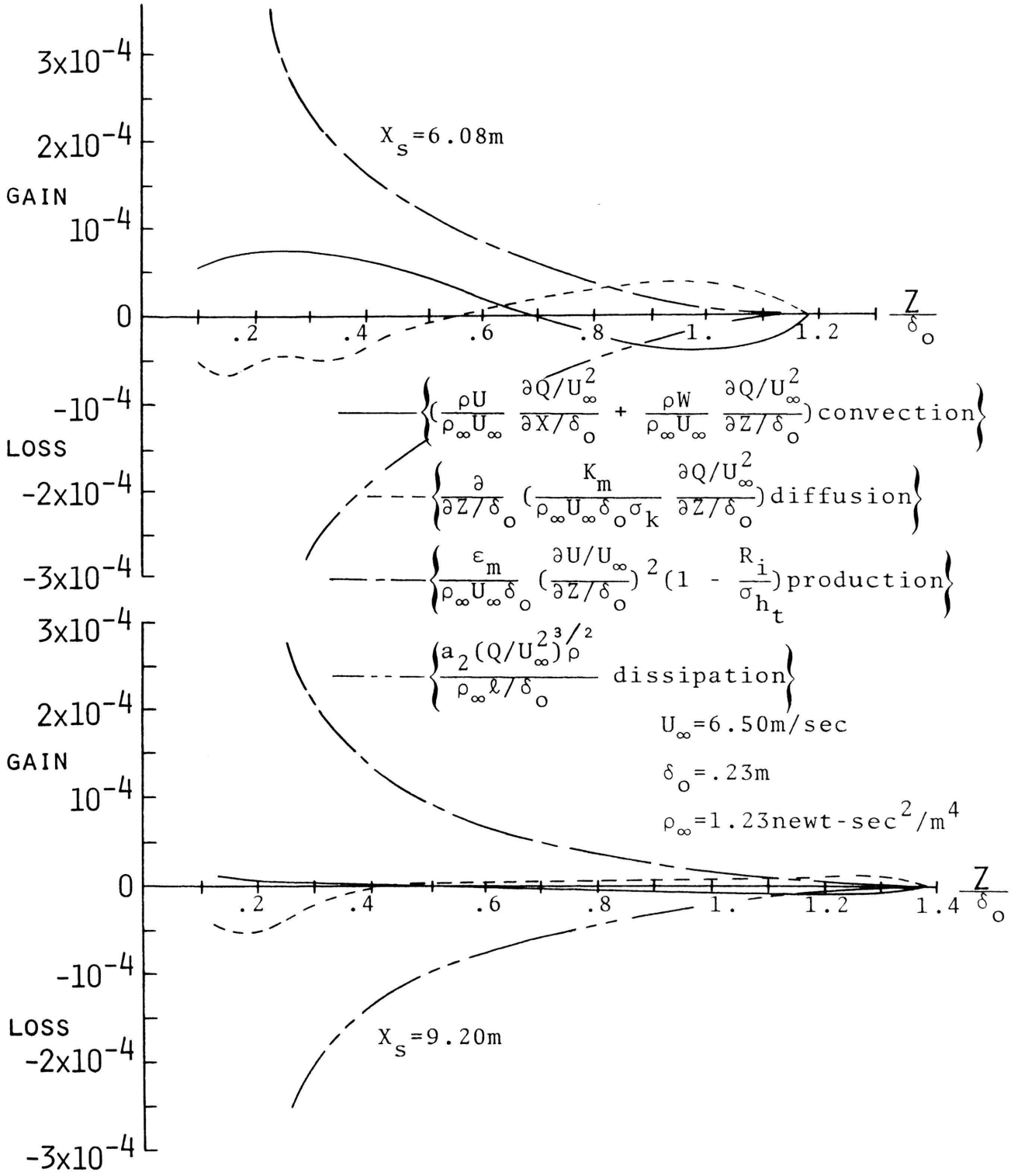

Figure 16. Balance of Turbulence Kinetic Energy in a Neutrally Stratified Turbulent Boundary Layer

in Figure 17. The results of the predicted velocity profiles appear to be in excellent agreement with the measured data.

Anhydrous ammonia gas was used as the diffusing quantity, with mean concentration profiles being measured at the same downstream locations from the source as the velocity field. Figure 18 shows the predicted concentration profiles in comparison with the experimental results. The concentration field is non-dimensionalized by the wall concentration value at X_s = .91 meter, where the subscript, W_o, denotes initial wall value. Beginning with the initial data measured at X_s = .91 meter, the numerical results appear to adjust to the correct shape and magnitude of the experimental data with reasonably good accuracy. The slight variation in attenuation of the ground concentration is due in part to the assumption of a constant mixed Schmidt number, σ_c. Limted turbulence intensity measurements were made at several locations, but did not prove to be sufficient in detail for analyzing the turbulence kinetic energy.

The synthetic line source data obtained by Malhotra (28) was used as an additional reference in order to verify the existing assumptions regarding neutral atmospheric flow. Although the turbulent diffusion of ammonia gas was measured from a point source, numerical integration by Malhotra (28) showed the concentration distributions to be very similar to actual line source data. The mean velocity and concentration profiles were measured at four downstream locations from the source using constant temperature hot

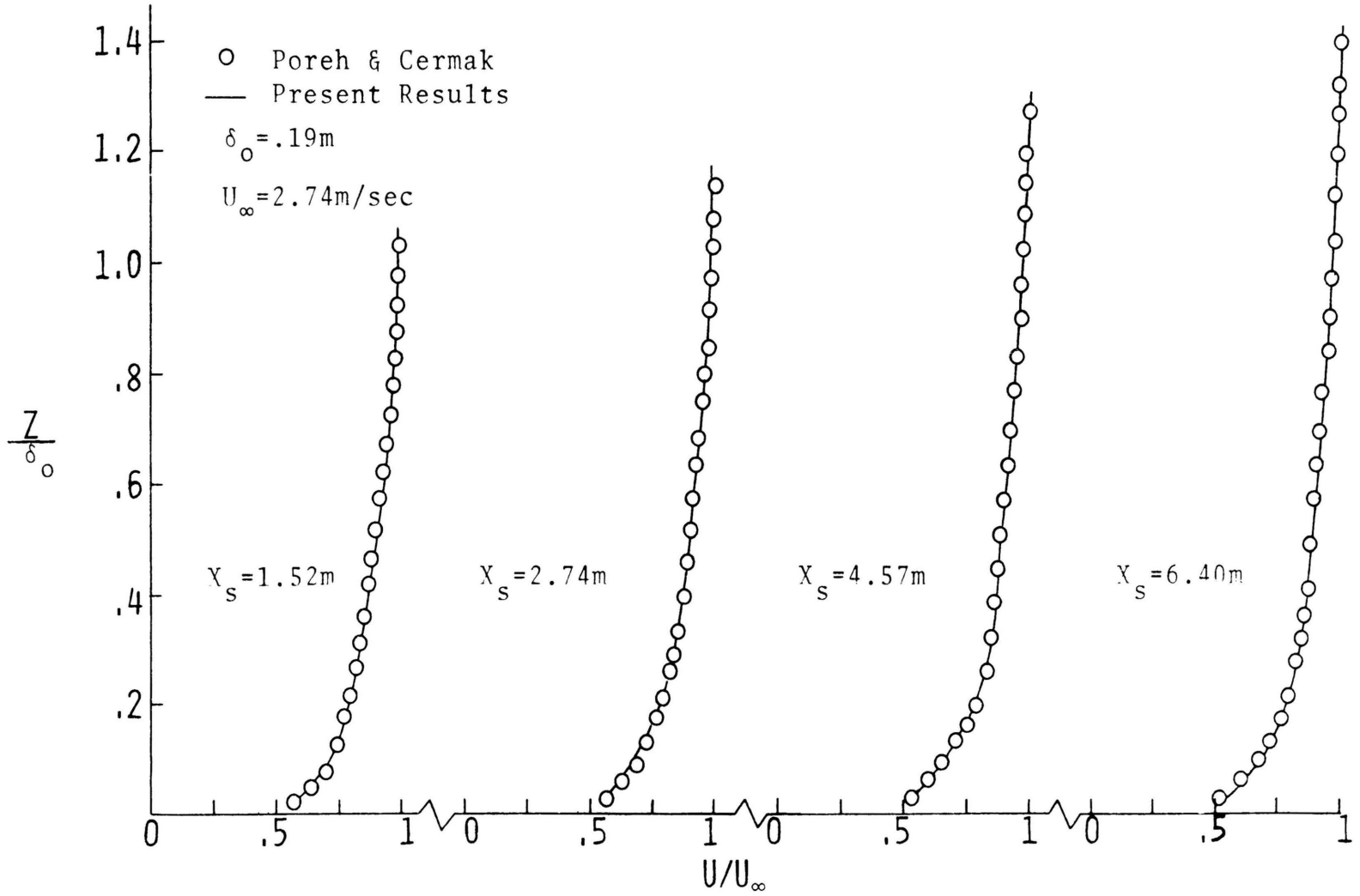

Figure 17. Comparison between Predicted Velocity and Experiment in a Neutrally Stratified Turbulent Boundary Layer

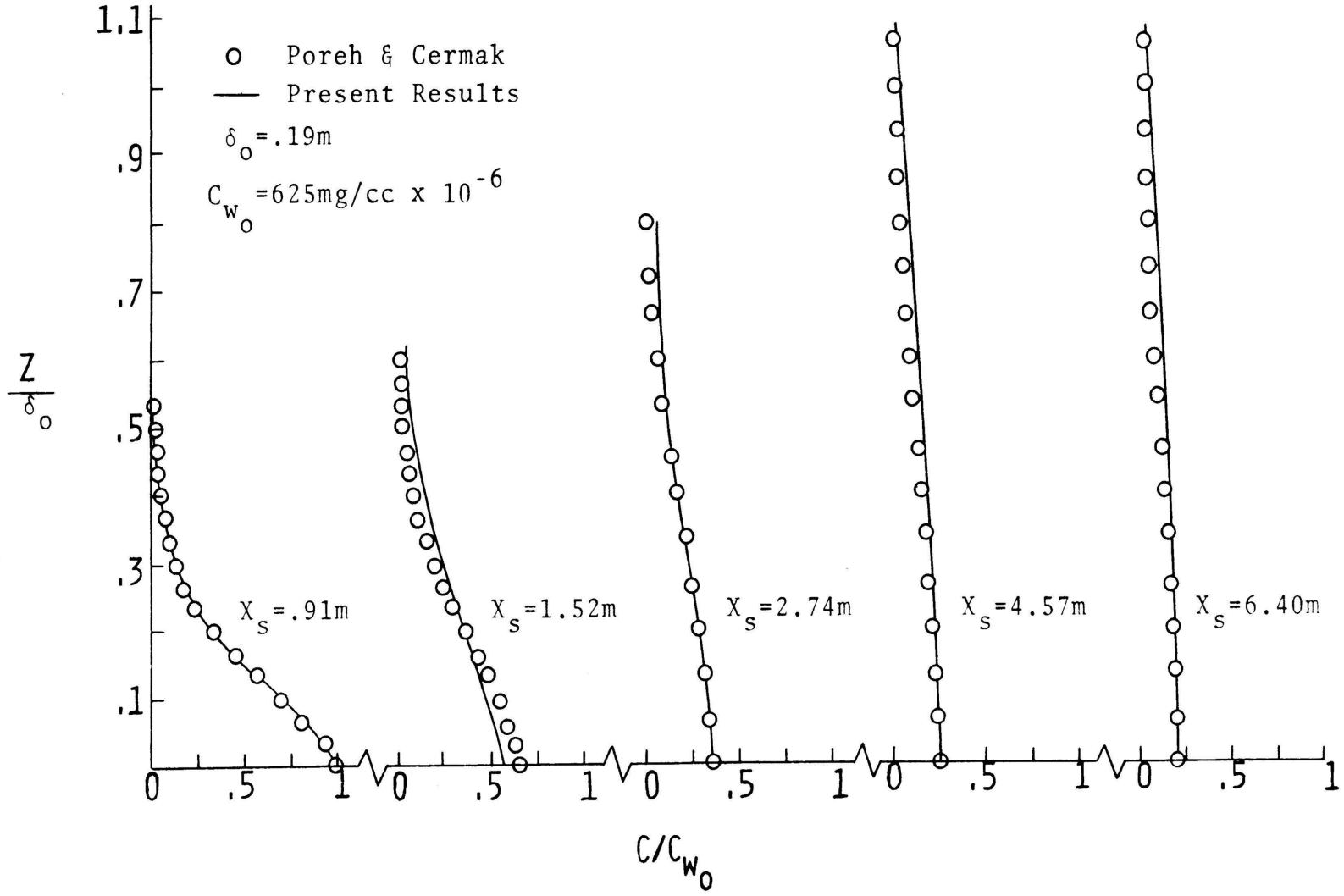

Figure 18. Comparison between Predicted Concentration and Experiment in a Neutrally Stratified Turbulent Boundary Layer

wire anemometry and gas sampling probes.

The comparison between the numerical results and the mean velocity profile data is shown in Figure 19. The starting condition for the numerical velocity profile was obtained from a 1/5.5 power law relation for the mean velocity field, which closely approximated the data of Malhotra (28). Agreement is good between the measured and predicted profiles, especially in calculating the boundary layer thickness and velocity profiles near the wall.

The concentration data at X_s = .30 meter was used as the initial condition for the concentration field, as shown in Figure 20, where C_{W_o} is the initial wall concentration. A slight underprediction of concentration occurs at X_s = .61 meter, but then begins to readjust to where the concentration is overpredicted at X_s = 2.13 meters.

An energy balance, similar to that made in Figure 16 for Schon and Mery (20), is shown in Figure 21 for two downstream locations. In this case the production and dissipation appear to be the significant terms in maintaining the energy balance throughout the boundary layer. Convection and diffusion are negligible except near the outer region where the diffusion contributes to a gain of turbulence kinetic energy, balancing the loss due to convection. The energy balance at X_s = 2.13 meters shows only a small change in magnitude from that at X_s = .61 meter, indicating that the boundary layer is nearly fully developed. A closer approximation to the actual starting conditions accounts for

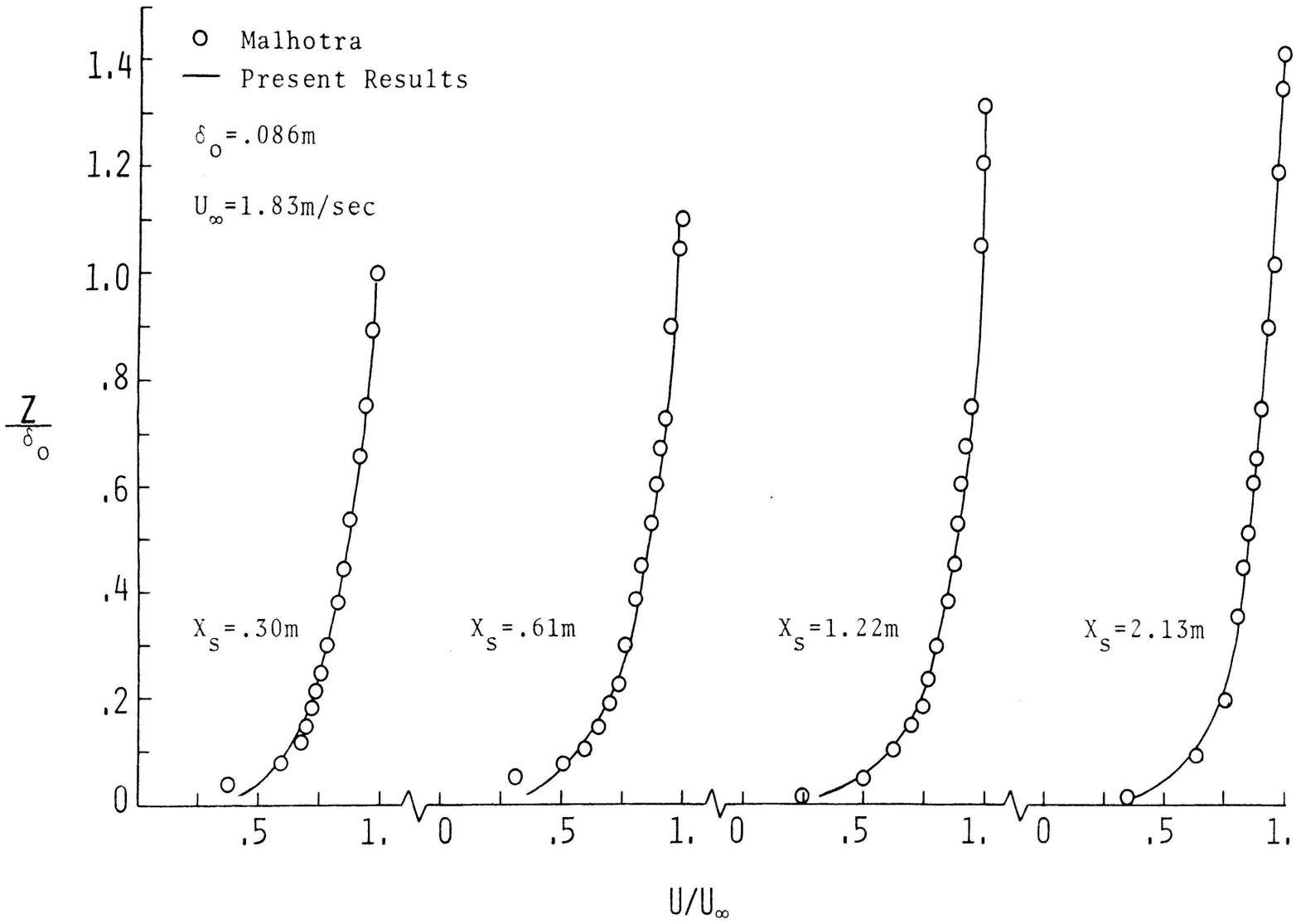

Figure 19. Comparison between Predicted Velocity and Experiment in a Neutrally Stratified Turbulent Boundary Layer

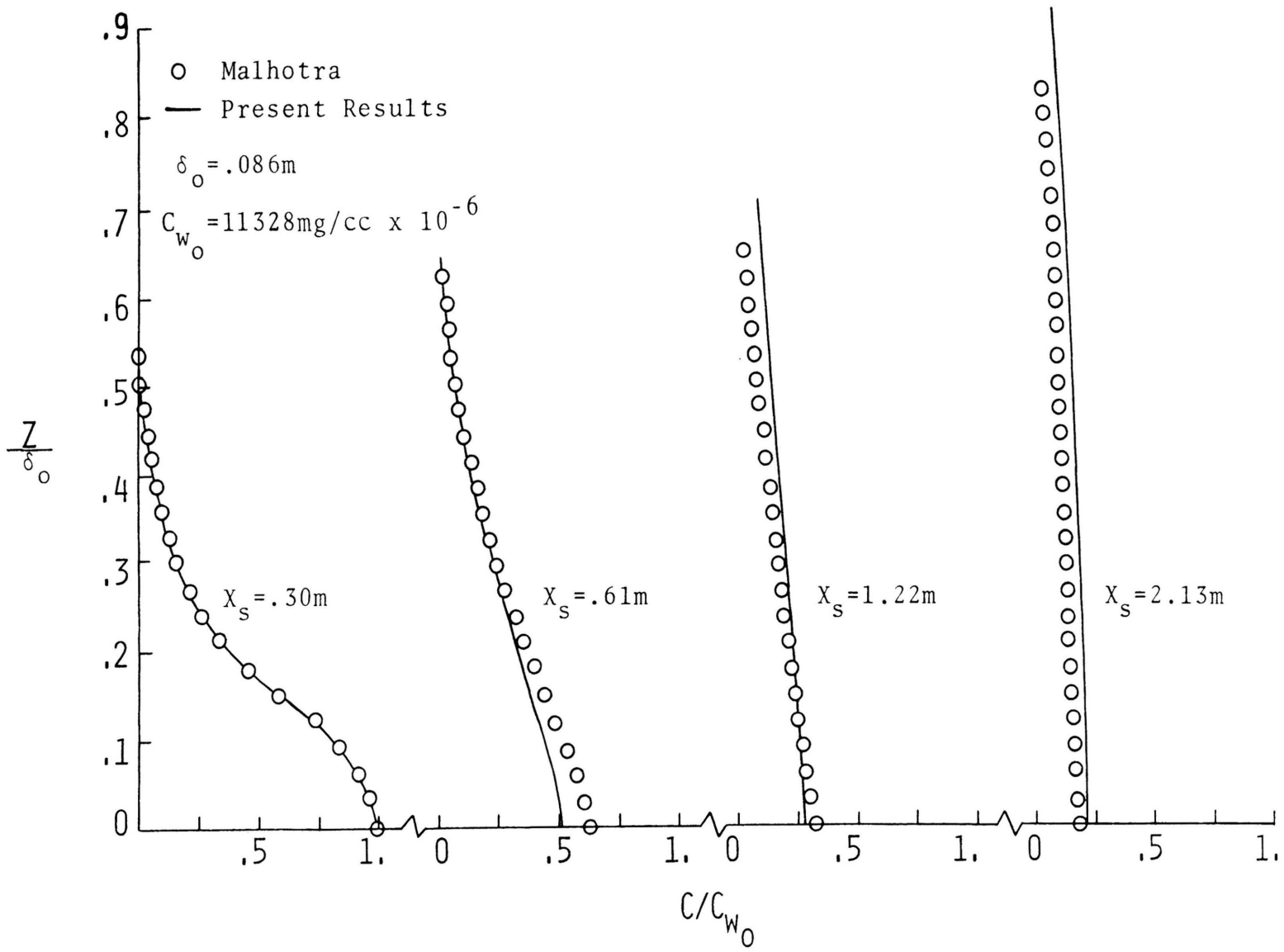

Figure 20. Comparison between Predicted Concentration and Experiment in a Neutrally Stratified Turbulent Boundary Layer

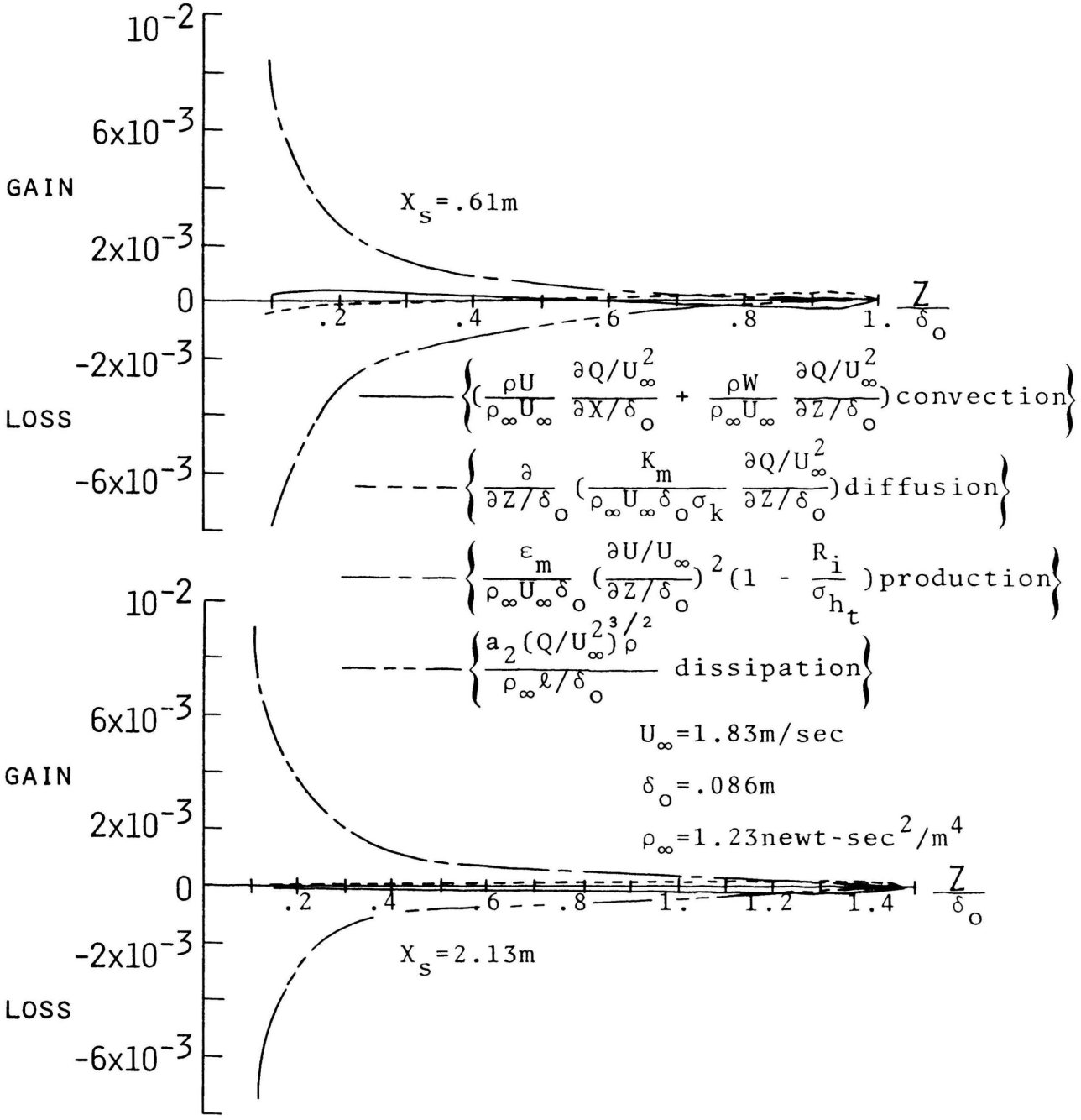

Figure 21. Balance of Turbulence Kinetic Energy in a Neutrally Stratified Turbulent Boundary Layer

the minimal change in the energy balance, as compared with the results from Schon and Mery (20).

2. Thermally Stratified Atmosphere

Based upon the results obtained from the neutral cases, the phenomenological model was used in an effort to predict flow phenomena in thermally stratified atmospheric boundary layers. The investigation was divided into two categories: stable and unstable stratified flows. Although buoyancy has an influential effect upon the turbulence kinetic energy, the relations formulated in the neutral case were used throughout in order to ascertain the feasibility of using a constant set of empirical data to avoid continuous alterations of the governing formulae.

a. Stable Atmosphere

Only one reference proved to be of any value in analyzing stably stratified flow data with the present numerical model. Using the Colorado State meteorological wind tunnel facilities, Arya (25) measured mean velocities, temperatures, and turbulence kinetic energy data at two downstream locations. Unfortunately, no concentration data was measured.

A comparison between the experimentally measured velocity profiles and the predictions are shown in Figure 22. A 1/7 power law assumption was used at X_s = 12.2 meters to estimate the velocity profile in the numerical scheme, and allowed to progress downstream to the two locations reported by Arya (25). Even though the initial boundary layer thickness, δ_o, was relatively large, the predicted velocity

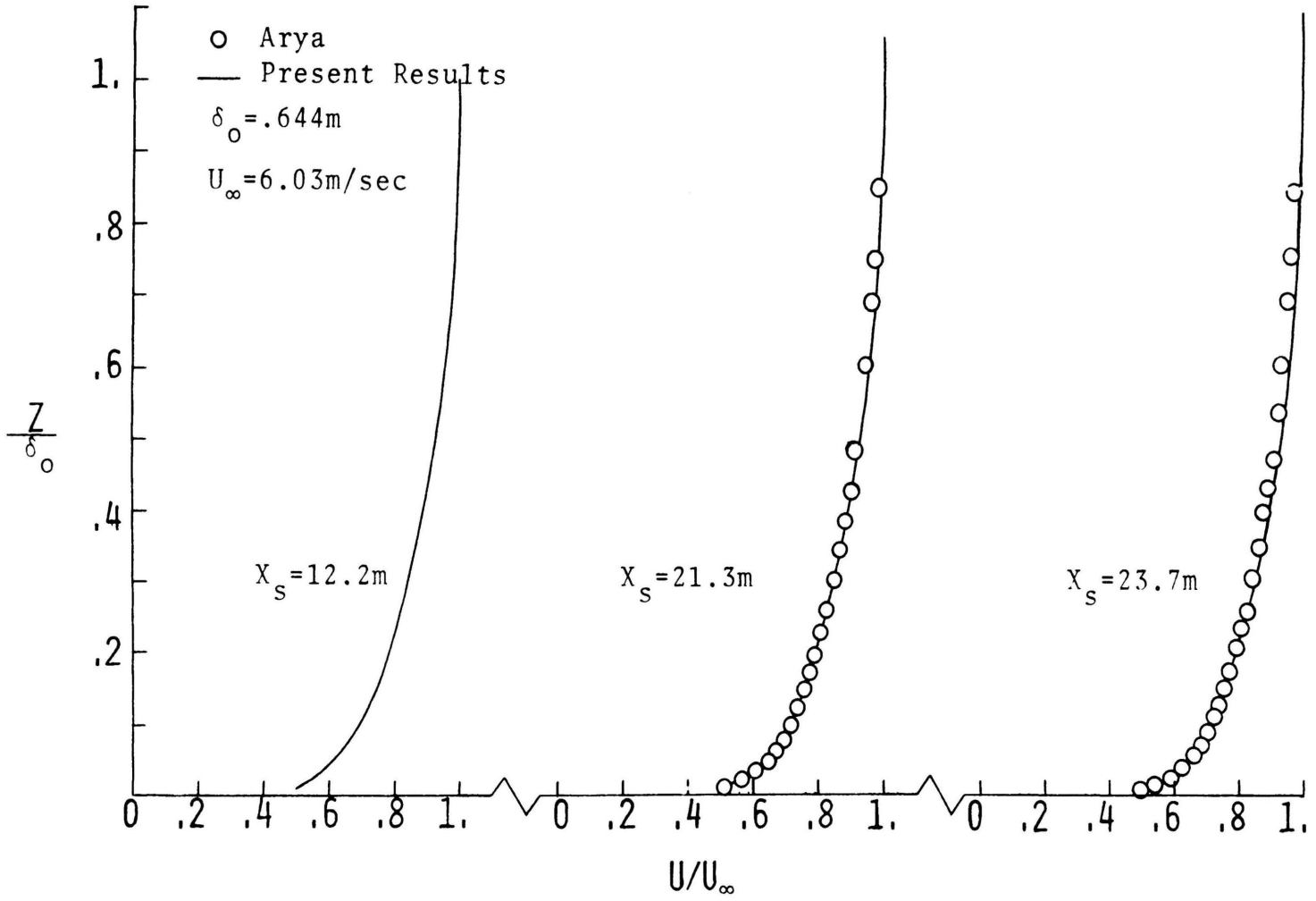

Figure 22. Comparison between Predicted Velocity and Experiment in a Stably Stratified Turbulent Boundary Layer

profiles show very good approximations as to shape and boundary layer thickness at X_s = 21.3 meters and X_s = 23.7 meters.

Figure 23 shows the non-dimensional temperature as a function of the hydrodynamic boundary layer thickness at X_s = 12.2 meters for both Arya's data and the predicted temperature profile. The initial temperature distribution was given by T_W at Z = 0 and T_∞ for Z greater than 0. The thermal boundary layer began developing at X_s = 12.2 meters. Comparison of the experimental data with the numerical results at the two downstream locations appear to be good. Prediction of the thermal boundary layer thickness, although indicated by Z/δ_o, is seen to be reasonable from the shape of the temperature profile. Arya (25) assumed δ_t/δ_o = .65, while the numerical model gave δ_t/δ_o = .70 at X_s = 23.7 meters.

The most noticeable comparison between experiment and prediction is seen in Figure 24 for the turbulence kinetic energy. Klebanoff's (65) turbulence kinetic energy profile was used to start the numerical solution at X_s = 12.2 meters with a_1 = 0.3 for the eddy coefficient of momentum. The wall value for the turbulence kinetic energy was extrapolated from the measured data at X_s = 21.3 meters. The underprediction of turbulence kinetic energy occurring within 10 per cent of the wall, at X_s = 21.3 meters and X_s = 23.7 meters, is to be expected since the eddy coefficient model is based upon a linear assumption for the wall value of turbulence kinetic energy. Once outside the region of maximum turbulence

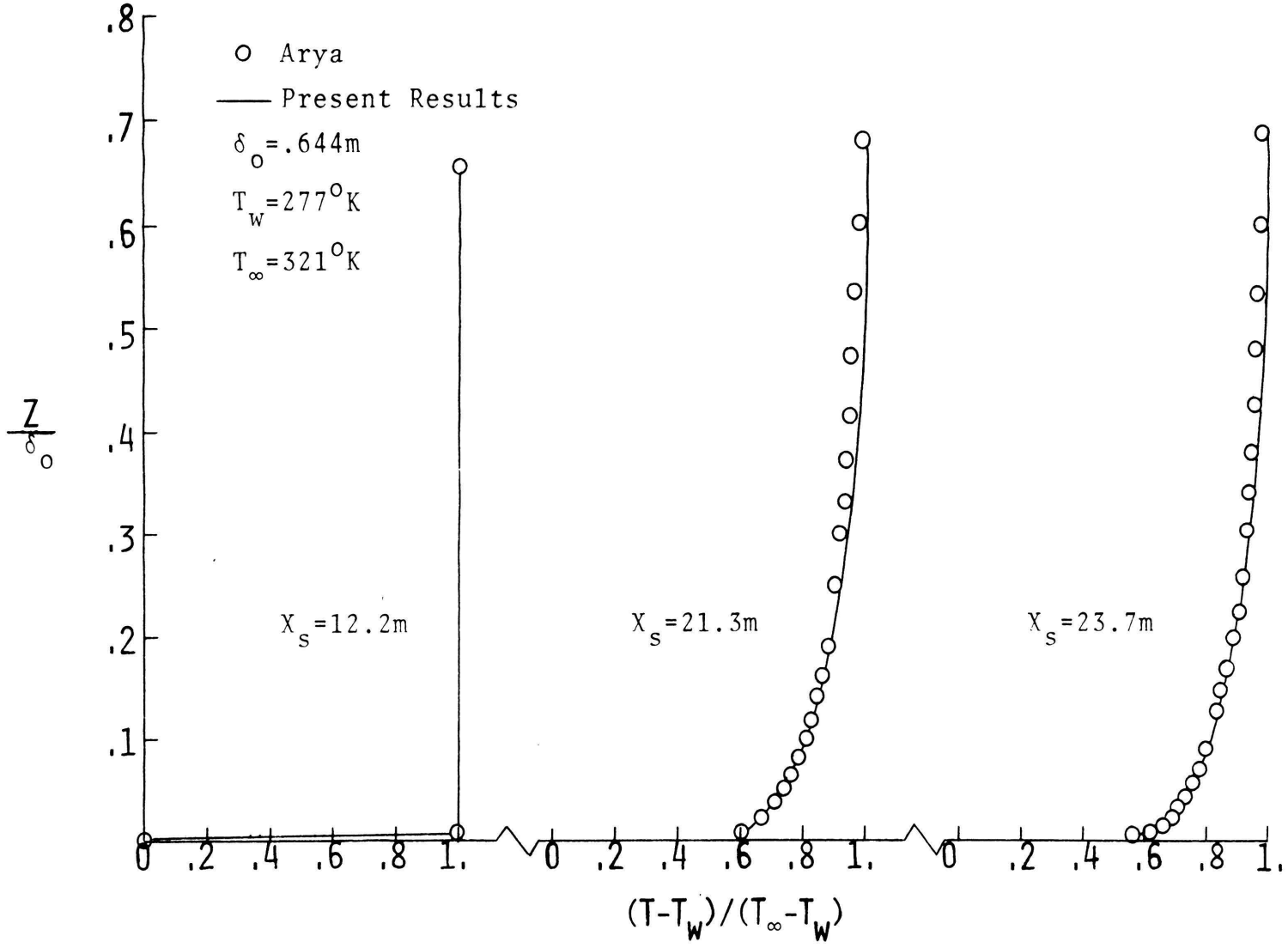

Figure 23. Comparison between Predicted Temperature and Experiment in a Stably Stratified Turbulent Boundary Layer

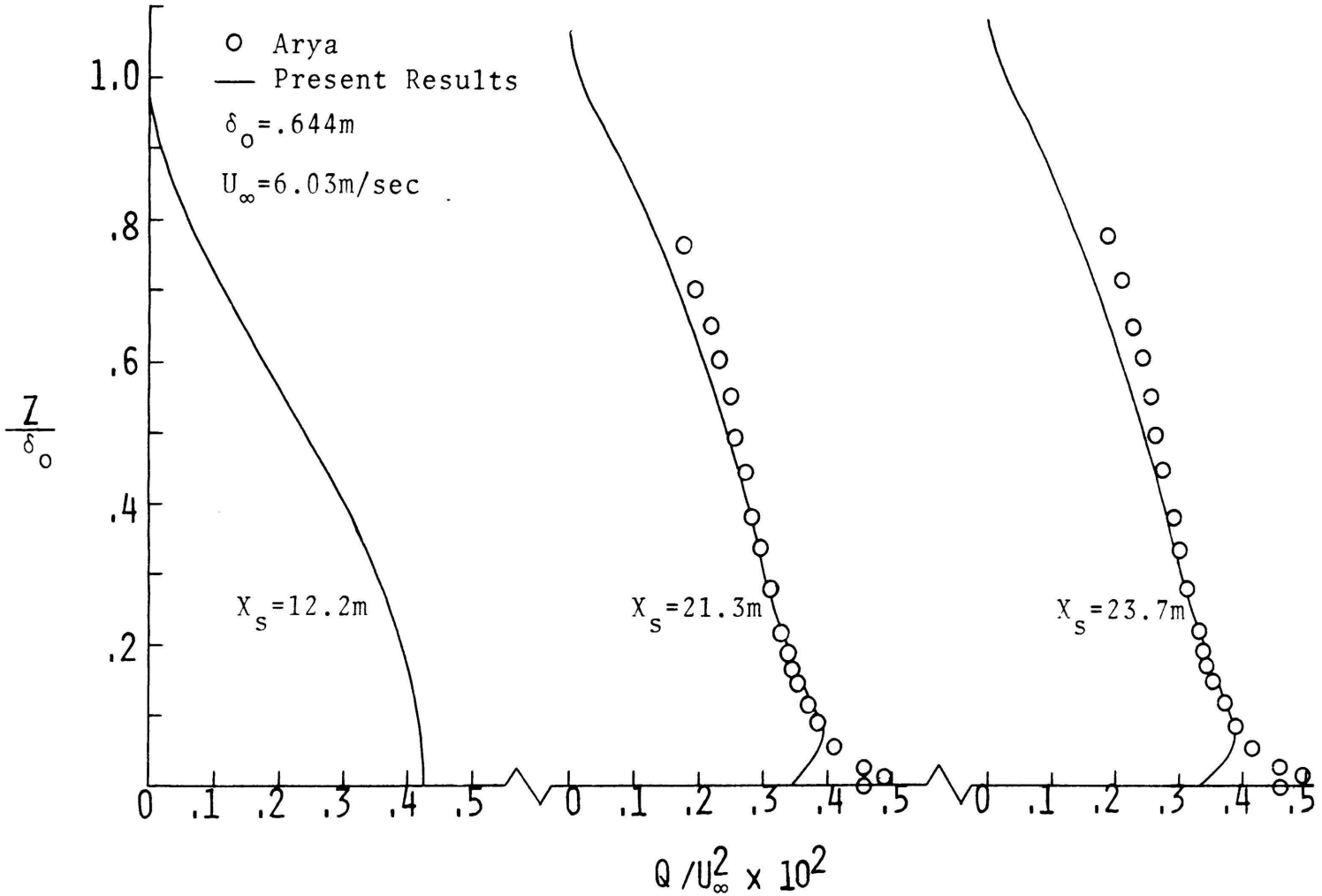

Figure 24. Comparison between Turbulence Kinetic Energy and Experiment in a Stably Stratified Turbulent Boundary Layer

kinetic energy, the predicted profiles begin to closely approximate the experimental data. The slight underestimation of the profiles for Z/δ_o greater than .50 is due to the assumption that the outer edge of the boundary layer is free of any turbulence, hence causing the turbulence kinetic energy to approach zero for Z/δ_o greater than 1. Accurate approximations for the turbulence kinetic energy under thermally stratified conditions using the Nevzglajdov model may become more feasible as additional data becomes available.

Energy balances at X_s = 21.3 meters and X_s = 23.7 meters are shown in Figure 25. A very slight decrease is seen to exist in the production and dissipation terms as the flow progresses downstream from X_s = 21.3 meters. This fact, along with the negligible contribution of the diffusional and convection terms and the similarities in the velocity profiles, indicate that the boundary layer is well developed. This condition was similarly observed by Arya (25).

Because the gradient Richardson number serves as a quantitative measure of the thermal stability, the distribution of R_i is plotted as a function of Z/δ in Figure 26. Agreement is good between the numerical predictions and the experimental data, especially within the region Z/δ less than 0.1. Since experimental data was not available for Z/δ greater than 0.5, the variation of R_i with Z/δ was plotted only to Z/δ = 0.5. A comparison of the local Richardson number with Z/L, the universal function described by the Monin-Obukhov (44) similarity theory, is

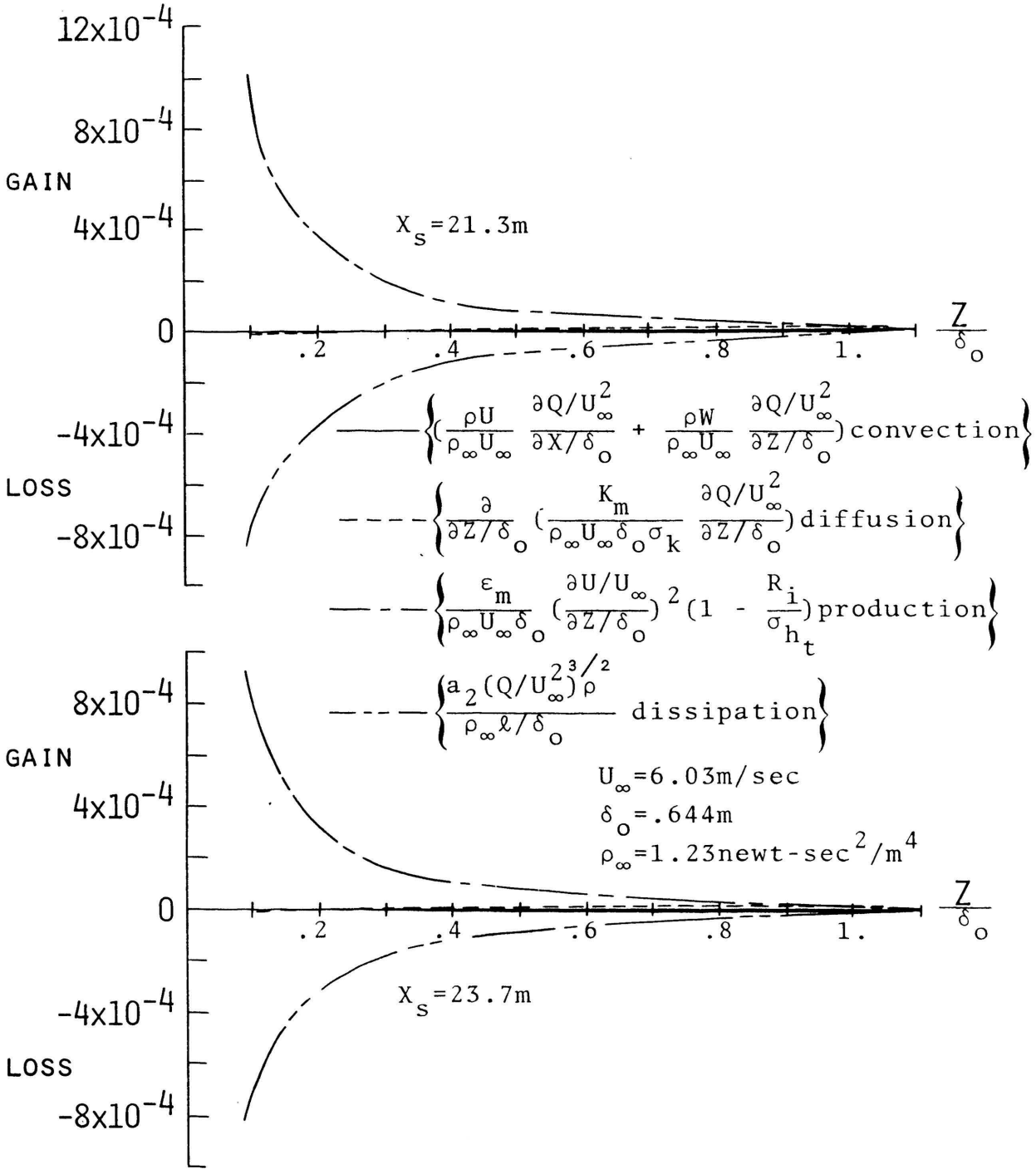

Figure 25. Balance of Turbulence Kinetic Energy in a Stably Stratified Turbulent Boundary Layer

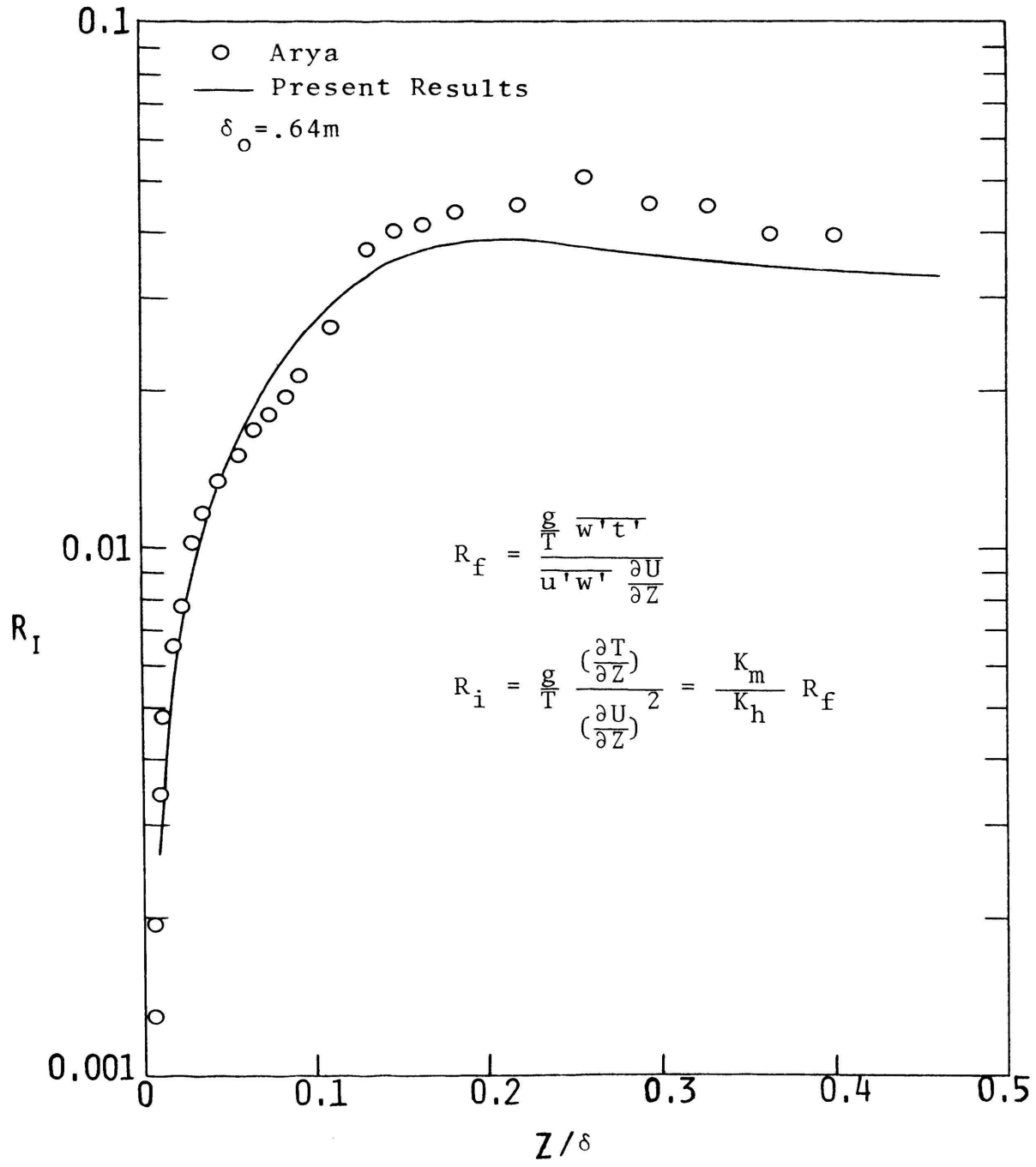

Figure 26. Variation of Richardson Number in a Stably Stratified Turbulent Boundary Layer

made with Arya's (25) data and the atmospheric data of Gurvich, as reported by Arya (25). Figure 27 shows Gurvich's curve to fit the data of Arya and the numerical results reasonable well.

b. Unstable Atmosphere

The data of Reynolds, et al (99), Malhotra (28), and Wieghardt (29) were used to verify the ability of the numerical model to predict flow phenomena in an unstable atmosphere. The data of Reynolds, et al (99) and Wieghardt (29), while not obtained from atmospheric wind tunnels, proved to be significant in formulating the numerical scheme and served as test cases for analyzing more general engineering situations. The experiments by Malhotra (28) were performed in an atmospheric wind tunnel for both neutral and unstable conditions for a ground level point source. Integration of the point source, as in the neutral case, was made in order to obtain synthetic line source plumes.

The experimental results of Reynolds, et al (99) were used to confirm the ability of the numerical scheme to accurately predict temperature and velocity profiles over an isothermal heated plate. Comparison between the analytical and experimental results for mean velocity at three locations is shown in Figure 28. The initial velocity profile was assumed to vary as a 1/5.6 power formula for the numerical model; this relation was found by Reynolds, et al (99) to adequately describe the experimental results. Predicted velocity distributions appear to be in excellent agreement

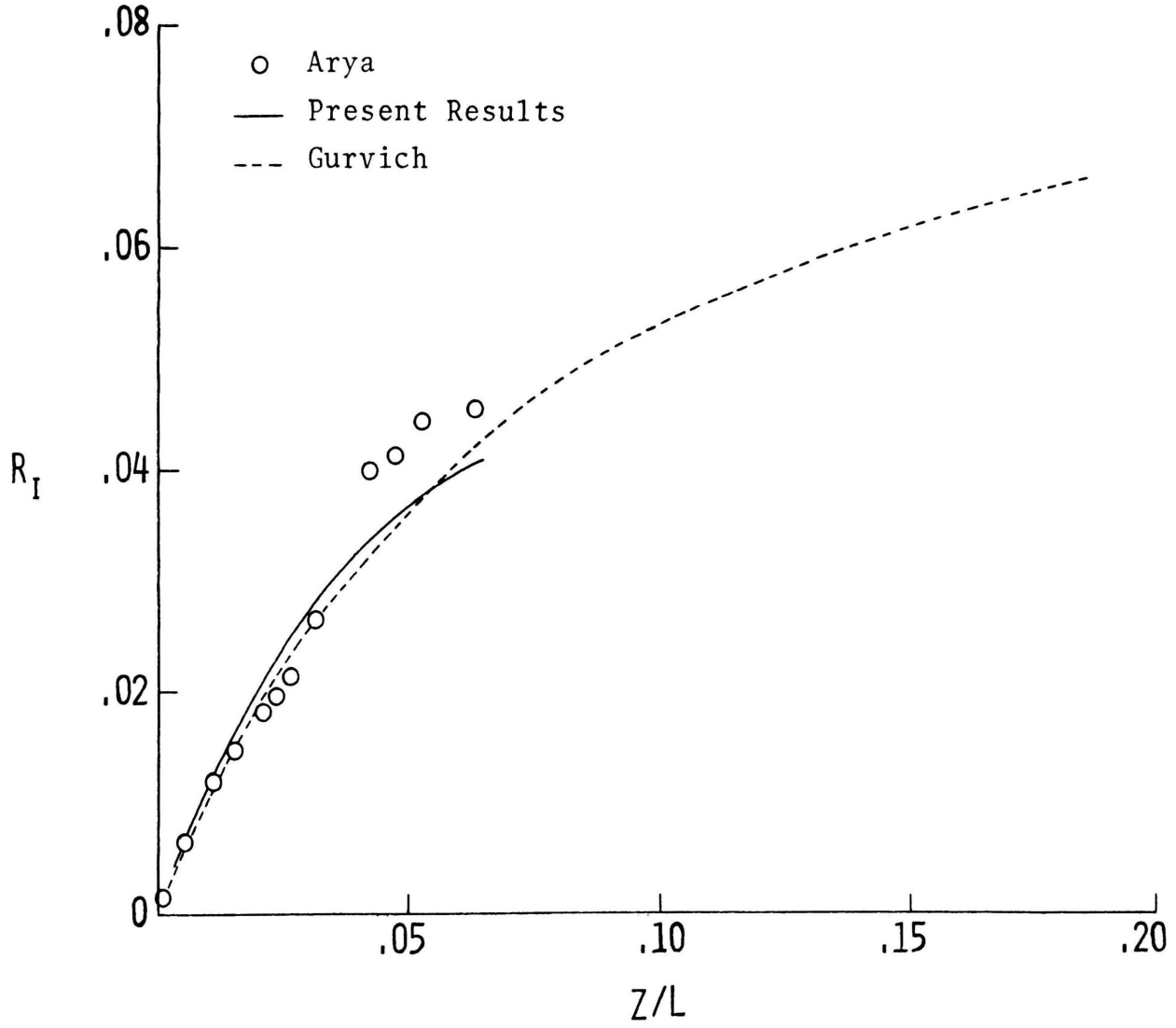

Figure 27. Variation of Richardson Number with Z/L in a Stably Stratified Turbulent Boundary Layer: Comparison with Atmospheric Data

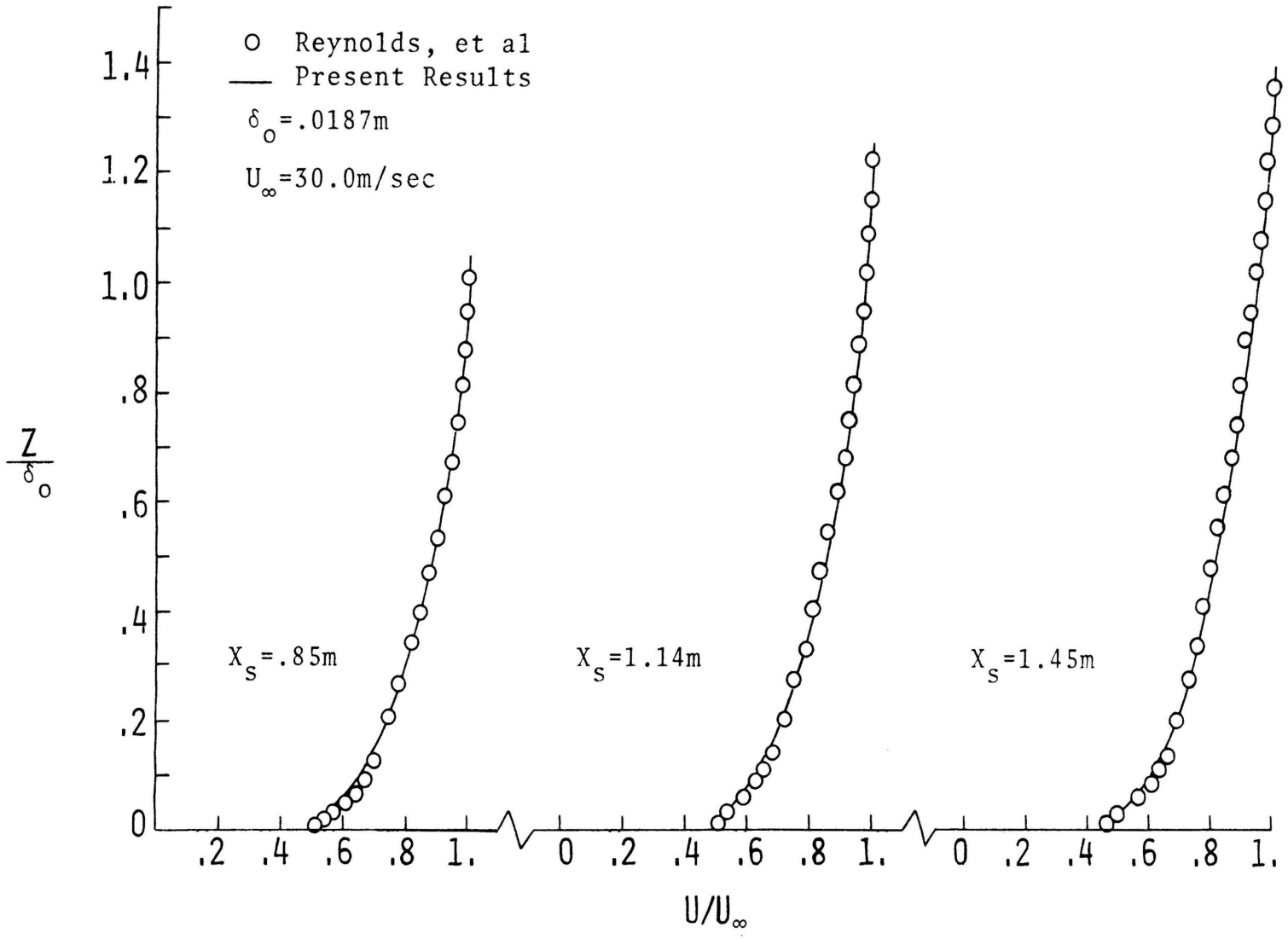

Figure 28. Comparison between Predicted Velocity and Experiment for Turbulent Boundary Layer Flow Over an Heated Plate

with the experimental data.

Temperature surveys were made at three locations on the plate, as shown in Figure 29. The initial temperature distribution in the numerical scheme was represented by a 1/5.6 power relation. This was similarly found by Reynolds, et al (99) to provide a best fit for the experimental data. The dimensionless temperature profiles predicted by the numerical model agree with the measured results throughout the entire boundary layer. The effect of the Richardson number in this case was found to be insignificant; this is to be expected since the boundary layer is too thin to reasonably approximate an atmospheric boundary layer.

An extensive amount of data was measured by Malhotra (28) in simulating unstable stratified flow in an atmospheric wind tunnel. Other works dealing with unstable stratification used elevated sources, or proved insufficient in supplying necessary data relevant to this study. Concentrations from a simulated point source were measured using ammonia as the diffusing gas for five downstream locations ranging from X_s = .30 meter to X_s = 1.83 meters. Synthetic line source distribution is obtained by assuming that the tranverse profile for a point source has a Gaussian form. Comparisons with the neutral line source data of Poreh and Cermak (21) were found by Malhotra (28) to be very good, particularly for the variation of surface concentration. Unfortunately, no actual line source data were available for comparison with the synthetic results for an unstable

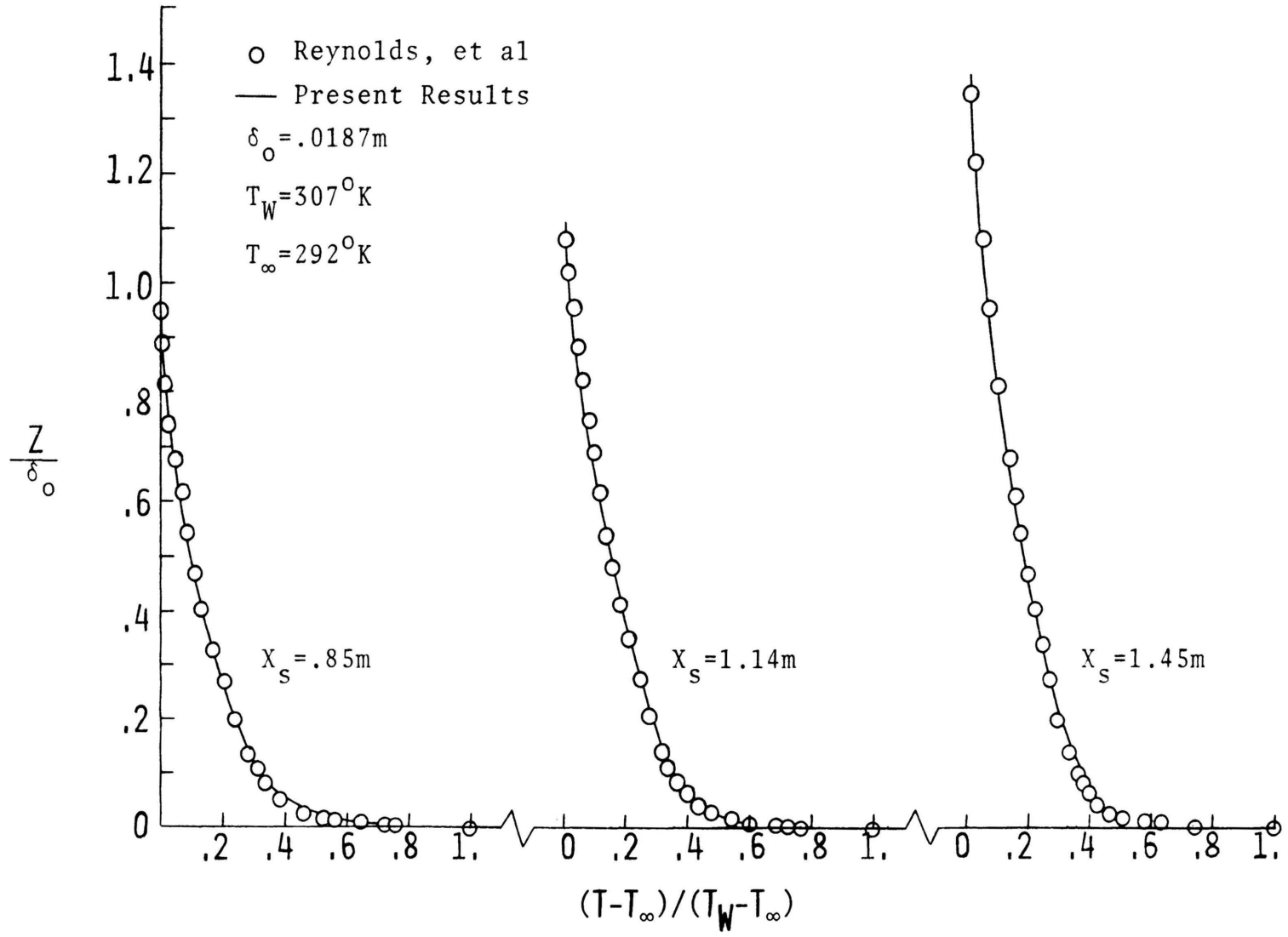

Figure 29. Comparison between Predicted Temperature and Experiment for Turbulent Boundary Layer Flow Over an Heated Plate

atmosphere.

The analytical results are compared with the measured mean velocity values in Figure 30. A mean free velocity of U_∞ = 2.74 m/sec was used in conjunction with a 1/5.5 power law relationship for velocity distribution as the initial conditions in the numerical program; this power law relation was empirically determined by Malhotra (28) from his experimental data. The numerical scheme can be seen to accurately predict downstream velocity profiles even in the near wall region. Use of the measured data for the initial profile showed minimal improvement over the initial power law assumption at succeeding downstream locations.

The isothermal heated surface was maintained at a constant difference of 64^{o}K with the free stream temperature. Using the initial temperature measured at X_s = .30 meter, non-dimensional temperature distributions are shown to be in good agreement with the experimental results in Figure 31. The slight deviation from the measured data in the lower 15 per cent of the boundary layer is due, in part, to the constant mixed Prandtl number, σ_h, used throughout this study. Although lacking sufficient data near the outer portion of the boundary layer, prediction of the thermal boundary layer development appears to be reasonably accurate.

Non-dimensional concentration profiles are shown in Figure 32 for both experimental and numerical results as a function of Z/δ_o. Measured data at X_s = .30 meter was used to generate the initial concentration distribution in

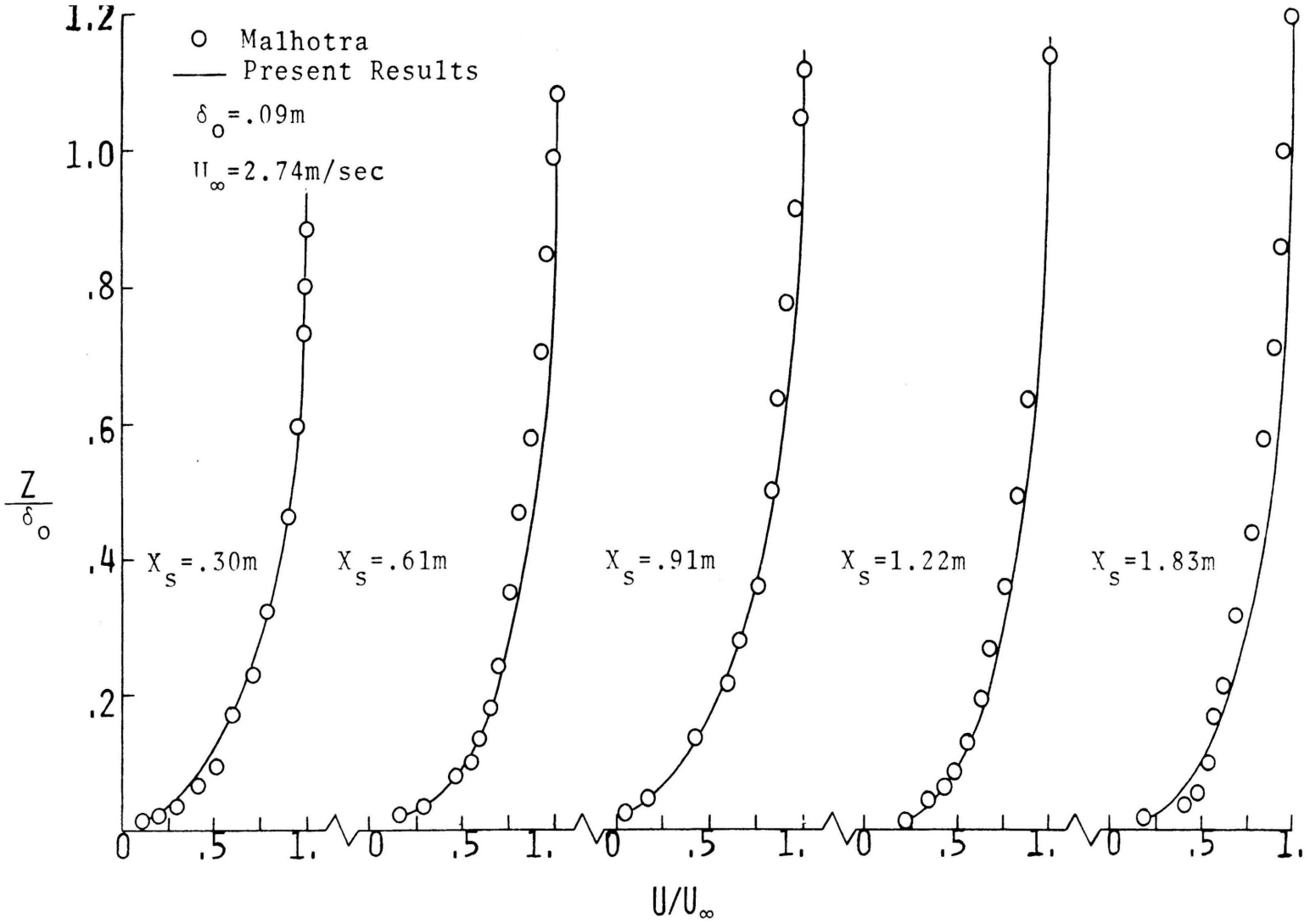

Figure 30. Comparison between Predicted Velocity and Experiment in an Unstably Stratified Turbulent Boundary Layer

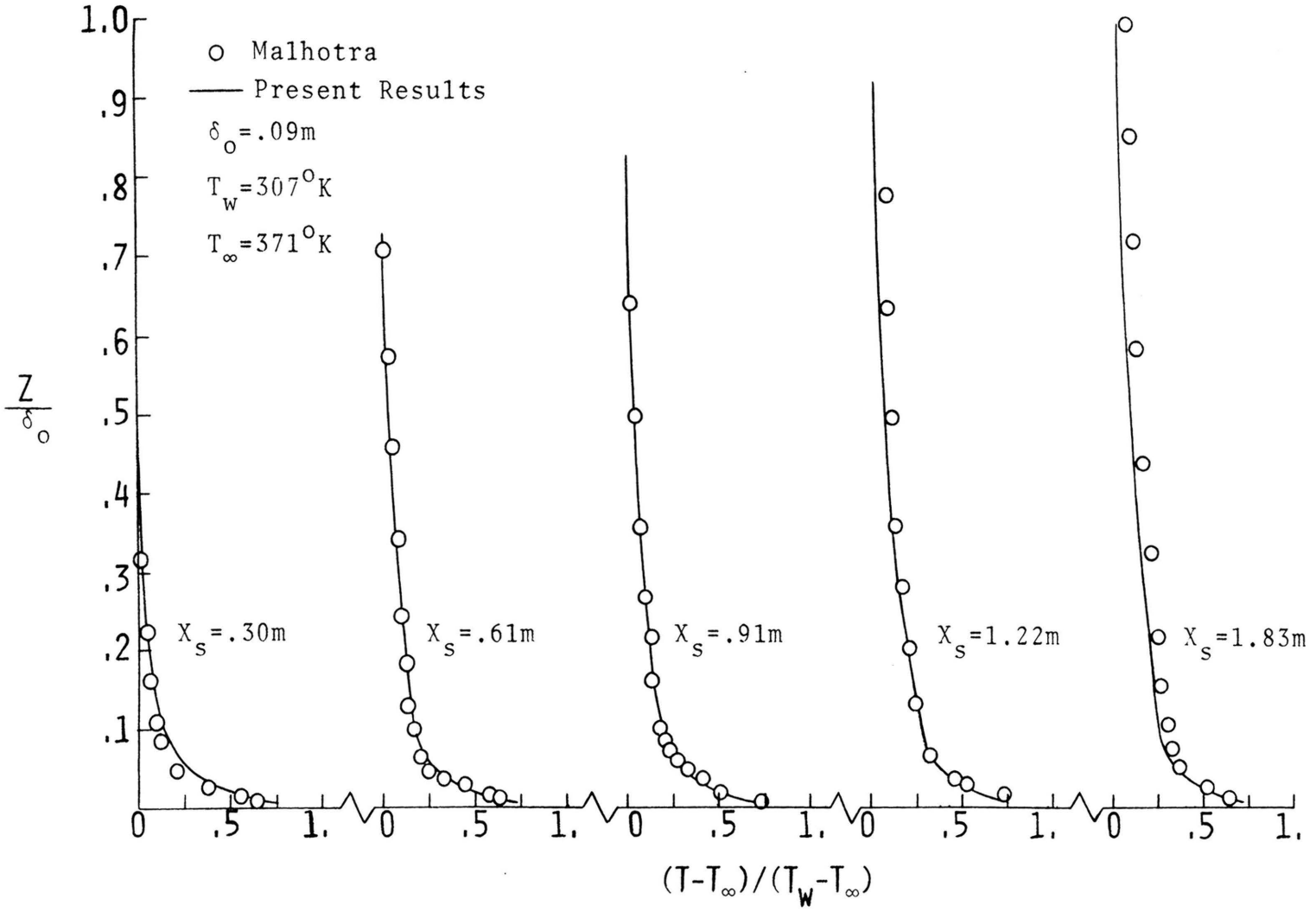

Figure 31. Comparison between Predicted Temperature and Experiment in an Unstably Stratified Turbulent Boundary Layer

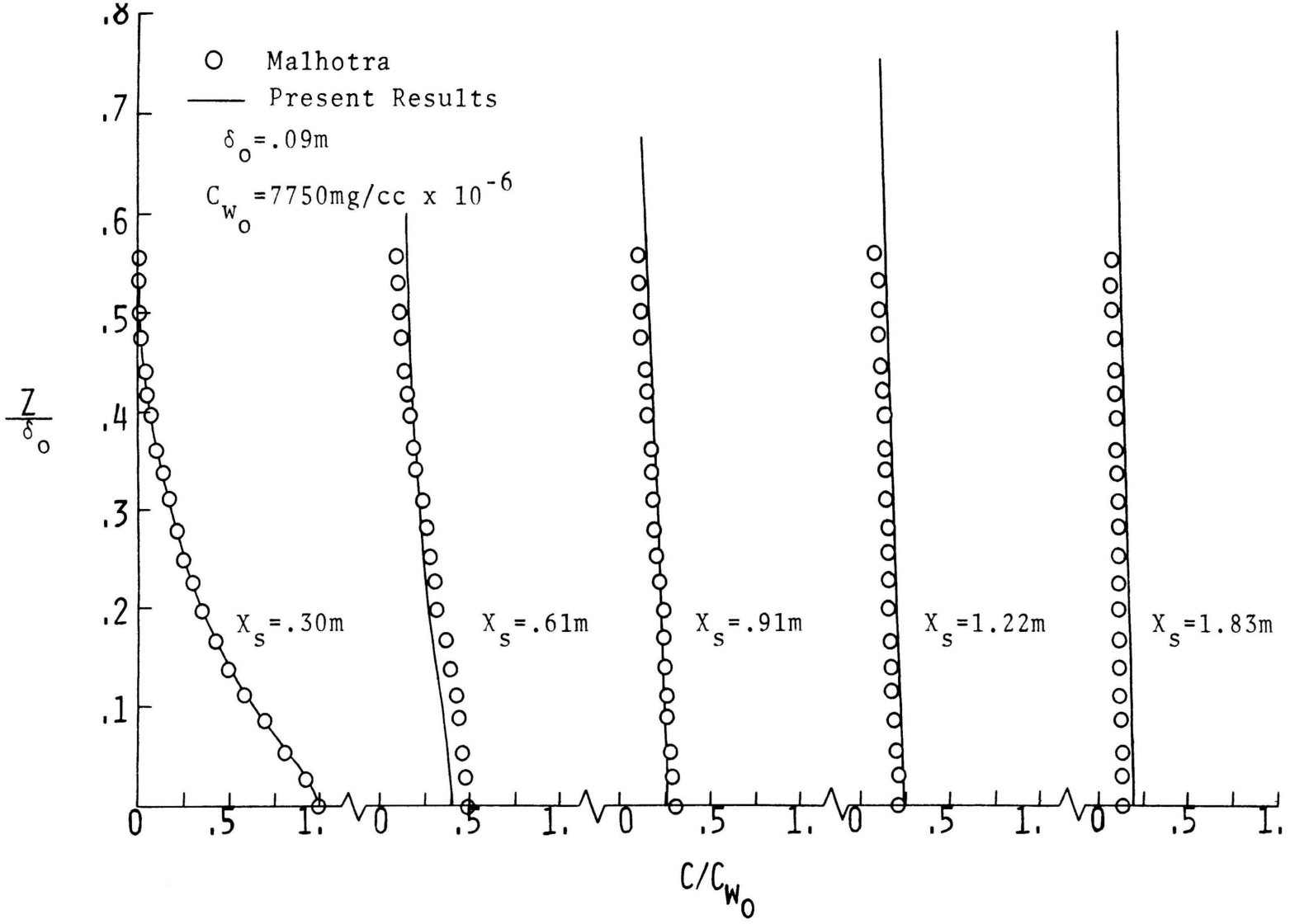

Figure 32. Comparison between Predicted Concentration and Experiment in an Unstably Stratified Turbulent Boundary Layer

the numerical model. Very rapid dissipation occurs within the first downstream location, X_s = .61 meter. The underpredicted values of the numerical results occurring at X_s = .61 meter and X_s = .91 meter result from an overestimation of the turbulence kinetic energy and friction velocity, u*. An increase in turbulence kinetic energy produces an increase in diffusion rates. Readjustment of the turbulence kinetic energy to more accurately simulate the first few concentration profiles results in substantial overprediction of the concentration at X_s = 1.83 meters. Regardless of the initial starting conditions, overprediction begins to occur at X_s = 1.22 meters. Reasonable prediction of the surface values for concentration, C_W, show the flux-Couette flow relationships to be adequate in establishing a suitable boundary condition.

An energy balance is shown in Figure 33 for two locations, X_s = .61 meter and X_s = 1.83 meters. The large contribution of convection and diffusion at X_s = .61 meter in the lower 50 per cent of the boundary layer is attributed to the assumed Klebanoff (65) turbulence kinetic energy profile as the starting conditions. At X_s = 1.83 meters, the production and dissipation completely dominate the energy balance, except near the outer region of the boundary layer where the diffusion becomes significant in balancing the negative contribution by convection and dissipation. Comparison of Figure 33 with the neutral datain Figure 21 shows the production of turbulence kinetic energy to be significantly

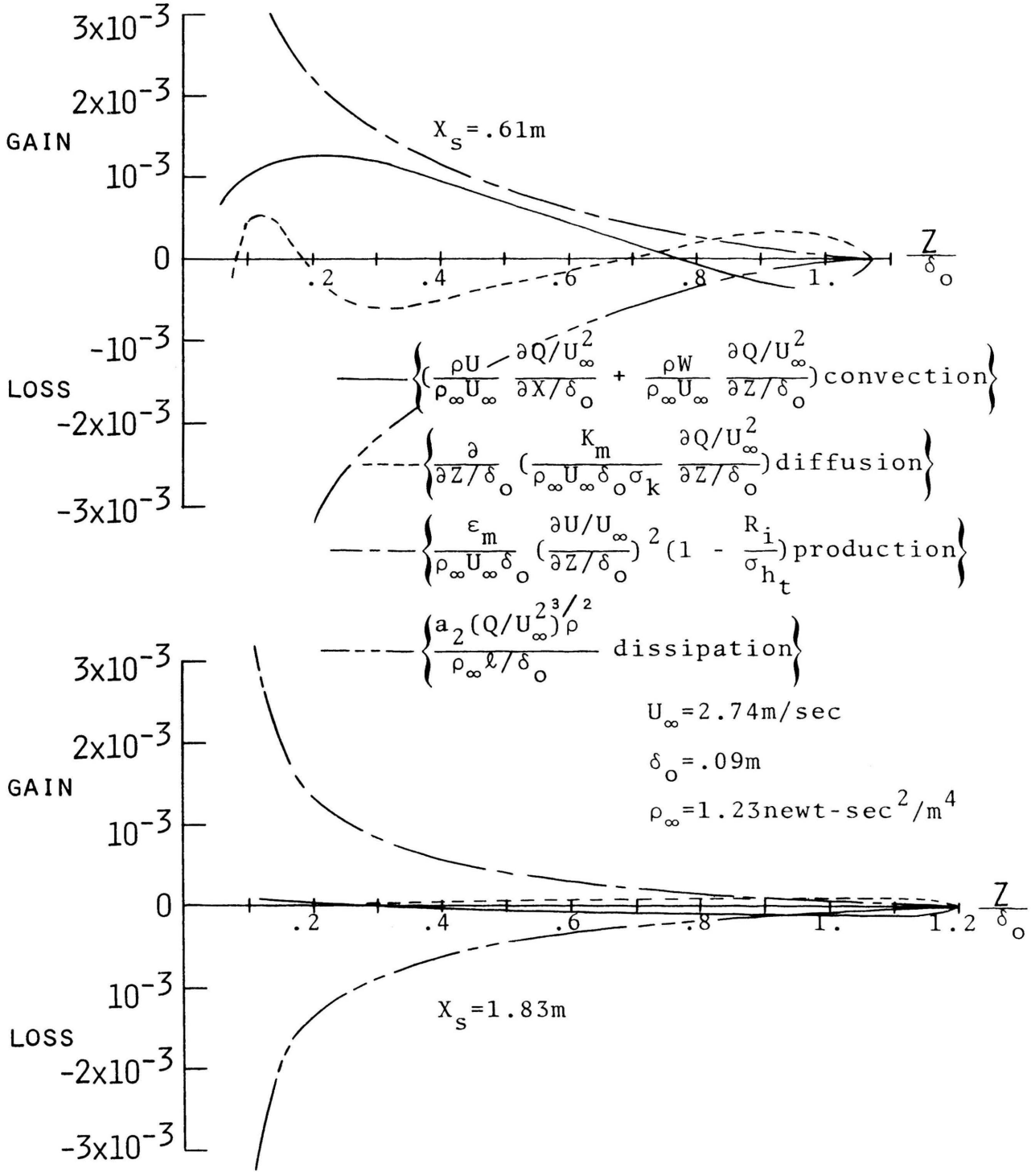

Figure 33. Balance of Turbulence Kinetic Energy in an Unstably Stratified Turbulent Boundary Layer

larger for the unstable case.

The variation of the Richardson number is shown in Figure 34 for three downstream locations. The initial Richardson number distribution at X_s = .61 meter is seen to reach a maximum near Z/δ_o = .50, and then diminish to zero as the outer region of the boundary layer is approached. This is due to the initially assumed power law distribution for the velocity profile in lieu of using the measured data of Malhotra (28). Since the Richardson number is calculated from the local temperature gradient divided by the square of the velocity gradient, any slight inaccuracy in calculating the velocity gradient results in a significant alteration in the Richardson number. Flattening of the Richardson number profiles at X_s = 1.22 meters and X_s = 1.83 meters are similarly seen in the data by Ayra (25), Figure 26. The increase in the Richardson number for Z/δ_o greater than .80 is caused by the velocity gradient approaching zero, i.e., the mean velocity is attempting to produce nearly vertical profiles in an effort to satisfy the free stream velocity boundary condition in the numerical model. A similar effect is observed in the temperature distribution. No actual Richardson number data were available from Malhotra (28).

Based upon the results obtained from the mass diffusion data of Malhotra (28) in an unstable atmospheric boundary layer, the numerical model was modified to analyze the diffusion of heat from a line source in an isothermal turbulent boundary layer. The numerical results are compared with the

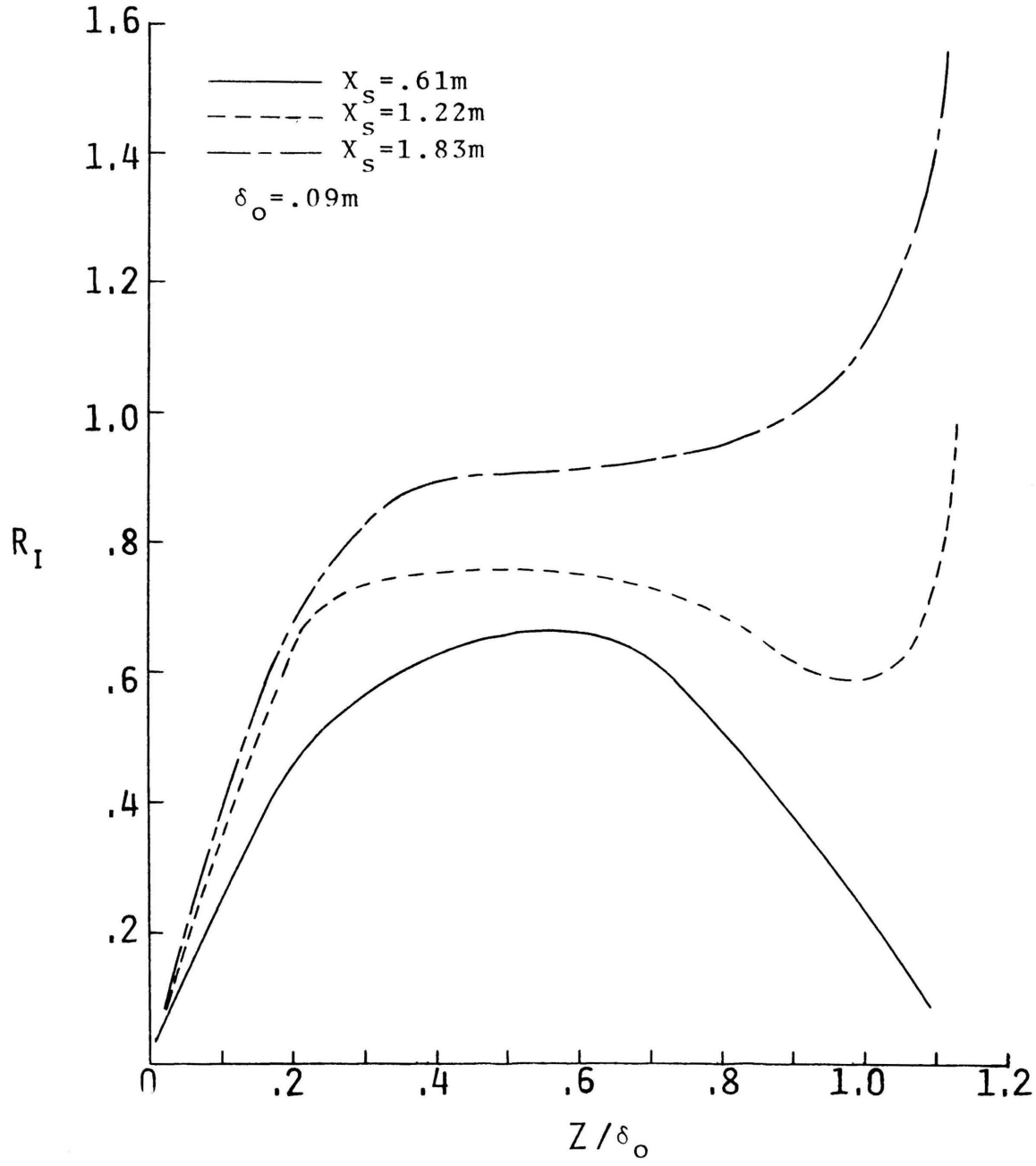

Figure 34. Variation of Richardson Number in an Unstably Stratified Turbulent Boundary Layer

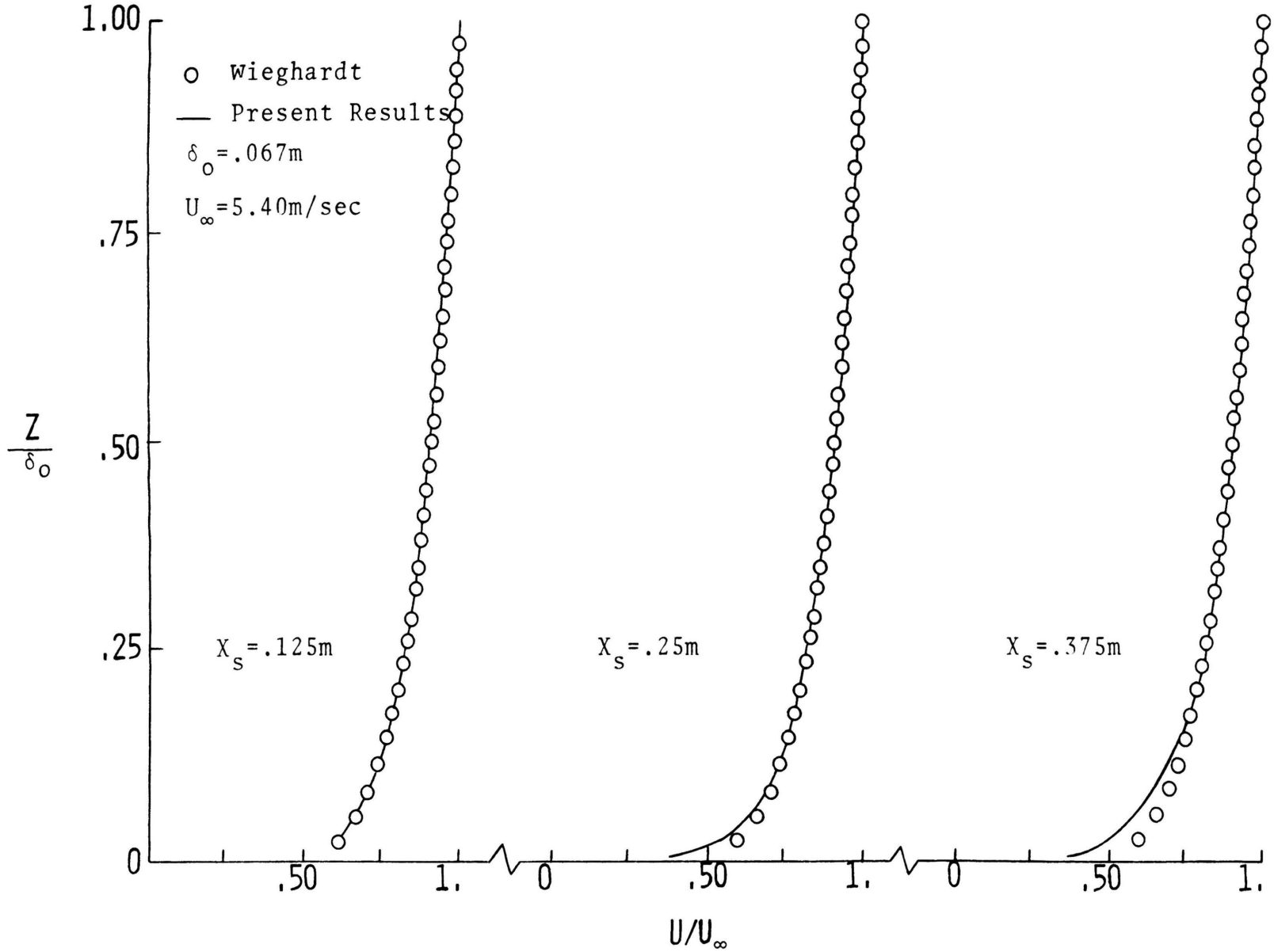

Figure 35a. Comparison between Predicted Velocity and Experiment for Turbulent Boundary Layer Flow Over a Faint Line Source of Heat: X_s=.125 - .375 meters

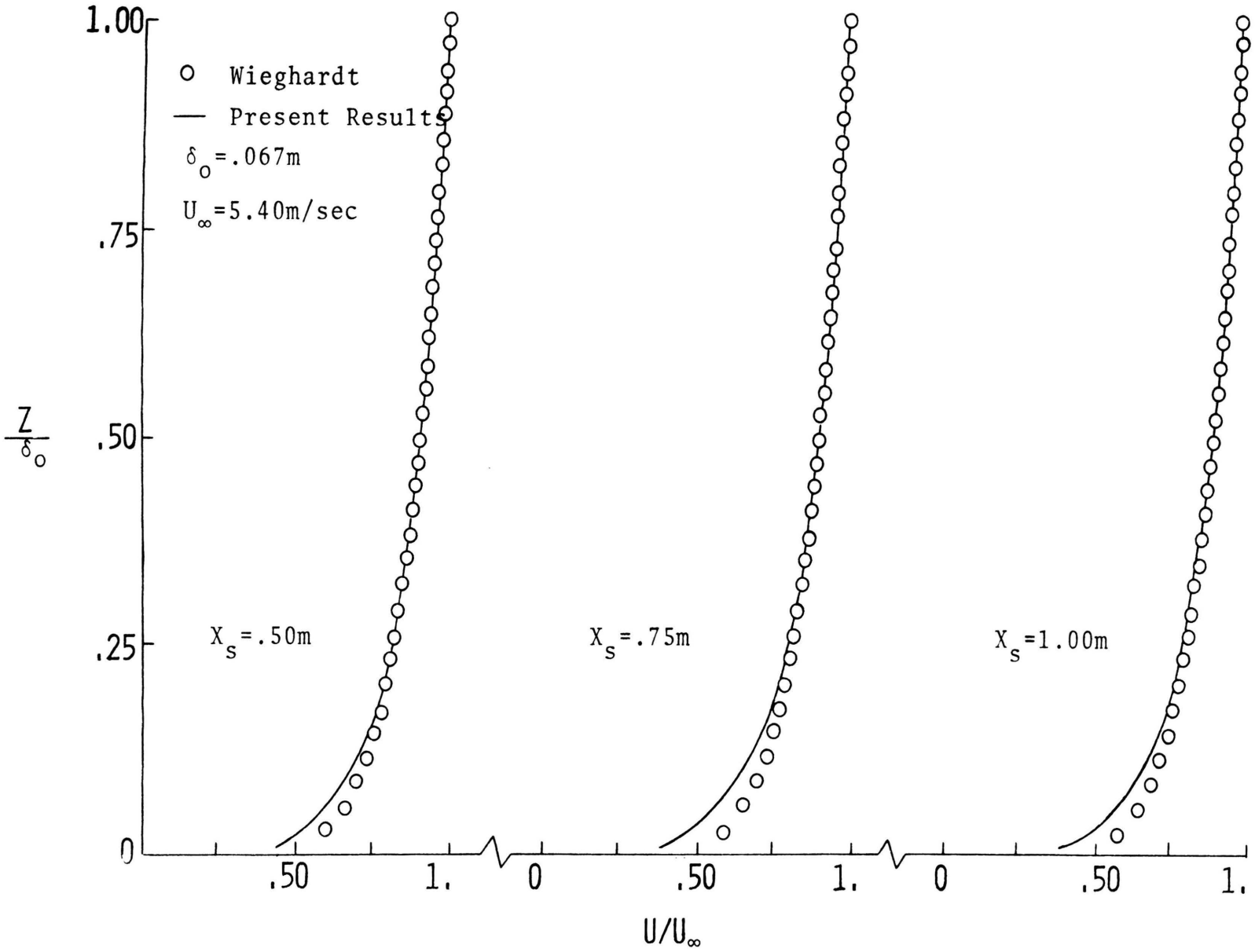

Figure 35b. Comparison between Predicted Velocity and Experiment for Turbulent Boundary Layer Flow Over a Faint Line Source of Heat: X_s=.50 - 1.00 meters

experimental heat diffusion data of Wieghardt (29) for mean velocity and temperature distributions at six locations downstream of a faint heat source. The mean velocity distributions predicted by the numerical scheme are compared with a 1/7 power law distribution used by Wieghardt (29) to approximate the measured velocity data. The boundary layer thickness was found by Wieghardt to vary as $\delta = .37X/(U_\infty X/\nu)^{.2}$, where X is the horizontal distance from the leading edge of the test plate. Wieghardt's results are plotted in Figures 35a and 35b as a function of the 1/7 power distribution and the empirical relation for δ. The numerical results are seen to deviate substantially in the near wall region within the first two downstream locations, $X_s = .25$ meter and $X_s = .375$ meter, but does not change significantly from $X_s = .50$ meter to $X_s = 1.00$ meter. For Z/δ_o greater than .20, the calculated values are in excellent agreement with the assumed power law profiles. The numerically calculated profiles are probably more realistic in describing actual flow conditions than the power law relation, since flow over a heated surface is altered in the near wall region by the steep temperature gradients.

A constant line source of heat was used to create the temperature field. The surface in this case is assumed to be adiabatic. The boundary condition for the temperature at the wall is given by the no flux relationship, $\frac{\partial T}{\partial X} = 0$. This results in a heat diffusion model exactly analogous to a mass diffusion case. The non-dimensional temperature is

shown in Figure 36 as a function of the measured wall temperature at X_s = .125 meter, i.e., T_W = 310°K. Ambient temperature was assumed to be constant, T_∞ = 293°K. The calculated temperature distributions depend upon the ability of the flux relations to accurately predict surface values for the temperature. Considerable underpredictions are seen to occur immediately downstream of the initial conditions. This may be due to a neglect of the conduction of heat along the plate in evaluating the experimental data. However, the relative spread and shape of the predicted heat diffusion profiles are very similar to the experimental results. Comparison of Wieghardt's (29) heat diffusion data with line source mass diffusion data was found by Malhotra (28) to be similar.

The numerical model appears to predict experimental results with reasonable accuracy in both neutral and thermally stratified atmospheric boundary layer flows. Based upon these preliminary test cases, a more realistic case was investigated dealing with the formation of advection fogs over a cold sea surface.

C. Advection Fog Formation

Because of insufficient information regarding ocean fogs, few studies are available in the literature. However, a considerable amount of theoretical analysis has been done in attempting to model fog. Specifically the numerical work done by Mack, et al (51), Fischer and Caplan (50), and Zdunkowski and Trask (54) have proved to be instrumental in

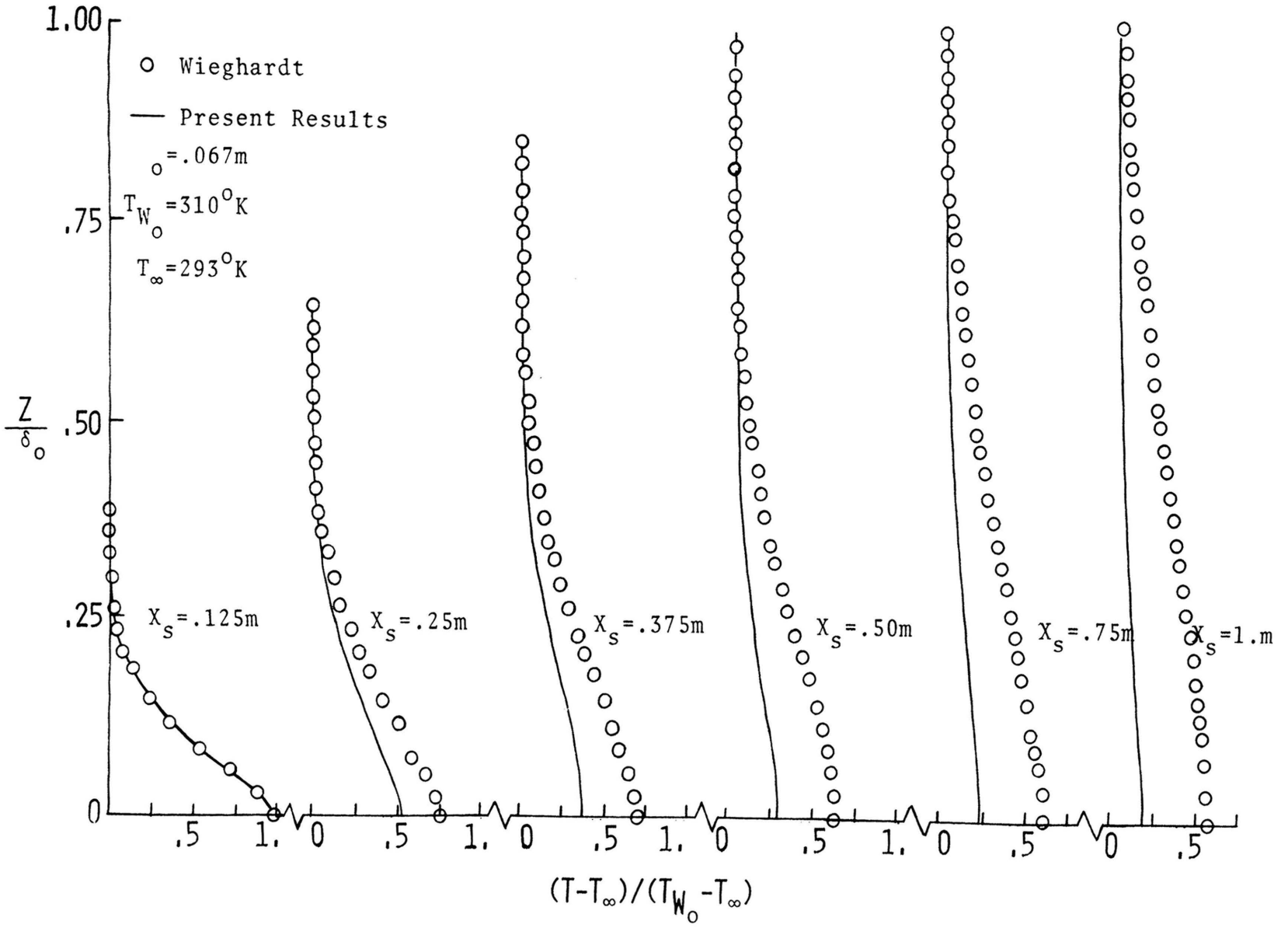

Figure 36. Comparison between Predicted Temperature and Experiment for Turbulent Boundary Layer Flow Over a Faint Line Source of Heat

developing the model used in this study.

The formation of advection fog is a combined phenomena of hydrodynamics and microphysics. Sea-air interaction produces the environment of moisture and sea salt particles in the lower boundary layer over the ocean surface. The microphysics of clouds regulate the condensation and coagulation of small water droplets at various atmospheric conditions which govern the formation and dissipation of advection fogs.

The principle mechanism used in this study to numerically simulate fog was to advect warm moist air over a cold surface with continuously decreasing temperature, as shown in Figure 37. Due to the continuously decreasing sea surface isotherms, the ambient temperature of the air is lowered until the dew point temperature is reached. This results in the condensation of water vapor into small liquid water droplets. In addition to the conventionally used equation of state and hydrostatics of the atmosphere, equations for water vapor content and liquid water content were used to satisfy the conservation of species. These equations take into consideration the balance of species concentration that results from advection, diffusion, condensation (or evaporation), and sedimentation of liquid water droplets. An additional source term has been added to the potential temperature equation to account for latent heat of phase change and heat addition by radiation. Formulation of these governing equations was based upon the numerical model developed by Mack, et al (51).

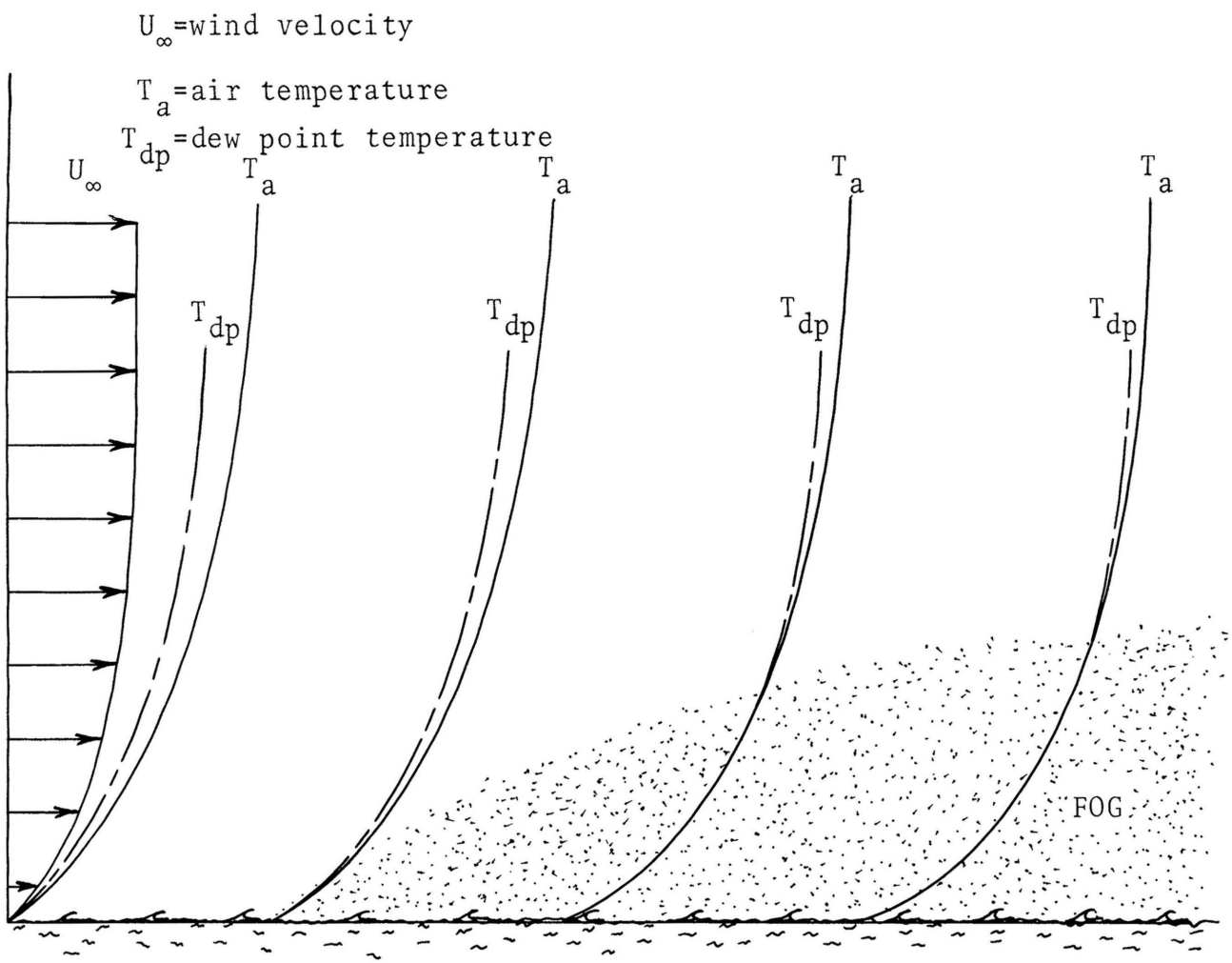

Figure 37. Advection Fog Over the Ocean Surface

A saturation adjustment procedure, developed by McDonald (100), has been used to account for the condensation of water vapor or the evaporation of liquid water. Since the air is heated by the release of latent heat of condensation, supersaturated water vapor at a grid point is converted into liquid water until saturation is achieved. Likewise, if the air is cooled, liquid water at a grid point is evaporated into unsaturated vapor until saturation occurs or the liquid water is exhausted. The vapor pressure computation at saturated conditions is obtained from an empirical formula derived by Murray (101). Barker (102) also makes use of these adjustment procedures in numerically predicting fog formation over the ocean.

Figure 38 shows the effect of wind velocity on fog development. Wind velocities of 3 and 6 m/sec were used in creating a hydrodynamic boundary layer with a thickness of 943 meters. Previous numerical models dealing with fog prediction usually neglected the effect of advection or used a simple expression for the velocity distribution in conjunction with the exchange coefficient of momentum. Qualitatively, the results shown here indicate that an increase in wind velocity results in a decrease of the fog layer height. The dark lines depicted by W_L from .10 to .30 in Figure 38 are lines of constant liquid water content. Liquid water content did not get much greater than .30 gm/m^3 over the horizontal distance of 7000 meters.

During the early stages of sea fog formation, advection

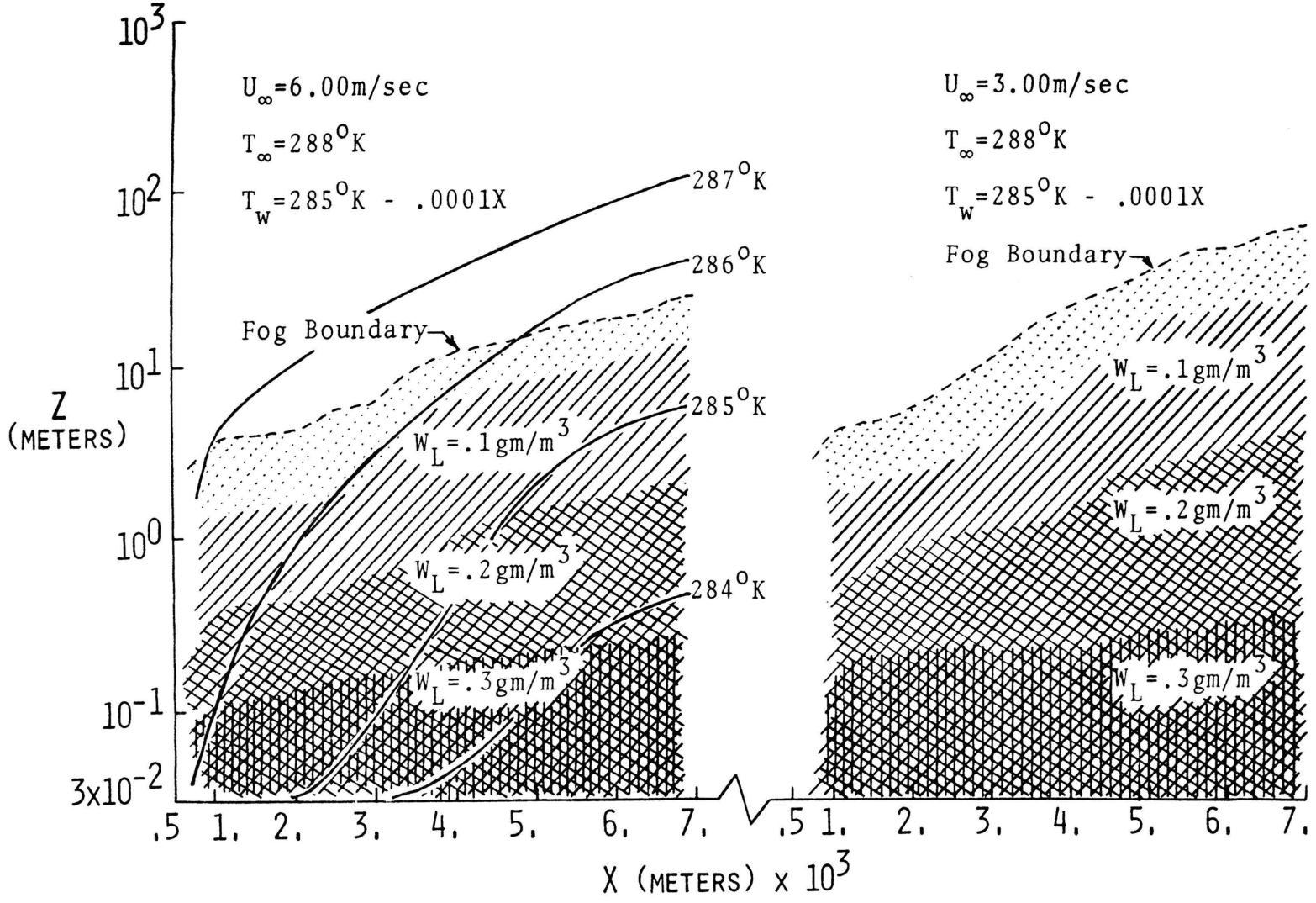

Figure 38. Influence of Wind Velocity on the Formation of Advection Fog

of warm moist air over decreasing isotherms is the dominant mechanism. When there is a temperature inversion near the ocean surface, fog particles can not move upward so long as moisture continues to be supplied through evaporation to the warmer air from a colder surface. Consequently, visibility begins to decrease. Radiation cooling of the warm fog particles and latent heat absorption of the ocean surface eventually overcome a temperature inversion. As the air temperature becomes equal or lower than the ocean surface temperature, the supply of moisture is stopped. The fog layer then becomes a stratus and gradually lifts from the surface.

V. CONCLUSION AND RECOMMENDATION

An analytical investigation of turbulent diffusion in thermally stratified boundary layers has been made by using a local phenomenological theory based upon the turbulence kinetic energy. This formulation specifies the eddy coefficient of momentum as a function of the turbulence kinetic energy, thus allowing the past history of the flow to be considered. This model also proved to be quite advantageous in terms of versatility and flexibility for various applications as well as simple in concept. Based upon the results of this investigation, the following conclusions have been reached:

1. Use of wind tunnel modeling in simulating actual atmospheric motion is still questionable. Although surface effects and thermal stratification can be modeled, the scale of turbulence is still a decided disadvantage to laboratory simulation. However, because of the random scattering of field data, well controlled laboratory modeling of the atmosphere has been found to provide suitable results for understanding the basic mechanisms of atmospheric diffusion. Undoubtedly more field data should be taken in an effort to correlate with experimental wind tunnel testing and numerical modeling.
2. A linear correlation between local turbulent shear stress and local turbulence kinetic energy has been found to exist in neutral atmospheres by analyzing atmospheric

wind tunnel data. Only one case, dealing with stable stratification, contained any turbulence data for a thermally stratified boundary layer, but did not contain any concentration data. A thorough investigation of thermally stratified flow should be experimentally undertaken in order to effectively establish a more realistic eddy coefficient model. Because of this lack of experimental data, the exchange coefficient of momentum used throughout this study was based upon data obtained from neutral cases.

3. The basic equations for the conservation of mass, momentum, stagnation enthalpy, species, and turbulence kinetic energy are needed to adequately describe atmospheric boundary layer flow. Closure of the governing equations is obtained from empirical models used to account for: production of turbulence kinetic energy, dissipation of turbulence kinetic energy, diffusion of turbulence kinetic energy, and the eddy coefficients.
4. The governing equations can be reduced to a generalized parabolic differential equation. The implicit finite difference scheme developed by Patankar and Spalding (58) is found to be very efficient with a minimum of computational inaccuracy. The use of algebraic Couette flow relations prove to be adequate in establishing near wall values for the independent variables.
5. A law of the wall expression is developed which can be applied to general engineering applications as well as

to thermally stratified atmospheric flow in order to calculate friction velocity, u*, at the surface. The shear stress and "slip" turbulence kinetic energy can be calculated as a function of the friction velocity and eddy coefficient model.

6. Use of constant mixed Schmidt and Prandtl numbers in accounting for exchange coefficients of heat and concentration reduce the need of empirically correlating relations for various flow conditions. Comparison with available experimental data show these parameters to be adequately represented by $\sigma_h = \sigma_c = .75$.
7. The use of the turbulence kinetic energy model and the numerical program appears to be an effective tool for solving atmospheric boundary layer phenomena. The diffusion of matter from a ground level line source can be reasonably predicted along with the effect of buoyancy by the numerical scheme.
8. Investigation of the formation of fogs over aequous surfaces shows the numerical scheme to give qualitative predictions pertaining to the shape and development of the liquid water content profiles. The basic equations of momentum, heat, and turbulence kinetic energy must be coupled with the species equation for liquid water content and water vapor content to describe marine fogs.
9. A saturation adjustment procedure can be performed upon the predicted temperature values to account for the formation or dissipation of liquid water content and water

vapor content under saturated atmospheric conditions.

10. The dominant growth mechanism during the early stages of sea fog development is the influence of wind velocity coupled with a continuously decreasing cold surface. An increase in wind velocity results in a decrease in height of the fog boundary.

Results obtained by using the turbulence kinetic energy approach in analyzing heat and mass diffusion in thermally stratified boundary layers, along with the ability of the numerical scheme to predict realistic fog development over an ocean surface, leads to the following recommendations:

1. There is an obvious need for more experimental data, particularly field measurements, in order to form any meaningful correlation between actual physical processes occurring in the atmosphere and either numerical or laboratory modeling techniques. In this particular study, a considerable amount of data was found to exist from atmospheric wind tunnel tests in which the atmospheric boundary layer had been carefully simulated and measured. Unfortunately, either turbulence kinetic energy data was available and no concentration measurements made, or vice versa. Without a complete set of data, only synthetic comparisons could be made between experiment and theory. In the case of fog formation studies, the analytical schemes far outweigh experimental studies because of physical limitations or economic reasons. This causes empirical relations to be extrapolated from

seemingly similar natural occurrances, resulting in gross estimations of the physical processes. A joint effort should be made by coordinating measurements of atmospheric phenomena with numerical analysis if a realistic model for describing atmospheric motion is to be achieved.

2. More extensive research should be made in accounting for the turbulence kinetic energy near wall regions. Elimination of any mixing length hypothesis in accounting for entrainment rates and Couette flow relations could result in more substantial relationships for describing the nature of turbulence without the need of establishing empirical formulae unique to only their specific application. A more thorough study should also be undertaken to investigate the use of variable mixed Prandtl and Schmidt relations to account for the exchange coefficients of heat and mass.
3. Comparisons between the experimental distributions of production and dissipation of turbulence kinetic energy are needed in an effort to better define the empirical models used to account for these terms. Recent use of partial differential equations to describe these two terms may prove to be a substantial improvement over existing one-equation models, providing that the additional empiricism necessary in formulating these equations can be kept to a minimum.
4. Since almost all boundary layers are three-dimensional

in reality, attempts to confine these flows to two-dimensional prediction procedures have met with some success, but only at the expense of gross simplifications or empirical relations common to only one set of experimental data. Development of a general numerical model for the calculation of transport processes in three-dimensional flows would give rise to more accurate predictions of flow phenomena occurring in the atmosphere as well as give insight into the general nature of turbulent flow.

BIBLIOGRAPHY

1. Fay, J. A., Joult, D. P. and Heywood, J. B. (1971), Fluid Physics of Pollution, AIAA Professional Study Series, 135 p.

2. Briggs, G. A. (1965), "A Plume Rise Model Compared with Observations," Journal of the Air Pollution Control Association, Vol. 15, No. 9, p. 433-438.

3. Hoult, D. P., Fay, J. A. and Forney, L. J. (1969), "A Theory of Plume Rise Compared with Field Observations," Fluid Physics of Pollution, AIAA Professional Study Series, p. 5-10.

4. Haagen-Smit, A. J. (1952), "Chemistry and Physiology of Los Angeles Smog," Industrial and Engineering Chemistry, Vol. 44, No. 6, p. 1342-1346.

5. Wynaard, J. E. and Cote, O. R. (1971), "The Budgets of Turbulent Kinetic Energy and Temperature Variance in the Atmospheric Surface Layer," JAS, Vol. 28, p. 190-201.

6. Webb, E. K. (1970), "Profile Relationships: The Log-Linear Range, and Extension to Strong Stability," Quarterly Journal of the Royal Meteorological Society, Vol. 96, p. 67-90.

7. Priestly, C. H. B. (1959), Turbulent Transfer in the Lower Atmosphere, University of Chicago Press.

8. Lumley, J. L. and Panofsky, H. A. (1964), The Structure of Atmospheric Turbulence, Interscience Publishers, p. 239.

9. Haugen, D. A., Barad, M. L. and Antanaitis, O. (1961), "Values of Parameters Appearing in Sutton's Diffusion Models," Journal of Meteorology, No. 18, p. 368-372.

10. Sutton, O. G. (1932), "A Theory of Eddy Diffusion in the Atmosphere," Proceedings of the Royal Society, Series A, Vol. 135, p. 143-165.

11. Sutton, O. G. (1953), Micrometeorology, McGraw-Hill Book Company, p. 333.

12. Kraus, E. B. (1967), "Wind Stress Along the Sea Surface," Advances in Geophysics, Academic Press, New York, Vol. 2, p. 213-255.

13. Deacon, E. L. (1962), "Aerodynamic Roughness of the Sea," Journal of Geophysical Research, Vol. 67, p. 3167-3172.

14. Hidy, G. M. (1972), "A View of Recent Air-Sea Interaction Research," Bulletin AMS, Vol. 53, No. 11, November, p. 1083-1102.

15. Roll, H. U. (1965), Physics of the Marine Atmosphere, International Geophysical Series, Vol. 7, Academic Press, New York, 426 p.

16. Cermak, J. E., Sandborn,V. A., Plate, E. J., Binder, G. J., Chuang, H., Meroney, R. N. and Ito, S. (1966), "Simulation of Atmospheric Motion by Wind-Tunnel Flow," CER66JEC-VAS-EJP-GJB-HC-Rnm-Si17, College of Engineering, Colorado State University, Fort Collins, Colorado.

17. Chuang, H. and Cermak, J. E. (1966), "Similarity-Law Profiles in Thermally Stratified Shear Flows," Proceedings of the International Symposium on Boundary Layers and Turbulence, September, Kyoto, Japan.

18. Plate, E. J. (1971), Aerodynamic Characteristics of Atmospheric Boundary Layers, U.S.A.E.C. Critical Review Series, TID-25465, 190 p.

19. Plate, E. J. and Lin, C. W. (1966), "Investigations of the Thermally Stratified Boundary Layer," Fluid Mechanics Paper No. 5, Fluid Dynamics and Diffusion Laboratory, Colorado State University, Fort Collins, Colorado.

20. Schon, J. P. and Mery, P. (1971), "A Preliminary Study of the Simulation of Neutral Atmospheric Boundary Layer Using Air Injection in a Wind Tunnel," Atmospheric Environment, Vol. 5, p. 299-311.

21. Poreh, M. and Cermak, J. E. (1964), "Study of Diffusion from a Line Source in a Turbulent Boundary Layer," International Journal of Heat Mass Transfer, Vol. 7, p. 1083-1095.

22. Quraishi, A. A. (1963), "Effects of Flexible Roughness Elements on Diffusion in a Turbulent Boundary-Layer," Ph. D. Dissertation, Engineering Mechanics, Colorado State University, Fort Collins, Colorado, 190 p.

23. Davar, K. S. (1961), "Diffusion From a Point Source Within a Turbulent Boundary-Layer, Ph. D. Dissertation, Engineering Mechanics, Colorado State University, Fort Collins, Colorado, 161 p.

24. Bhaduri, S. (1963), "Mass Diffusion from a Point Source in a Turbulent Boundary Layer Over a Rough Surface," Ph. D. Dissertation, Engineering Mechanics, Colorado State University, Fort Collins, Colorado, 167 p.

25. Arya, S. P. S. (1968), "Structure of Stably Stratified Turbulent Boundary Layer," Technical Report, CER68-69SPSA10, Fluid Dynamics and Diffusion Laboratory, Colorado State University, Fort Collins, Colorado, 157 p.

26. Fleagle, R. G. and Businger, J. A. (1963), An Introduction to Atmospheric Physics, Academic Press, Third Printing, 346 p.

27. Chaudhry, F. H. and Meroney, R. N. (1969), "Turbulent Diffusion in a Stably-Stratified Shear Layer," Technical Report, C-0423-5, Colorado State University, Fort Collins, Colorado.

28. Malhotra, R. C. (1962), "Diffusion From a Point Source in a Turbulent Boundary-Layer with Unstable Density Stratification," Ph. D. Dissertation, Engineering Mechanics, Colorado State University, Fort Collins, Colorado, 171 p.

29. Wieghardt, K. (1948), "Uber Ausbreitungsvorgange in Turbulenten Reibungsschichten," Z. angew. Math. Mech. (ZAMM), Vol. 28, No. 11, 12, November-December, p. 346-355.

30. Poreh, M. (1961), "Diffusion From a Line Source into a Turbulent Boundary Layer," Ph. D. Dissertation, Engineering Mechanics, Colorado State University, Fort Collins, Colorado, 100 p.

31. Rao, K. S., Nee, V. W. and Yang, K. T. (1971), "Mass Diffusion in a Neutral or Thermally Stratified Atmospheric Surface Layer," Technical Report No. 71-28, EPA, 132 p.

32. Monin, A. S. and Yaglom, A. M. (1969), Statistical Fluid Mechanics, Part I, Nauka Press, Moscow, English Translation, 1971, IT Press 769 p.

33. Boussinesq, T. V. (1877), "Theorie de l'ecoulement Tourbillant," Mem. Pre. par. div. Sav., Vol. 23, 46 p.

34. Richardson, L. F. (1920), "The Supply of Energy From and to Atmospheric Eddies, "Proceedings of the Royal Society, Series A, Vol. 97, No. 686, p. 354-373.

35. Prandtl, L. (1925), "Uber die Ausgegildete Turbulenz," Z. angew. Math. Mech. (ZAMM), Vol. 5, p. 136-139.

36. Prandtl, L. (1945), "Uber ein Neues Formelsystem fuer die Ausgebildete Turbulenz," Nachrichten I. Akad. d. Wiss. (Goettingen), Vol. 6.

37. Taylor, G. I. (1932), "The Transport of Vorticity and Heat Through Fluids in Turbulent Motion," Proceedings of the Royal Society, Series A, Vol. 135, 685 p.

38. Von Karman, T. (1930), "Mechanische Aehnibichkeit und Turbulenz," Nach. Gesell, Wiss. Goettingen, Math, Phy. Klass, Vol. 5, 58 p.

39. Hinze, J. O. (1959), Turbulence, McGraw-Hill Book Company, 586 p.

40. van Driest, E. R. (1956), "On Turbulent Flow Near a Wall," Journal of Aeronautical Sciences, Vol. 23 1007 p.

41. Patankar, S. V. (1967), "Heat and Mass Transfer in Turbulent Boundary Layers," Ph. D. Dissertation, Department of Mechanical Engineering, Imperial College, London, England, 201 p.

42. Cebeci, T., Smith, A. M. O., and Mosinskis, G. J. (1970), "Solution of the Incompressible Turbulent Boundary-Layer Equations With Heat Transfer," Journal of Heat Transfer, Transactions of ASME, Series C, Vol. 92, No. 1, p. 33-43.

43. Cebeci, T. and Mosinskis, G. J. (1971), "Calculation of Incompressible Turbulent Boundary Layers With Mass Transfer, Including Highly Acclerating Flows," Journal of Heat Transfer, Transactions of ASME, Series C. Vol. 93, p. 271-280.

44. Monin, A. S. and Okukhov, A. M. (1954), "Basic Laws of Turbulent Mixing in the Ground Layer of the Atmosphere," Trudy Geofiz. Inst. ANSSSR, Vol. 151, No. 24, p. 163-187.

45. Ellison, T. H. (1957), "Turbulent Transport of Heat and Momentum From an Infinite Rough Plane," Journal of Fluid Mechanics, Vol. 2, p. 456-466.

46. Townsend, A. A. (1958), "Turbulent Flow in a Stably Stratified Atmosphere," Journal of Fluid Mechanics, Vol. 5, p. 361-372.

47. Yamamoto, G. and Shimamuki, A. (1960), "Numerical Solution of the Equation of the Atmospheric Diffusion," Scientific Report, Tokyo University, Tokyo, Japan, Series 5, Vol. 14, p. 24-35.

48. Yamamoto, G. and Shimanuki, A. (1964), "The Determination of Lateral Diffusivity in Diabatic Condition Near the Ground From Diffuison Experiments," Journal of Atmospheric Sciences, Vol. 11, p. 187-196.

49. Estoque, M. A. (1963), "A Numerical Model of the Atmospheric Boundary Layer," Journal of Geophysical Research, Vol. 68, No. 4, p. 1103-1113.

50. Fisher, E. L. and Caplan, P. (1963), "An Experiment in Numerical Prediction of Fog and Stratus," Journal of Atmospheric Sciences, Vol. 20, p. 425-437.

51. Mack, E. J., Eadie, W. J., Rogers, C. W., Kocmond, W. C. and Pilie, R. J. (1972), "A Field Investigation and Numerical Simulation of Coastal Fog," Cornell Aeronautical Lab., CAL No. CJ-5055-M-1, Project Fog Drops Annual Summary Report, 136 p.

52. Blackadar, A. K. (1962), "The Vertical Distribution of Wind and Turbulent Exchange in a Neutral Atmosphere," Journal of Geophysical Research, Vol. 67, p. 3095-3102.

53. Heisenberg, W. (1948), "Zur Statistischen Theorie der Turbulenz," Z. Physik, Vol. 124, p. 628-657.

54. Zdundowski, W. G. and Trask, D. C. (1971), "Application of a Radiative-Conductive Model to the Simulation of Nocturnal Temperature Changes over Different Soil Types," Journal of Applied Meteorology, Vol. 10, No. 5, p. 937-948.

55. Wu, S. S. (1965), "A Study of Heat Transfer Coefficients in the Lowest 400 Meters of the Atmosphere," Journal of Geophysical Research, Vol. 70, p. 1801-1808.

56. Nee, V. W. and Kovasznay, L. S. G. (1969), "A Simple Theory of the Turbulent Shear Flows," The Physics of Fluids, Vol. 13, p. 473-484.

57. Kolmogorov, A. M. (1942), "Equations of Turbulent Motion of an Incompressible Fluid," Izv. Akad. Mauk.SSSR Ser. Phys., Vol. 6, p. 56-58.

58. Patankar, S. V. and Spalding, D. B. (1967), "A Finite-Difference Procedure for Solving the Equations of the Two-Dimensional Boundary Layer," International Journal of Heat Mass Transfer, Vol. 10, p. 1389-1411.

59. Glushko, G. S. (1965), "Turbulent Boundary Layer on a Flat Plate in an Incompressible Fluid," NASA TT F-10, 080. Translated from Izvestiya Akademii Nak SSSR, Seriya Mekanika, No. 4, p. 13-23.

60. Wolfshtein, M. (1969), "The Velocity and Temperature Distribution in One-Dimensional Flow with Turbulence Augmentation and Pressure Gradient, International Journal Heat Mass Transfer, Vol. 12, p. 301-318.

61. Wolfshtein, M. (1970), "Some Solutions of the Plane Turbulent Impinging Jet," Journal of Basic Engineering, Transactions of ASME, December, p. 915-922.

62. Gosman, A. D., Pun, W. M., Runchal, A. K., Spalding, D. B. and Wolfshtein, M. (1969), Heat and Mass Transfer in Recirculating Flows, Academic Press, London, 338 p.

63. Bradshaw, P., Ferris, D. H. and Attwell, M. P. (1967), "Calculation of Boundary-Layer Development Using the Turbulent Energy Equation," Journal of Fluid Mechanics, Vol. 28, Part 3, p. 593-616.

64. Nevzglajdov, V. (1945), "A Phenomenological Theory of Turbulence," Journal of Physics, (USSR), Vol. 9, p. 235-243.

65. Klebanoff, P. S. (1955), "Characteristics of Turbulence in a Boundary Layer With Zero Pressure Gradient," NACA Rep. 1247, 19 p.

66. Bradshaw, P. (1967), "The Turbulence Structure of Equilibrium Boundary Layers," Journal of Fluid Mechanics, Vol. 29, Part 4, p. 625-645.

67. Harsha, P. T. and Lee, S. C. (1970), "Correlation Between Turbulent Shear Stress and Turbulent Kinetic Energy," AIAA Journal, Vol. 9, No. 8, p. 1508-1510.

68. Byrne, W. M. (1970), "Use of the Turbulent Kinetic Energy Equation in Prediction of Nonequilibrium Turbulent Boundary Layers," Ph. D. Dissertation, Mechanical Engineering, University of Missouri, Rolla, Missouri, 117 p.

69. Lee, S. C. and Harsha, P. T. (1970), "Use of Turbulent Kinetic Energy in Free Turbulent Mixing Studies," AIAA Journal, Vol. 8, No. 6, p. 1026-1032.

70. Lee, S. C., Pepper, D. W., Byrne, W. M. and Tai, R. C. (1973), "Heat, Mass, and Momentum Transfer in Turbulent Boundary Layer Flows," to be presented at the Fifth International Heat Transfer Conference, Tokyo, Japan, September, 1974.

71. Jones, W. P. and Launder, B. E. (1972), "The Calculation of Low-Reynolds-Number Phenomena With A Two-Equation Model of Turbulence," Journal of Heat Transfer, Transactions of ASME, Vol. 20, 8 p.

72. Gibson, M. M. and Spalding, D. B. (1972), "A Two-Equation Model of Turbulence Applied to the Prediction of Heat and Mass Transfer in Wall Boundary Layers," Journal of Heat Transfer, Transactions of ASME, Vol. 15, 8 p.

73. Launder, B. E., Morse, A., Rodi, W. and Spalding, D. B. (1972), "The Prediction of Free Shear Flows - A Comparison of the Performance of Six Turbulence Models," NASA Conference on Free Shear Flows, Langley Field, Hampton, Virginia, July 20-21.

74. Donaldson, C. DuP. (1972), "Construction of a Dynamic Model of the Production of Atmospheric Turbulence and the Dispersal of Atmospheric Pollutants," ARAP Report No. 175, 123 p.

75. Reynolds, O. (1894), "On the Dynamical Theory of Incompressible Viscous Fluids and the Derermination of the Criterion," Philosophical Transactions of the Royal Society, Vol. 186, Part A, p. 123-164.

76. Weinstein, A. (1973), "Comments on Thrust of Air Force Fog Program," presented to the First Conference in Marine Fogs, University of Missouri, Rolla, Missouri, January, 1973.

77. Patankar, S. V. and Spalding, D. B. (1972), "A Calculation Procedure for Heat, Mass and Momentum Transfer in Three-Dimensional Parabolic Flows," International Journal of Heat Mass Transfer, Vol. 15, p. 1787-1806.

78. Deardorff, J. W. (1970), "A Numerical Study of Three-Dimensional Turbulent Channel Flow at Large Reynolds Numbers," Journal of Fluid Mechanics, Vol. 41, No. 2, p. 453-480.

79. Kasahara, A. and Washington, W. M. (1971), "General Circulation Experiments With a Six-Layer NCAR Model, Including Orography, Cloudiness and Surface Temperature Calculations," Journal of Atmospheric Sciences, Vol. 28, No, 5, p. 657-701.

80. Deardorff, J. W. (1972), "Parameterization of the Planetary Boundary Layer for Use in General Circulation Models," Monthly Weather Review, Vol. 100, No. 2, p. 92-106.

81. Lilly, D. K. (1971) "Progress in Research on Atmospheric Turbulence," IUGG, p. 332-341.

82. Taylor, G. I. (1920), "Diffusion by Continuous Movements," Proceedings of the London Mathematical Society, Vol. 20, p. 196-212.

83. Frenkiel, F. N. (1953), "Turbulent Diffusion: Mean Concentration Distribution in a Flow Field of Homogeneous Turbulence," Advances in Applied Mechanics, Vol. 3, p. 61-107.

84. Gifford, F. A. (1962), "Diffusion in the Diabatic Surface Layer," Journal of Geophysical Research, Vol. 67, p. 3207-3212.

85. Klug, W. (1968), "Diffusion in Atmospheric Surface Layer: Comparisons of Similarity Theory With Observations," Quarterly Journal of the Royal Meteorological Society, Vol 94, p. 555-562.

86. Batchelor, G. K. (1964), "Diffusion From Sources in a Turbulent Boundary Layer," Arch. Mech. Stosowanej, Vol. 3, p. 661-670.

87. Schilichting, H. (1968), Boundary-Layer Theory, McGraw-Hill Book Company, 747 p.

88. Pepper, D. W. and Lee, S. C. (1973), "The Effects of Turbulent Mixing on Advection Fogs," American Geophysical Union, Washington, D. C., April 16-20.

89. Harsha, P. T. (1970), "Free Turbulent Mixing: A Critical Evaluation of Theory and Experiment," Ph. D. Dissertation, Aerospace Engineering, University of Tennessee, p. 603.

90. Tai, R. C. (1969), "The Use of Turbulence Energy Equation in Boundary Layer Study," M. S. Thesis, Mechanical and Aerospace Engineering, University of Missouri, Rolla, Missouri, 65 p.

91. Naudascher, E. (1965), "Flow in the Wake of Self-Propelled Bodies and Related Sources of Turbulence," Journal of Fluid Mechanics, Vol. 22, Part 4, p. 625-656.

92. Lee, S. C., Harsha, P. T., Auiler, J. E. and Lin, C. L. (1972), "Heat Mass and Momentum Transport in Free Turbulent Mixing," Proceedings 1972 Heat Transfer and Fluid Mechanics Institute, Stanford University Press, p. 215-230.

93. Lin, C. C. (1959), Turbulent Flows and Heat Transfer, Princeton University Press, Princeton, New Jersey, p. 102-376.

94. Julien, H. L., Kays, W. M. and Moffat, R. J. (1971), "Experimental Hydrodynamics of the Accelerated Turbulent Boundary Layer With and Without Mass Injection," ASME Paper No. 71-HT-F.

95. Thielbahr, W. J., Kays, W. M. and Moffat, R. J. (1969), "The Turbulent Boundary Layer: Experimental Pressure Gradient," Report No. HMT-5, Stanford University, p. 166.

96. Julien, H. L. (1969), "The Turbulent Boundary Layer on a Porous Plate: Experimental Study of the Effects of a Favorable Pressure Gradient," Ph. D. Dissertation, Mechanical Engineering, Stanford University, Palo Alto, California.

97. Richtmyer, R. D. (1957), Difference Methods for Initial-value Problems, Interscience Publishing, Inc., New York, 238 p.

98. Malhotra, R. C. and Cermak, J. E. (1964), "Mass Diffusions in Neutral and Unstably Stratified Boundary-Layer Flows," International Journal of Heat Mass Transfer, Vol. 7, p. 169-186.

99. Reynolds, W. C., Kays, W. M. and Kline, S. J. (1958), "Heat Transfer in the Turbulent Incompressible Boundary Layer: I-Constant Wall Temperature," NASA, Memo. 12-1-58W, 36. p.

100. McDonald, J. E. (1963), "The Saturation Adjustment in Numerical Modelling of Fog," Journal of Atmospheric Sciences, Vol. 20, p. 476-478.

101. Murray, F. W. (1967), "On the Computation of Saturation Vapor Pressure," Journal of Applied Meterology, Vol. 6, p. 203-204.

102. Barker, E. H. (1973), "Oceanic Fog, A Numerical Study," EPRF, Naval Postgraduate School, Technical Paper No. 6-73, 65 p.

VITA

The author, Darrell Weldon Pepper, was born on May 14, 1946, in Kirksville, Missouri. He graduated from Pattonville High School, St. Ann, Missouri, in June, 1964, and entered the University of Missouri - Rolla in September, 1964. He received the degree of Bachelor of Science in Mechanical Engineering in May, 1968, and is a member of Pi Tau Sigma and Sigma Xi.

He enrolled in the Graduate School of the University of Missouri - Rolla in September, 1968, and worked as a graduate assistant in the Department of Mechanical and Aerospace Engineering until June, 1969. The author joined the Graduate Center for Cloud Physics Research in June, 1969, where he has worked as a research assistant until the present time under THEMIS Contract N00014-68-A-0497 (2357-2228) and ONR Contract N00014-69-A-0141-0006. He received the degree of Master of Science in Aerospace Engineering in December, 1970.

The author married the former Miss Jeanne Limbacher of Tucson, Arizona, on August 16, 1969.

APPENDIX A: FOG FORMATION ANALYSIS

Fogs are normally classified into three types: radiation fog, advection fog, and combined-process fog. A fog occurring over the ocean is predominantly an advection fog, resulting either from warm humid air passing over a cold ocean surface or cold air passing over a warm surface (steam fog). Fogs resulting from warm air blowing over a cold surface occur frequently over the North Atlantic Ocean during the summer, often lasting for days or weeks.

A. Governing Equations

In order to understand the physics of the air-sea system, the conservation equations for continuity, momentum, species, and energy have been coupled with the turbulence kinetic energy equation. Closure of the set of equations is obtained by using the phenomenological model of Nevzglajdov. The governing equations are given in terms of the X-Z coordinate system for atmospheric boundary layer flow as follows:

1. Conservation of Mass

$$\frac{\partial}{\partial X}(\rho U) + \frac{\partial}{\partial Z}(\rho W) = 0 \qquad \text{(A-1)}$$

2. Conservation of Longitudinal Momentum

$$\rho\left(U\frac{\partial U}{\partial X} + W\frac{\partial U}{\partial Z}\right) = \frac{\partial}{\partial Z}\left(K_m\frac{\partial U}{\partial Z}\right) - \frac{dP}{dX} \qquad \text{(A-2)}$$

where $K_m = \mu + \varepsilon_m$.

3. Conservation of Potential Temperature

$$\rho\left(U\frac{\partial\theta}{\partial X} + W\frac{\partial\theta}{\partial Z}\right) = \frac{\partial}{\partial Z}\left(\frac{K_m}{\sigma_h}\frac{\partial\theta}{\partial Z}\right) + \frac{1}{C_p}\left(L_h C_s + \frac{\partial R}{\partial Z}\right)\left(\frac{1000}{P}\right)^{2/7} \qquad (A\text{-}3)$$

where θ is the potential temperature given by the adiabatic relation

$$\theta = T\left(\frac{1000_{mb}}{P}\right)^{2/7} \qquad (A\text{-}4)$$

The cross stream gradient of potential temperature is expressed as

$$\frac{\partial\theta}{\partial Z} = \frac{\theta}{T}\left(\frac{\partial T}{\partial Z} + \Gamma\right) \qquad (A\text{-}5)$$

where $\Gamma = g/C_p$, the adiabatic lapse rate. The term $L_h C_s$ is the latent heat of condensation for water vapor (592 cal/gm) times the source function for condensation or evaporation; C_p represents the specific heat of air at constant pressure (.24 cal/gm - ^oK). The radiation flux divergence term, $\partial R/\partial Z$ (cal/cc), is defined by the relation

$$\frac{\partial R}{\partial Z} = 1.6\beta'\sigma T_w^4 K_\omega \rho W_L \exp\left[-1.6K_\omega\rho\int_z^{z_t} W_L(z')dz'\right] \qquad (A\text{-}6)$$

where β', the fraction of longwave radiation emitted from the earth's surface, is given as $\beta' = .25$, $K_\omega = 1.5 \times 10^3$ cm^2/gm for the mass absorption coefficient for fog, σ the Stefan-Boltzmann constant, T_w the surface temperature of the earth, W_L the liquid water mixing ratio, ρ the density of air, and z_t the height of the fog layer.

The treatment of radiation in this model is based upon the previous work by the Calspan Corporation regarding the

numerical simulation of advection fog. Infrared radiation at the earth's surface, R_w, is given by the relation

$$R_w = \beta' \sigma T_w^4 \tag{A-7}$$

where $\beta' = .25$, signifying that the net upward flux of radiation is 25 per cent of the blackbody radiation emitted from the earth's surface at temperature T_w. The radiation flux at a height, Z, is subsequently written as

$$R = \beta' \sigma T_w^4 \exp\left[-1.6 K_\omega \rho \int_z^{z_t} W_L(z')dz'\right] \tag{A-8}$$

where the exponential term represents the presence of fog. The resulting expression for the radiative flux divergence, equation (A-6), is valid for a fog which has droplet radii less than 10μm.

4. Conservation of Turbulence Kinetic Energy

$$\rho\left(U\frac{\partial Q}{\partial X} + W\frac{\partial Q}{\partial Z}\right) = \frac{\partial}{\partial Z}\left(\frac{K_m}{\sigma_k}\frac{\partial Q}{\partial Z}\right) + \varepsilon_m\left(\frac{\partial U}{\partial Z}\right)^2\left(1 - \frac{R_i}{\sigma_h}\right) - D_Q \tag{A-9}$$

where ε_m is the eddy coefficient of momentum, $K_m = \mu + \varepsilon_m$, D_Q the dissipation of turbulence kinetic energy, given as

$$D_Q = \frac{a_2 \rho Q^{\frac{1}{2}}}{\delta} \tag{A-10}$$

and R_i, the gradient Richardson number, given as

$$R_i = \frac{g}{T_m}\frac{\partial\theta/\partial Z}{(\partial U/\partial Z)^2} \tag{A-11}$$

where $T_m = \frac{1}{2}(T_w + T_\infty)$.

5. Conservation of Species

The conservation of species is given by the equations

for water vapor mixing ratio, W_v, and liquid water mixing ratio, W_L. The conservation of water vapor mixing ratio is expressed as

$$\rho(U\frac{\partial W_v}{\partial X} + W\frac{\partial W_v}{\partial Z}) = \frac{\partial}{\partial Z}(\frac{K_m}{\sigma_c}\frac{\partial W_v}{\partial Z}) - C_s \qquad \text{(A-12)}$$

The conservation of liquid water mixing ratio is written as

$$\rho(U\frac{\partial W_L}{\partial X} + W\frac{\partial W_L}{\partial Z}) = \frac{\partial}{\partial Z}(\frac{K_m}{\sigma_c}\frac{\partial W_L}{\partial Z}) + C_s + \frac{\partial}{\partial Z}(W_t W_L) \qquad \text{(A-13)}$$

where C_s in both equations represents the source function for condensation or evaporation and W_t is the terminal velocity of fog drops. The mean terminal velocity, W_t, is based upon the Calspan expression, for droplet radii less than 20μm,

$$W_t = 5.3 \times 10^3(\frac{W_L}{N})^{2/3} \qquad \text{(A-14)}$$

where N is the number of drops per unit volume and W_L the liquid water mixing ratio. Assuming a constant drop concentration of N = 50/cc, equation (A-14) becomes

$$W_t = 400 W_L^{2/3} (\text{cm/sec}) \qquad \text{(A-15)}$$

If $W_L = 2.44 \times 10^{-4}$, corresponding to a liquid water content of 0.30 gm/m^3, $W_t \simeq 1.5$ cm/sec.

B. Saturation Adjustment

Appropriate computations at each grid point yield values for T, W_v, and W_L according to equations (A-3), (A-12), and (A-13). The source term, C_s, allows for contributions to these independent variables of the heating or cooling of the air, evaporation of liquid water content,

and condensation of water vapor.

Following the procedure outlined by McDonald (100) and Mack, et al (51), values for T, W_V, and W_L are calculated at each horizontal step increment, neglecting condensation or evaporation. A saturation adjustment procedure is then applied to these three variables, external to the solution procedure for the governing equations. By considering the heating of the air due to the release of latent heat of condensation, supersaturated water vapor at a grid point is converted into liquid water until saturation is achieved. Likewise, if the air is in a subsaturated state, liquid water at a grid point is evaporated into water vapor until saturation is obtained or the liquid water becomes exhausted. The following derivation of the saturation adjustment procedure is based principally upon the method of McDonald (100).

Water vapor content can be described by either mixing ratio, which is the ratio of the mass of water vapor to the mass of dry air, or vapor pressure. Vapor pressure will be used here in keeping with McDonald's formulation. The derivation will be described for the case where the vapor pressure, p_o, exceeds the saturation vapor pressure, p_{s_o}, corresponding to a temperature, T_o. The final relations are the same for either supersaturation or subsaturation, except for sign changes.

A parcel of air attains a temperature, T_o, corresponding to a point at a vapor pressure, p_o. After accounting

for all the terms appearing in the governing equations except C, the saturation adjustment is performed. This is shown in Figure A-1, where p_o lies above the saturation vapor pressure curve, $p_s(T)$. The adjustment procedure must therefore condense excess vapor onto the existing fog drops. This condensation creates a release of latent heat, which tends to raise T, causing the characteristic points (p, T) and (p_s, T) to mutually approach each other.

In a saturation adiabatic process, condensation produces a release of latent heat within the system, but no heat is added to or removed from the system. As an air parcel lifts adiabatically, the temperature of the parcel decreases at the adiabatic lapse rate until saturated. Further lifting results in the release of latent heat by the parcel. This process can be expressed by the First Law of Thermodynamics as

$$-Ld\omega_s = C_v dT + pdv \qquad \text{(A-16)}$$

where L is the latent heat of vaporization and ω_s the mass of water vapor condensed per unit mass of air. Equation (A-16) can be combined with the equation of state to give

$$-Ld\omega_s = C_p dT - vdp \qquad \text{(A-17)}$$

The heating, dT, resulting from a small amount of adiabatic-isobaric condensation can be represented by

$$-Ld\omega_s = C_p dT \qquad \text{(A-18)}$$

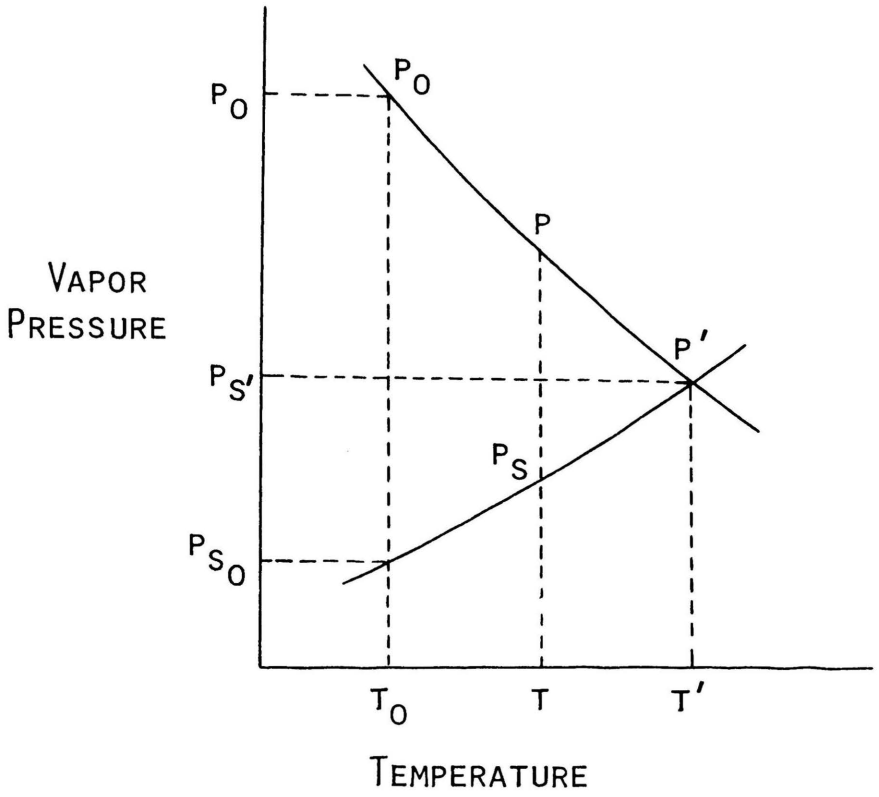

Figure A-1. Saturation Adjustment Procedure

Since $\omega_s = m_v/m_a$, where m_v denotes the mass of water vapor and m_a the mass of dry air, the mixing ratio can be rewritten, with the use of the equation of state, as

$$\omega = \frac{m_v}{m_a} = \frac{p_s v/R_v T}{p_a v/R_a T} \tag{A-19}$$

or

$$\omega = \frac{R_a}{R_v}\frac{p_v}{p_a} = .622\ \frac{p_v}{p_a} \tag{A-20}$$

where the subscripts v and a denote vapor and air respectively. The total pressure of the mixture of water vapor and air, p, can be introduced in equation (A-20)

$$\omega = \varepsilon\ \frac{p_v}{p - p_v} \tag{A-21}$$

where $\varepsilon = .622$ and $p = p_a + p_v$. Equation (A-21) is normally referred to as specific humidity. Since $p >> p_v$,

$$\omega \simeq \varepsilon\ \frac{p_v}{p} \tag{A-22}$$

For saturated conditions, $\omega_s \simeq \varepsilon\ p_s/p$. Therefore, equation (A-18) can be rewritten as

$$-\frac{L\varepsilon}{p}\ dp_s = C_p dT \tag{A-23}$$

Equation (A-23) specifies the line along which condensational heating takes place, shown in Figure A-1 passing through the points (p_o, T_o) and (p_s', T'). As the vapor pressure decreases, temperature rises, causing the saturation vapor pressure to increase. The final saturated state occurs at (p_s', T').

The Clausius-Clapeyron equation is normally written as

$$\frac{dp_s}{p_s} = \frac{L}{R_v}\frac{dT}{T^2} = \frac{L\varepsilon}{R_a T^2} \qquad \text{(A-24)}$$

which describes the variation in saturated water vapor pressure with T. This can be rewritten to a good approximation for the saturation vapor pressure curve as

$$\frac{(p_s' - p_{s_o})}{T' - T_o} = \frac{p_{s_o}\varepsilon L}{R_a T_o^2} \qquad \text{(A-25)}$$

However, equation (A-23) implies that

$$\frac{p_o - p_s'}{T' - T_o} = \frac{C_p p}{\varepsilon L} \qquad \text{(A-26)}$$

Inspection of Figure A-1 shows that

$$p_o - p_s' = (p_o - p_{s_o}) - (p_s' - p_{s_o}) \qquad \text{(A-27)}$$

Substituting equation (A-27) into equation (A-26), and making use of equation (A-25), yields the relation

$$p_o - p_{s_o} = \frac{(T' - T_o)\varepsilon L p_{s_o}}{RT_o^2} + \frac{pC_p(T' - T_o)}{\varepsilon L} \qquad \text{(A-28)}$$

Rearrangement of equation (A-28) for the adjusted temperature, T', gives

$$T' = T_o + \frac{(p_o - p_{s_o})\varepsilon L R T_o^2}{pC_p RT_o^2 + \varepsilon^2 L^2 p_{s_o}} \qquad \text{(A-29)}$$

which is the governing equation in the saturation adjustment procedure for the temperature, equation (A-3). Once T' is known, equation (A-29) can be used to determine the

final vapor pressure, p_s',

$$p_s' = p_{s_o} + \frac{\varepsilon L p_{s_o}}{R T_o^2} (T' - T_o) \qquad \text{(A-30)}$$

The amount of condensate portioned among the fog drops is governed by equation (A-26), where

$$p_o = p_s' + \frac{C_p p}{\varepsilon L} (T' - T_o) \qquad \text{(A-31)}$$

The total pressure, p, is solved by using equation (A-22).

The only unknown appearing throughout equations (A-29), (A-30), and (A-31) is p_{s_o}, the saturation vapor pressure for water at T_o. This is calculated at every grid point by the relation

$$p_{s_o} = 6.1078 \exp \left\{ \frac{17.269(T_o - 273.16)}{(T_o - 35.86)} \right\} \qquad \text{(A-32)}$$

Equation (A-32), derived by Murray (101), gives reasonably accurate results, over a wide range of temperatures.

C. Vertical Grid Control

An expanding vertical grid system is employed which provides high resolution near the surface where the independent variables change significantly with height. A total of 55 grid intervals are used with the vertical grid spacing expanding by 1.2 per level, beginning at 1 cm above the surface. This places the upper boundary at a distance of 943 m above the surface; sufficiently far enough away so that the upper boundary does not influence the steep gradient region. This essentially reduces the need of Couette flow relations to account for the near wall region; however, they need not

be removed from the computer program. Although liquid water content does not necessarily begin to appear at the 1 cm level, the fog does attempt to settle to the surface as the flow proceeds downstream. The radiation flux divergence from the surface influences the heat flux within the first few levels. Since the radiation effect quickly dampens with height, use of a more coarse grid network may lead to a total neglect of radiation in the model.

D. Boundary and Initial Conditions

The boundary conditions are specified as follows:

Surface ($Z = 0$)

$$U = 0$$

$$T = T_w - .0001X$$

$$W_L = 0$$

$$\frac{\partial W_v}{\partial Z} = 0$$

$$Q = \tau_w / a_1 \rho$$

Free Stream ($Z \to \infty$)

$$U = U_\infty$$

$$T = T_\infty$$

$$Q = 0$$

$$W_v = 0$$

$$W_L = 0$$

The initial conditions for the dependent variables are specified at $X = 0$ by the relations:

$U = U_{\infty}(Z/\delta)^{1/5.5}$, $\delta = 943$ if U is not known

$T = T_{\infty}(Z/\delta_t)^{1/5.5}$, $\delta_t \simeq .7\delta$ if T is not known

$Q = \tau_w/a_1\rho = u^{*2}/a_1$

$W_v = W_v$ at saturation, if W_v is not known

$W_L = 0$